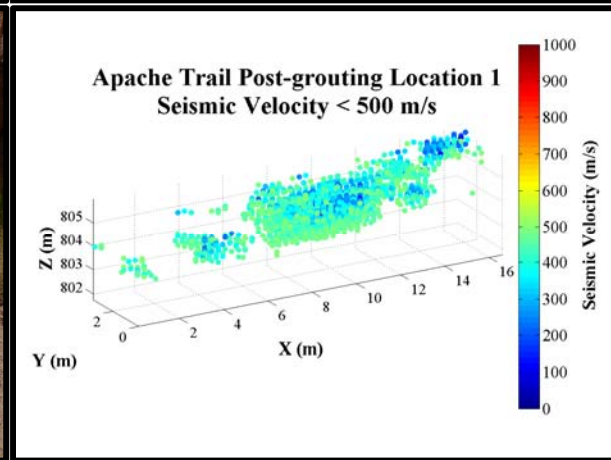
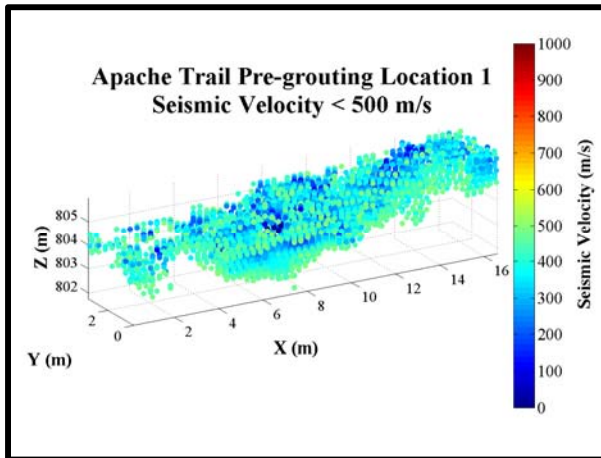


VERIFICATION OF GROUTING Using 3D Seismic Tomography

Publication No. FHWA-CFL/TD-11-007

September 2011



U.S. Department
of Transportation
**Federal Highway
Administration**



Central Federal Lands Highway Division
12300 West Dakota Avenue
Lakewood, CO 80228

FOREWORD

Compaction grouting is one of the most common ground improvement techniques in geotechnical practice. Traditional quality assurance methods for compaction grouting typically involve evaluation of grout injection parameters and intrusive point measurements. One issue with these methods is that they may not reflect the entire treated soil volume. A geophysics-based evaluation method such as 3D seismic tomography provides an alternative technique to evaluate the volumetric improvement of soil profiles before and after compaction grouting. Specifically, 3D seismic tomographic images can be used to visualize and quantify the distribution in compression wave (p-wave) velocities to measure and estimate spatial variations in improvement of subsurface materials in a rapid, non-intrusive, and inexpensive manner.

The Federal Lands Highway (FLH) of the Federal Highway Administration (FHWA) performs a variety of roadway stabilization projects, many of which include the use of grouting technologies. Three-dimensional seismic tomography was applied in this study to two roadway rehabilitation projects to investigate its suitability in quality assurance programs for shallow grouting of poor roadway subgrades. This study presents the details of these projects as well as related grouting field operations, seismic data collection procedures, and raw 3D seismic tomography results. Several analytical methods are proposed to interpret the tomography results to quantify the degree of improvement in the seismic velocity distributions at the sites following grouting. The potential applications of 3D seismic tomography for verifying effectiveness of future compaction grouting projects is explored and recommendations are made based on lessons learned.



David J. Scott, P.E., Acting Director of Project Delivery
Federal Highway Administration
Central Federal Lands Highway Division

Notice

This document is disseminated under the sponsorship of the U.S. Department of Transportation in the interest of information exchange. The U.S. Government assumes no liability for the use of the information contained in this document. This report does not constitute a standard, specification, or regulation.

Quality Assurance Statement

The FHWA provides high-quality information to serve Government, industry, and the public in a manner that promotes public understanding. Standards and policies are used to ensure and maximize the quality, objectivity, utility, and integrity of its information. FHWA periodically reviews quality issues and adjusts its programs and processes to ensure continuous quality improvement.

Cover Photos, clockwise from top left: Pre-grouting seismic tomography, compaction grouting at Zion National Park site, post-grouting seismic tomography, and seismic data collection at Apache Trail site.

Technical Report Documentation Page

1. Report No. FHWA-CFL/TD-11-007	2. Government Accession No.	3. Recipient's Catalog No.	
4. Title and Subtitle <i>Verification of Grouting Using 3D Seismic Tomography</i>		5. Report Date September 2011	
		6. Performing Organization Code	
7. Author(s) Christopher Lynch and Matthew DeMarco (FHWA-CFLHD); and John S. McCartney (University of Colorado at Boulder)		8. Performing Organization Report No.	
9. Performing Organization Name and Address Federal Highway Administration Central Federal Lands Highway Division 12300 W. Dakota Avenue, Suite 210 Lakewood, CO 80228		10. Work Unit No. (TRAIS)	
		11. Contract or Grant No.	
12. Sponsoring Agency Name and Address Federal Highway Administration Central Federal Lands Highway Division 12300 W. Dakota Avenue, Suite 210 Lakewood, CO 80228		13. Type of Report and Period Covered Final Report	
		14. Sponsoring Agency Code HFTS-16.4	
15. Supplementary Notes <i>Program Development Team:</i> Christopher Lynch, Khamis Haramy, Marilyn Dodson, Roger Surdahl, FHWA-CFLHD; Phil Sirles, Zonge International, Colorado; Alan Rock, GSR, Inc.			
16. Abstract <p>Compaction grouting is one of the most common ground improvement techniques in geotechnical practice. Traditional quality assurance methods for compaction grouting typically involve evaluation of grout injection parameters and intrusive point measurements. One issue with these methods is that they may not reflect the entire treated soil volume. A geophysics-based evaluation method such as 3D seismic tomography provides an alternative technique to evaluate the volumetric improvement of soil profiles before and after compaction grouting. Specifically, 3D seismic tomographic images can be used to visualize and quantify the distribution in compression wave (p-wave) velocities to measure and estimate spatial variations in improvement of subsurface materials in a rapid, non-intrusive, and inexpensive manner.</p> <p>The Federal Lands Highway of the Federal Highway Administration perform a variety of roadway stabilization projects, many of which include the use of grouting technologies. Three-dimensional seismic tomography was applied in this study to two roadway rehabilitation projects to investigate its suitability in quality assurance programs for shallow grouting of poor roadway subgrades. This study presents the details of these projects as well as related grouting field operations, seismic data collection procedures, and raw 3D seismic tomography results. Several analytical methods are proposed to interpret the tomography results to quantify the degree of improvement in the seismic velocity distributions at the sites following grouting. The potential applications of 3D seismic tomography for verifying effectiveness of future compaction grouting projects is explored and recommendations are made based on lessons learned.</p>			
17. Key Words COMPACTION GROUTING, GEOPHYSICS, SEISMIC, TOMOGRAPHY, VOID-FILL		18. Distribution Statement No restriction. This document is available to the public from the sponsoring agency at the website http://www.cflhd.gov .	
19. Security Classification (of this report) Unclassified	20. Security Classification (of this page) Unclassified	21. No. of Pages 118	22. Price NA

SI* (MODERN METRIC) CONVERSION FACTORS

APPROXIMATE CONVERSIONS TO SI UNITS

Symbol	When You Know	Multiply By	To Find	Symbol
LENGTH				
in	inches	25.4	millimeters	mm
ft	feet	0.305	meters	m
yd	yards	0.914	meters	m
mi	miles	1.61	kilometers	km
AREA				
in ²	square inches	645.2	square millimeters	mm ²
ft ²	square feet	0.093	square meters	m ²
yd ²	square yard	0.836	square meters	m ²
ac	acres	0.405	hectares	ha
mi ²	square miles	2.59	square kilometers	km ²
VOLUME				
fl oz	fluid ounces	29.57	milliliters	mL
gal	gallons	3.785	liters	L
ft ³	cubic feet	0.028	cubic meters	m ³
yd ³	cubic yards	0.765	cubic meters	m ³
NOTE: volumes greater than 1000 L shall be shown in m ³				
MASS				
oz	ounces	28.35	grams	g
lb	pounds	0.454	kilograms	kg
T	short tons (2000 lb)	0.907	megagrams (or "metric ton")	Mg (or "t")
TEMPERATURE (exact degrees)				
°F	Fahrenheit	5 (F-32)/9 or (F-32)/1.8	Celsius	°C
ILLUMINATION				
fc	foot-candles	10.76	lux	lx
fl	foot-Lamberts	3.426	candela/m ²	cd/m ²
FORCE and PRESSURE or STRESS				
lbf	poundforce	4.45	newtons	N
lbf/in ²	poundforce per square inch	6.89	kilopascals	kPa

APPROXIMATE CONVERSIONS FROM SI UNITS

Symbol	When You Know	Multiply By	To Find	Symbol
LENGTH				
mm	millimeters	0.039	inches	in
m	meters	3.28	feet	ft
m	meters	1.09	yards	yd
km	kilometers	0.621	miles	mi
AREA				
mm ²	square millimeters	0.0016	square inches	in ²
m ²	square meters	10.764	square feet	ft ²
m ²	square meters	1.195	square yards	yd ²
ha	hectares	2.47	acres	ac
km ²	square kilometers	0.386	square miles	mi ²
VOLUME				
mL	milliliters	0.034	fluid ounces	fl oz
L	liters	0.264	gallons	gal
m ³	cubic meters	35.314	cubic feet	ft ³
m ³	cubic meters	1.307	cubic yards	yd ³
MASS				
g	grams	0.035	ounces	oz
kg	kilograms	2.202	pounds	lb
Mg (or "t")	megagrams (or "metric ton")	1.103	short tons (2000 lb)	T
TEMPERATURE (exact degrees)				
°C	Celsius	1.8C+32	Fahrenheit	°F
ILLUMINATION				
lx	lux	0.0929	foot-candles	fc
cd/m ²	candela/m ²	0.2919	foot-Lamberts	fl
FORCE and PRESSURE or STRESS				
N	newtons	0.225	poundforce	lbf
kPa	kilopascals	0.145	poundforce per square inch	lbf/in ²

*SI is the symbol for the International System of Units. Appropriate rounding should be made to comply with Section 4 of ASTM E380.
(Revised March 2003)

TABLE OF CONTENTS

1. INTRODUCTION.....	1
2. GROUND IMPROVEMENT	3
2.1. Void-Fill Grouting.....	3
2.2. Compaction Grouting.....	4
2.3. Field Procedures.....	5
2.4. Grouting Verification Methods	6
3. BACKGROUND ON GEOPHYSICAL METHODS	9
3.1. Seismic Methods	10
3.1.1. 2D vs. 3D Geophysical Methods	11
3.1.2. 3D Seismic Tomography	13
3.1.3. GSR3D Seismic Tomography Software	16
3.1.4. Assumptions and Limitations of GSR3D	18
3.1.5. GSR3D Historical Case Study #1: Rocky Mountain National Park.....	18
4. CASE STUDY 1: ZION NATIONAL PARK.....	21
4.1. Soils and Site Conditions	22
4.2. Pre-Grouting Geophysical Investigation.....	23
4.2.1. Site #1 Grid Layout (172+54 – 174+04)	24
4.2.2. Site #2 Grid Layout (177+26 – 178+76)	25
4.2.3. Equipment and Data Collection.....	26
4.3. Observation of Compaction Grouting.....	28
4.3.1. Equipment and Methods	29
4.3.2. Additional Observations	30
4.3.3. Comments and Suggestions from Contractor	31
4.3.4. For Further Consideration.....	31
4.3.5. Reinforced Fill (177+26 to 179+37).....	32
4.4. Post-Grouting Geophysical Investigation	32
5. CASE STUDY 2: APACHE TRAIL, TONTO NATIONAL FOREST	35
5.1. Soils and Site Conditions	36
5.2. Pre-Grouting Geophysical Investigation.....	38
5.3. Observation of Compaction Grouting.....	39
5.4. Post-Grouting Geophysical Investigation	39
6. RESULTS	41
6.1. Zion National Park Results	41
6.1.1. Difference Tomography.....	45
6.2. Apache Trail Results.....	46
6.2.1. Difference Tomography.....	48
6.3. Ray Densities.....	48

VERIFICATION OF GROUTING USING 3D SEISMIC TOMOGRAPHY - TABLE OF CONTENTS

7. DATA ANALYSIS.....	51
7.1. Improvement of a Target Velocity Range.....	51
7.2. Seismic Velocity Difference Quantification	54
7.2.1. Possible Explanations for Decreased Velocities following Grouting.....	55
7.3. 3D Spatial Analysis.....	56
7.4. Comparison with 2D Seismic Refraction Results	59
7.5. Comparison with Consultant Findings at Zion National Park	63
8. RECOMMENDATIONS.....	65
8.1. Changes to Design of 3D Seismic Tomography Grouting Verification Programs	66
8.2. Cost Comparison between Sites	66
8.3. Effect of Different Geophone Spacings	67
8.4. Improvements to Quality Assurance and Quality Control Programs.....	68
8.5. Use of Pre-Grouting Tomography for Design of Grouting Plans	69
8.6. Future Work	70
9. CONCLUSION	73
REFERENCES.....	75
APPENDIX A – LOCATION MAPS AND PLAN DRAWINGS.....	81
APPENDIX B – DATA COLLECTION LAYOUT DIAGRAMS	89
APPENDIX C – SEISMIC TOMOGRAPHY	95
APPENDIX D – SEISMIC DIFFERENCE TOMOGRAPHY	99
APPENDIX E – RAY DENSITIES	103

FIGURES

Figure 2.1. Schematic. (a) Bottom-up, and (b) top-down compaction grouting (after ASCE, 2010) 6

Figure 3.1. Chart. (L) Most commonly used geophysical methods; and (R) most common applications of geophysics among state DOTs and selected federal and Canadian transportation agencies (after NCHRP, 2006) 10

Figure 3.2. Schematic. Simplified seismic refraction process showing reflected waves and arrivals as recorded by geophones. 12

Figure 3.3. Graph. A comprehensive interpretation of body-, air-, and surface-wave events on seismic travel-time plots (after Park et al. 2001). 12

Figure 3.4. Schematic. (L) Illustration of raypaths normal to the surface of a propagating wavefront and (R) reflected and refracted waves resulting from an incident p-wave. 13

Figure 3.5. Schematic. Source and receiver locations along with raypath coverage for typical (L) surface seismic and (R) subsurface seismic surveys. 15

Figure 3.6. Flowchart. Simplified processing procedure utilized by GSR3D. 17

Figure 3.7. Photo. Photographs showing (L) differential settlement of roadway and (R) compaction grouting operations at Rocky Mountain N.P. 19

Figure 3.8. Graph. Pseudo 3D difference tomography from Rocky Mountain National Park, Colorado, compaction grouting site, showing seismic velocity differences (L) less than 3000 ft/s and (R) greater than 3000 ft/s, on a scale of 0 to 7000 ft/s. 20

Figure 4.1. Schematic. Typical compaction grouting profile and layout at the Zion National Park. 21

Figure 4.2. Photo. Voids beneath roadway surface daylighting at Zion National Park: (L) Large void opening resembling a pothole, more than 0.5 m (1.5 ft) in width; and (R) small hole in pavement surface observed to open to a much larger void beneath pavement. 23

Figure 4.3. Photo. Layouts of the (L) 10-ft (3-m) geophone spacing for grid #1 and (R) 5-ft (1.5-m) geophone spacing for grid #1 at Zion National Park, during pre-grouting seismic data collection. 25

Figure 4.4. Photo. Layout of the 10 ft (3.0 m) geophone spacing at Zion National Park, grid #2 during (L) pre-grouting and (R) post-grouting seismic data collection. 26

Figure 4.5. Photo. Twenty-four channel Geometrics Geode seismograph. 26

Figure 4.6. Photo. (L) Sledge hammer; and (R) aluminum strike plate. 27

Figure 4.7. Photo. Asphalt thickness greater than 1 m (3 ft) observed at Zion National Park, site due to repeated maintenance patching to correct settlement. 32

Figure 5.1. Schematic. Typical grouting profile and layout at Apache Trail Wall 1. 35

Figure 5.2. Photo. Panoramic photograph showing locations 1 to 4, from right to left, along Wall 3 at Apache Trail, with stationing advanced from approximately 300+00 at the right to 304+50 at the left. 36

Figure 5.3. Photo. Photographs of Apache Trail retaining walls: clockwise from top left: (1) Location 1; (2) Location 2; (3) Location 3; (4) and (5) Location 5, Wall 1; (6) large void daylighting at the roadway surface at Location 4. 37

Figure 5.4. Photo. (L) Laptop, seismograph, and battery setup; and (R) geophones deployed on landstreamers at Apache Trail. 38

VERIFICATION OF GROUTING USING 3D SEISMIC TOMOGRAPHY - TABLE OF CONTENTS

Figure 6.1. Schematic. Schematic illustrating the viewing perspective for the tomography generated for both Zion National Park, and Apache Trail sites, relative to the typical site conditions. 41

Figure 6.2. Graph. Typical shot record for 3D layout 2.5.1 at Zion National Park, with clearly distinguishable first arrivals. 42

Figure 6.3. Graph. Manual training picks used for GSR3D autopicker for Zion National Park sites: (a) 10-ft (3-m) geophone spacing; and (b) 5-ft (1.5-m) geophone spacing. 43

Figure 6.4. Screenshot. Typical GSR3D screenshot showing manual training picks (in red) and resulting trained autopicks (in blue) used processing of seismic data for Zion National Park pre-grouting location 1.5.2. 44

Figure 6.5. Graph. Typical shot record for 3D layout at Apache Trail, with clear first arrivals and pre-trigger delay interval shown. 46

Figure 6.6. Graph. Manual training picks used for GSR3D autopicker for Apache Trail sites. 47

Figure 6.7. Screenshot. Typical GSR3D screenshot showing manual training picks (in red) and resulting trained autopicks (in blue) for Apache Trail pre-grouting location 1. 47

Figure 7.1. Graph. Pre- and post-grouting tomography for Apache Trail Location 1, showing data points having seismic velocities less than a targeted velocity of 500 m/s. 51

Figure 7.2. Graph. Pre- and post-grouting tomography for Apache Trail Location 1, showing data points having seismic velocities less than a targeted velocity of 250 m/s. 52

Figure 7.3. Graph. Nearest neighbor distance plots for Apache Trail Location 1 pre-grouting (left) and post-grouting (right) for seismic velocities less than 250 m/s. 57

Figure 7.4. Graph. Tri-histogram plots for Apache Trail Location 1 pre-grouting (upper) and post-grouting (lower) for seismic velocities less than 250 m/s, showing a closer packing of points following grouting. 58

Figure 7.5. Schematic. Results from 2D seismic refraction analysis for Line 4 at Apache Trail, as performed previously by AMEC (2007) using SeisOpt2D, which corresponds to Location 5 of the 3D tomography study performed here. 61

Figure 7.6. Graph. 2D slice of 3D seismic tomography results from Apache Trail Location 5, shown in the same orientation as the results from the 2D refraction survey. Slice shown for values of $-1 \text{ ft} < y < 1 \text{ ft}$ ($-0.3 \text{ m} < y < 0.3 \text{ m}$). 61

Figure 7.7. Schematic. Results from 2D seismic refraction analysis for Line 8 at Apache Trail, as performed previously by AMEC (2007) using SeisOpt2D, which corresponds to Location 3 of the 3D tomography study performed here. 62

Figure 7.8. Graph. 2D slice of 3D seismic tomography results from Apache Trail Location 3, shown in the same orientation as the results from the 2D refraction survey. A slice is shown for values of $0 < y < 1.5 \text{ ft}$ ($0 < y < 0.5 \text{ m}$). 62

TABLES

Table 2.1. Guidelines for design of compaction grouting programs (after Warner 2010) 5

Table 2.2. Advantages and disadvantages of compaction grouting applications (after Abdelrahman et al. 2003)..... 5

Table 3.1. Range of Velocities for Compressional Waves in Soil and Rock (after ASTM D5777-00)..... 11

Table 4.1. Compaction grouting summary for Zion National Park..... 22

Table 4.2. Source and receiver summary for Zion National Park pre-grouting seismic survey.¹ 24

Table 4.3. Grouting location summary for Zion National Park..... 28

Table 5.1. Grouting summary for Apache Trail..... 36

Table 5.2. Source and receiver summary for Apache Trail..... 39

Table 5.3. Grout mix used at Apache Trail..... 39

Table 6.1. Pre- and post-grouting tomography summary for Zion National Park..... 45

Table 6.2. Difference tomography calculation summary for Zion National Park..... 46

Table 6.3. Pre- and post-grouting tomography summary for Apache Trail..... 48

Table 6.4. Difference tomography calculation summary for Apache Trail..... 48

Table 7.1. Effectiveness values for all sites, with corresponding target velocity range and recorded grout volumes..... 53

Table 7.2. Effectiveness values for all sites, with corresponding target velocity range and recorded grout volumes..... 53

Table 7.3. Seismic velocity improvement factors for all sites, along with reported grout volumes injected at each site..... 55

Table 7.4. Summary of Spatial Analysis 3D nearest neighbor distance analyses for Apache Trail sites, with values shown for percent change from pre- to post-grouting for each parameter, for data sets having seismic velocities less than 250 m/s..... 59

Table 7.5. Summary of Spatial Analysis 3D autocorrelation analyses for Apache Trail sites, with values shown for percent change from pre- to post-grouting for each parameter, for data sets having seismic velocities less than 250 m/s..... 59

Table 7.6. Summary for previous 2D and new 3D seismic surveys..... 60

Table 8.1. Considerations for and potential limitations to performing 3D seismic tomography for grouting verification of roadway applications..... 66

Table 8.2. Pay scale for potential inclusion into performance-based specifications for grouting work..... 68

Table 8.3. Scoring rubric framework for grouting programs..... 69

Table 8.4. Verification method hierarchy for grouting programs..... 69

ACKNOWLEDGEMENTS

All the FHWA Central Federal Lands Highway Division (CFLHD) project team members who contributed to this project, including but not limited to Matthew DeMarco, Marilyn Dodson, Khamis Haramy, Justin Henwood, Emilio Burgos, and David Merenich, are greatly thanked for their contributions to this work, both in the office and in the field. Special thanks are extended to Bob Welch and to the FHWA CFLHD Technology Deployment Coordinator, Roger Surdahl, for financial support of this investigation. Professor John S. McCartney of the University of Colorado at Boulder is also recognized for his guidance and contributions to this work.

National Park Service staff, as well as Kenneth Baumgartner and Spencer Wingfield of CH2MHill, are thanked for their assistance and cooperation with the work performed at Zion National Park, Utah. The kind efforts of Carolyn Burg and Helen Pape from the FHWA CFLHD for their assistance with travel arrangements are also greatly appreciated. Sincere thanks also go to Alan Rock of Geostructural Seismic Research, Inc., without whose efforts this study would have been greatly hindered.

1. INTRODUCTION

Compaction grouting is a widely used soil improvement technique in geotechnical engineering practice. In this technique, cementitious grout is injected under pressure through boreholes into the subsurface with the goals of filling voids and densifying the surrounding soil profile. The costs associated with grouting can be significant for owners, especially when injected grout quantities exceed the initial estimated quantities. These costs are encumbered further due to difficulties in verifying the magnitude of improvement resulting from compaction grouting. The main objective of this report is to address the problem of verification by evaluating the use of 3D seismic tomography to infer the volumetric improvement in soil behavior from compaction and void-fill grouting. Three-dimensional seismic tomographic can be used to visualize and quantify the distribution in compression wave (p-wave) velocities in order to measure and estimate spatial variations in improvement of subsurface materials. Compression waves may also be referred to as seismic, or primary waves, and are the fastest-traveling of all direct body waves.

Specifically, 3D seismic tomographic evaluations were performed at two roadway rehabilitation projects which employed compaction and void-fill grouting to stabilize loose and deteriorating regions of subgrade soils. Case Study 1 is located in Zion National Park, Utah, and Case Study 2 is located along a section of Arizona State Route 88 northeast of Phoenix, AZ, referred to as “Apache Trail.” Both sites were constructed nearly a century ago. Geotechnical issues have arisen at these sites because cut and fill techniques were used to traverse the mountainous terrain, resulting in relatively shallow depths to bedrock from approximately 0.6 to 6.0 meters (2 to 20 feet) with relatively poor drainage. The soils at the two sites, consisting mostly of silty to sandy gravels with some cobbles and boulders, provide a particular challenge for compaction grouting do to their variable saturation and shallow depths. Accordingly, these sites were found to be good candidates for the use of seismic evaluation for compaction grouting verification as opposed to traditional verification approaches such as standard penetration testing (SPT) or cone penetration testing (CPT).

Seismic data resulting from the surveys before and after grouting operations were processed using commercial tomographic software. Several analytical techniques were used in this study to evaluate the seismic data to assess the quality of ground improvement. The results of these analyses were also interpreted based on the known grout quantities injected at each site.

Chapter 2 provides a brief overview of ground improvement, with a review of grouting methods and applications, including relevant information relating to site investigation, applications, design, equipment, and procedures. Chapter 3 provides an introduction to geophysical testing methods, including an overview of conventional 2D seismic refraction methods as well as relatively new 3D seismic tomography methods. This chapter also provides a background on the calculations incorporated into the software used to process the seismic data as part of this investigation (GSR3D), along with an overview of prior applications of this software to other civil engineering problems including other compaction grouting verification studies.

The details of the project at Zion National Park, Utah (Case Study 1) are documented in Chapter 4, while the details of the project at Apache Trail (Case Study 2) are documented in Chapter 5. The seismic tomography results from these two sites are presented in Chapter 6, along with the

details of the processing procedures and characterization of the tomography and difference tomography calculations. The analytical techniques developed to use the 3D seismic tomography results to verify the quality of grouting at these two sites are presented in Chapter 7. This chapter also includes a comparison of results from this study with those from a previously documented 2D seismic refraction investigation at the Apache Trail site (AMEC 2007).

Recommendations for potential future applications of these methods based on the lessons learned from the investigation design and seismic data collection and processing are summarized in Chapter 8. The conclusions of this study and lessons learned are summarized in Chapter 9. This report also includes several appendices. Location maps for the two projects are presented in Appendix A, along with plan drawing detail sheets from the project files to permit a better understanding of the site layouts. Layouts of the geophysical equipment arrangements are presented in Appendix B. Typical raw seismic tomography results are included in Appendix C and seismic difference tomography results are included in Appendix D. Finally, ray densities calculated for the tomography generated can be found in Appendix E. The results in Appendices C, D and E provide additional information to support the discussion in Chapters 8 and 9.

2. GROUND IMPROVEMENT

The main motivations for ground improvement are to address site-specific issues such as excessive surface settlement, erosion, excessive seepage, or weak zones. Settlement usually occurs due to changes in the state of stress due to increased foundation load magnitudes, changes in groundwater elevation, seismic loading, or excavations adjacent to existing foundations leading to decreased embedment depth and confining pressure. Erosion can occur beneath a foundation due to flow of surface water, as well as at greater depths due to piping in embankments or failure of sewers and storm drains. Preexisting or developing voids beneath foundations or within embankments can also result in particle mobility and destabilization of soil structure, ultimately resulting in settlement problems.

Ground improvement techniques have become increasingly accepted by engineers as a means of mitigating problematic soils determined to have either low bearing capacity or high settlement potential. Some of the typical goals of ground improvement methods are to increase soil density (and therefore frictional strength, stiffness, etc.), fill voids within the soil mass, improve drainage conditions or create a barrier to natural groundwater flow, and control or prevent settlement.

Compaction grouting is a ground improvement method that has been used successfully for decades (Warner 2003) for a variety of applications, including improvement of soil conditions at undeveloped sites and stabilization of historic structures where settlement was found or predicted to be unacceptably large. Advances in technology, equipment, and admixtures have allowed compaction grouting to be applied to a broad range of geotechnical problems. A considerable record of case histories, many providing quantitative verification of improvement, indicates that compaction grouting is a reliable technique for ground improvement and settlement control. Additionally, ground improvement technologies have been shown (Spaulding et al. 2008) to have significantly lower carbon footprints compared to certain conventional foundation approaches, which is often a question of interest in sustainability analyses.

Many types of grouting are currently employed in practice, covering a variety of grout materials and injection procedures. USACE (2008) released an engineering and design manual titled *Grouting Technology*, which provides technical criteria and guidance for grouting applications for civil works, covering procedures, materials, equipment, and applications of the many proven grouting methods available. Bruce and Dugnani (1994) summarized some of the most common grouting practices utilized in the United States, providing additional historical perspective to some of the advances made in this field.

2.1. Void-Fill Grouting

While not the most common method of grouting available today, void-fill grouting has a descriptively simple goal. Where voids, or cavities, are known or suspected to exist within a soil mass, this technique aims primarily to fill and stabilize these openings with a mixture of grout. Cavities can exist as continuous channels resulting from removal or abandonment of pipes, large voids resulting from mining operations, large voids common in lava tube or karstic environments, or eroded material resulting from flow of water. Warner (2004) described the fastest and least costly method of void filling using commercially available concrete pumps with

ready-mixed concrete or mortar. Since the primary objective of void-fill grouting programs is the filling of existing cavities more than the compaction of loose material surrounding the injected grout, little research has been found relating to the verification of such programs, other than field monitoring used to observe whether the problems originally related to the cavities ceased following grouting. Holmquist et al. (2003) summarized void-fill grouting procedures and verification methods used to mitigate mine subsidence due to abandoned underground coal mines.

2.2. Compaction Grouting

Compaction grouting refers to a ground improvement method that is used to increase soil density (and therefore frictional strength, stiffness, etc.), while filling or closing voids within the soil mass, improving drainage conditions or creating a barrier to natural groundwater flow, and controlling or preventing excessive settlements. The only major grouting technology to have originated in the United States, compaction grouting has been described as a “uniquely American” ground improvement method (Baker et al. 1983), pioneered on the West Coast of the United States in the 1950’s to repair settled structures. This method has been successfully used for decades to improve soil conditions at undeveloped sites and to stabilize and retrofit historic structures where settlement was found or predicted to be unacceptably large. Compaction grouting refers to the process by which low-slump, typically less than 2.5 cm (1 in), grout is injected underground at modest pressures, usually between 700 and 3500 kPa (100 and 500 psi). A complete review of compaction grouting has recently been presented by the American Society of Civil Engineers (ASCE 2010), providing an overview of grouting mechanics, investigations, design, procedures, analysis, and applications for the technique. In an effort to promote good practice in compaction grouting, the *Compaction Grouting Consensus Guide* (ASCE 2010) was released by the Geo-Institute of the American Society of Civil Engineers. That document provided the following general summary of the compaction grouting process:

“Compaction grouting is a ground improvement technique that improves the strength and/or stiffness of the ground by slow and controlled injection of low-mobility grout. The soil is displaced and compacted as the grout mass expands. Provided the injection process progresses in a controlled fashion, the grout material remains as a growing mass within the ground and does not permeate or fracture the soil. This behavior enables consistent densification around the expanding grout mass, resulting in stiff inclusions of grout surrounded by soil of increased density.”

Compaction grouting is typically achieved by sequencing the injection locations from primary to secondary, and sometimes to tertiary borings, arranged in a repeating pattern across the area to be improved. Mitigation of historic structures is costly, especially if the structure must be impacted, making compaction grouting a cost-effective method for improving foundation stability without adversely impacting structural or aesthetic aspects. Warner (2010) presented a useful outline of important factors to consider for the use of compaction grouting, summarized in Table 2.1, gathered from nearly sixty years of personal experience in the application of this method. Adbelrahman et al. (2003) provided a useful list of advantages and disadvantages to performing compaction grouting, summarized in Table 2.2. Compaction grouting may also be referred to as limited mobility or limited mobility displacement grouting, giving emphasis to the

fact that the low-slump (< 1 in.) grout used in the process is not intended to intersperse within the surrounding soil.

Table 2.1. Guidelines for design of compaction grouting programs (after Warner 2010)

Investigation	Planning	Rules for Proper Performance
<ul style="list-style-type: none"> • Soil Type / Grain Size Distribution • Consolidation Properties • Moisture Content • Permeability • Depth to Competent Strata • Grout Confinement 	<ul style="list-style-type: none"> • Acceptable Grout Hole Size Range • Upstage, Downstage, or Combined • Grout Mix / Aggregate Gradation • No Clay or Admixtures • Refusal Criteria (surface displacement, maximum pressure or volume) • Leveling Requirements and Accuracy 	<ol style="list-style-type: none"> 1. Start on Competent Formation 2. Acceptable Grout Rheology 3. Appropriate Pumping Rate (< 8 psi/min.) 4. Proper Injection Sequence 5. Good Surface Monitoring

Table 2.2. Advantages and disadvantages of compaction grouting applications (after Abdelrahman et al. 2003)

Advantages	Disadvantages
<ul style="list-style-type: none"> • Minimum disturbance to structures and surrounding ground 	<ul style="list-style-type: none"> • Relatively ineffective at shallow depths (low confining pressures)
<ul style="list-style-type: none"> • Minimum risk during construction 	<ul style="list-style-type: none"> • Prohibitive costs for problem soils at great depths
<ul style="list-style-type: none"> • Supports all portions of a structure 	<ul style="list-style-type: none"> • Possibly ineffective adjacent to unsupported slopes
<ul style="list-style-type: none"> • Loose/problem soil can be treated irrespective of depths or thickness of layers 	<ul style="list-style-type: none"> • Challenging to verify improvement
<ul style="list-style-type: none"> • Can be combined with other methods 	<ul style="list-style-type: none"> • Danger of filling underground pipes with grout
<ul style="list-style-type: none"> • No harmful vibrations to nearby structures/utilities 	<ul style="list-style-type: none"> • Effectiveness questionable in saturated clays
<ul style="list-style-type: none"> • Reduction in liquefaction potential 	<ul style="list-style-type: none"> • Expense

Some of the more favorable ground conditions for this technique are zones of loose material that may have originated due to poor construction practices or developed over time due to movement of groundwater or inadequate drainage design. Grout is injected through boreholes at various depths into this loose material to create bulbs of grout due to the low mobility of the grout mix used. These bulbs not only densify surrounding soil, but under ideal conditions can result in columns of grout.

2.3. Field Procedures

Weaver (2000) provided a valuable comparison of common “rules of thumb” followed by both American and European grouting contractors for compaction grouting. Figure 2.1 shows two different construction procedures that can be used for grouting, based on the advancement of the injected grout column. The simplest, fastest, and cheapest method is known as bottom-up, where

the casing is advanced to the full depth of the zone to be treated, with grouting proceeding upward in stages as the casing is removed, usually until insufficient confinement is obtained. For situations where greater improvement is required at shallow depths (1-3 m), or where surface heave must be carefully controlled, the top-down method can be used. The additional time and costs involved in the top-down method, as each stage must be re-drilled to advance the casing to the next stage, are offset by the grouting verification provided by drilling as well as the increased confinement at the surface. A combination of the two methods can also be used, with the first stage being injected at the most shallow depth, and the remaining stages advancing upward from the deepest depth as in the bottom-up method.

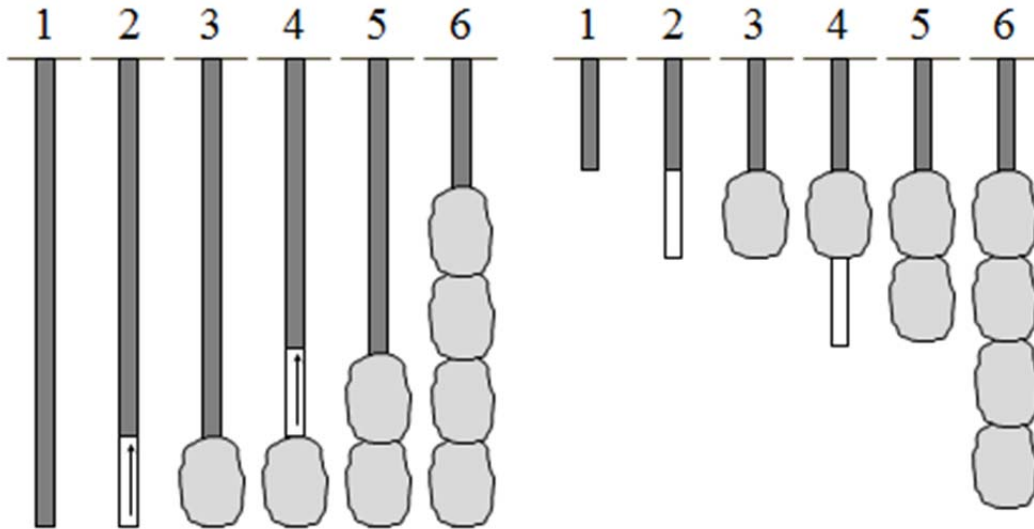


Figure 2.1. Schematic. (a) Bottom-up, and (b) top-down compaction grouting (after ASCE, 2010)

2.4. Grouting Verification Methods

Verification of the grouting process can be considered important for a number of reasons. To the engineer, perhaps of greatest interest is whether the grouting program designed and carried out indeed performed as intended, resulting in the desired outcome in the properties of the soil being treated. Additionally, verification can ensure that the grout injected into the ground actually improved the targeted area, which can particularly be a concern where the soil being treated overlies highly fractured bedrock or karstic terrain, where injected grout can possibly migrate through these features away from the targeted soil. Hydrofracturing of the soil, where high injection pressures can cause brittle fracturing of the soil resulting in lenses or “wings” of grout instead of the bulbs intended, is also a significant concern during compaction grouting, limiting the allowable injection pressures and rates. Frequently, the only records that exist for the quantities of injected grout are the manual logs recorded by the grouting contractor, necessitating careful inspector attention to confirm. For these and many other reasons, reliable and cost-effective methods are desired to verify the achievement of grouting programs.

A considerable record of case histories, many providing quantitative results of improvement, indicates that compaction grouting can be used successfully for ground improvement and

settlement control. One challenge with the use of compaction grouting for soil improvement is the quality assurance testing needed to verify that the target soil volume has been improved.

Verification methods available for use in grouting operations cover a wide range of technologies. ASCE (1995) published a thorough review of available grouting verification methods, including case histories highlighting advantages and disadvantages to the various methods available at the time. Several relationships have been proposed for verification of grouting based on changes in soil properties such as void ratio, density, and relative density.

Standard Penetration Test (SPT) or Cone Penetration Test (CPT) measurements before and after ground treatment are the most commonly used field testing quality assurance methods for compaction grouting. The primary issue with these methods is that they only quantify the degree of improvement at point locations and do not reflect the improvement of the soil from a volumetric basis. Additionally, site conditions may prevent access of the large equipment required to perform these tests, availability may be limited, and high mobilization costs may make these methods financially unachievable, especially for smaller projects.

Baez and Henry (1993) described verification methods used for a compaction grouting program designed to densify a layer of very loose sand to silty sand underlying a dam. Corrected SPT values obtained following grouting ranged between 11 and 38, compared to an average of 4 before treatment. Where post-grouting SPT values were found to be lower than required, a quaternary (fourth) injection phase was applied. Boulanger and Hayden (1995) conducted a collective review of case histories on improvement of liquefiable soils by compaction grouting, where significant increases in CPT penetration (tip) resistance were achieved for soils ranging from slightly silty sand to silt. Observations included changes in penetration resistance for increases in elapsed time following grout injection, as well as due to differences in field procedures followed, most notably bottom-up versus top-down techniques. For most situations, Boulanger and Hayden recommended that the bottom-up method could be effectively used at shallow depths, provided appropriate procedures are followed (multi-phase approach, decreased spacing between injections). Miller and Roycroft (2004) concluded that compaction grouting could be effectively used to mitigate liquefaction of susceptible soils and to create a buttress zone to protect structures. Their analysis included CPT results gathered for a variety of different injection spacings, which allowed for a quantification of liquefaction potential and factors of safety at different depths throughout the soil profile both before and after compaction grouting. They found densification to be achieved in all cases considered in their study, with maximum benefits occurring for sands at 1.5 m (5 ft) injection spacing.

Orense (2008) compiled a more recent review of two case histories on compaction grouting, finding improvements in strength and lateral earth pressure of the soil, in addition to SPT values, as a result of compaction grouting. Strauss et al. (2004) successfully utilized compaction grouting to mitigate settlement occurring due to weak alluvium beneath highway approach fills after performing a test program to verify effectiveness and establish minimum improvement requirements. Welsh and Burke (2009) provided some recent examples of effective applications of compaction grouting for settlement remediation due to erosion and piping resulting from unsealed joints in storm drains below a freeway in California. Their work also described the use

of compaction grouting for liquefaction mitigation in Japan following the 1995 Kobe earthquake, and for the prevention of sinkhole development in karstic regions of Pennsylvania.

While SPT and CPT verification methods can be considered the most common traditional grouting verification methods, a variety of alternative methods have been considered. Laboratory testing methods for verification of compaction grouting have been explored by Nichols and Goodings (2000) and El-Kelesh and Matsui (2008). Full-scale field excavations (Brown and Warner 1973; Warner 2003) have also produced valuable insights into the grouting process. Real-time data logging instrumentation has been demonstrated by Geraci (2007) and Schuyler and Gularte (2008) successfully incorporated tiltmeters, which measure rotation, to monitor the movement of a bridge deck during compaction grouting beneath a bridge foundation.

Simple devices such as crack gauges, or more sophisticated devices such as strain gauges, could be installed along sensitive structures, which would allow for the continuous visual or electronic monitoring of strain or movement of the structure. Surveying methods can also be employed, allowing for periodic verification of the position of a structure or the elevation of a roadway surface. One of the most simple and reliable devices that can accomplish monitoring of elevation change is a basic water manometer, but traditional and laser-based surveying instruments have also been successfully utilized to accomplish this task.

Mitchell et al. (1995) presented a considerable study of case histories from sites where ground improvement methods had been subjected to real life earthquake events. Hausler and Sitar (2001) presented a summary of more than 90 case histories relating to the performance of improved sites, collected from 14 earthquakes in Japan, Taiwan, Turkey, and the United States, which included two compaction grouting sites.

Although the available literature on injection monitoring and SPT-CPT testing show that these techniques are important tools to use as part of a quality assurance program, they only provide point measurements. An alternative approach is through the use of 3D seismic tomography, a volumetric, three-dimensional, non-destructive geophysics-based evaluation method. 3D seismic tomography uses seismic refraction of compression waves (p-waves) to determine the depths and seismic velocities of subsurface layers using a seismic wave generated at the surface. Further discussion of this method can be found in Chapter 3 following a brief overview of geophysical methods in general.

3. BACKGROUND ON GEOPHYSICAL METHODS

The field of geophysics has been defined as “the science of applying the principles of physics to investigations relating to the structure and properties of the earth” (CLFHD 2003) in order to measure physical properties of interest as well as characterize their distribution. A wide variety of geophysical technologies are available to engineers today, several of which could potentially be used for verification of grouting. Applications of geophysical imaging, as well as nondestructive test (NDT) methods, have seen significant increase and acceptance in recent years, due largely to their ability to rapidly and accurately gather information of interest to engineers.

Several publications can be found that comprehensively detail the various geophysical methods available to engineers, summarizing relevant background theory along with informative figures, tables, and case studies. One of the earliest, from the United States Army Corps of Engineers, titled *Geophysical Exploration for Engineering and Environmental Investigations* (USACE 1995), was intended to provide an introduction to geophysical exploration for engineering, geological, and environmental investigations. A more recent publication titled *Application of Geophysical Methods to Highway Related Problems* (CFLHD 2003) was intended to be used as a technical manual and focused on providing information for both traditional geophysical as well as emerging non-destructive testing (NDT) methods to geotechnical and highway engineers for various transportation engineering applications. The most recent publication of this type was published by the Center for Geotechnical Practice and Research, titled *Geophysical Primer for Geotechnical Engineers* (Rutledge et al. 2005), and also included a sample of geophysical contractors, equipment suppliers, and available software.

The National Cooperative Highway Research Program released a document titled *Synthesis 357: Use of Geophysics for Transportation Projects* (NCHRP 2006), which reported on “current knowledge and practice, without the detailed directions usually found in handbooks or design manuals.” U.S. State and Canadian provincial departments of transportation (DOTs) and U.S. federal transportation agencies were surveyed to primarily investigate which agencies were using geophysics and for what purposes, limiting the scope to how geophysical methods were being applied by geotechnical engineers during highway planning and construction activities. Figure 3.1 illustrates responses received regarding the most commonly used geophysical methods and applications within the agencies responding to the survey.

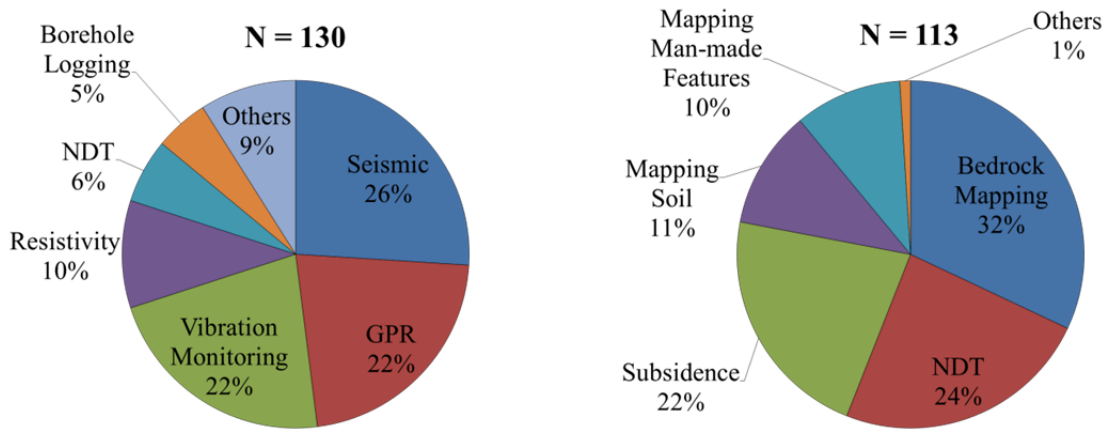


Figure 3.1. Chart. (L) Most commonly used geophysical methods; and (R) most common applications of geophysics among state DOTs and selected federal and Canadian transportation agencies (after NCHRP, 2006)

3.1. Seismic Methods

Seismic refraction is generally considered an efficient, cost-effective, and non-destructive method that can be used in a wide-variety of applications to characterize subsurface materials. This technique has been applied in the fields of petroleum, mining, geotechnical, environmental and hydrological engineering, to name a few, over the last several decades for a seemingly unlimited variety of subsurface characterization needs.

Seismic refraction can be defined as a geophysical method used to determine the depths and seismic velocities of subsurface layers using a seismic wave generated at the surface. Normally, low frequency seismic energy is emitted by a seismic source such as a sledgehammer and collected using geophones, which measure the arrival of the seismic wave, typically at a location some distance away from the location where the wave was introduced. Successful application and processing of traditional 2D seismic refraction relies on the assumptions that seismic wave velocities increase with depth through the subsurface profile and boundaries between subsurface layers are generally planar. One of the most significant limitations to the seismic refraction approach is introduced by the groundwater table. The compressional, or seismic, wave propagation speed through water is typically 1450 m/s (4750 ft/s) and is temperature-dependent. When saturated soils are encountered by a seismic wave, the true p-wave velocity through the soil medium is obscured by the high p-wave velocity of the water.

Many years of experience in performing seismic refraction studies have resulted in a variety of empirical charts providing typical seismic p-wave velocities of various geomaterials, such as the ranges provided in Table 3.1. Excavation equipment manufacturers (Anon. 1987; Anon. 1988) have also provided charts relating rippability of soils and rocks to seismic p-wave velocities, which are commonly cited in the literature. More recently, Rucker and Ferguson (2006) observed correlations between seismic velocities and soil cementation stage classifications resulting from three projects in Arizona.

Table 3.1. Range of Velocities for Compressional Waves in Soil and Rock (after ASTM D5777-00)

Materials	Velocity	
	ft/s	m/s
Natural Soil and Rock		
Weathered surface material	800 to 2000	240 to 610
Gravel or dry sand	1500 to 3000	460 to 915
Sand (saturated)	4000 to 6000	1220 to 1830
Clay (saturated)	3000 to 9000	915 to 2750
Water*	4700 to 5500	1430 to 1665
Sea water*	4800 to 5000	1460 to 1525
Sandstone	6000 to 13000	1830 to 3960
Shale	9000 to 14000	2750 to 4270
Chalk	6000 to 13000	1830 to 3960
Limestone	7000 to 20000	2134 to 6100
Granite	15000 to 19000	4575 to 5800
Metamorphic rock	10000 to 23000	3050 to 7000

*Depending on temperature and salt content.

3.1.1. 2D vs. 3D Geophysical Methods

Conventional 2D seismic refraction is based upon wave theory as related to plane waves. Huygen’s principle describes the refraction of an incident ray upon a boundary between two media of different seismic velocities. The most elementary relation describing this refraction phenomenon is the law of refraction, or Snell’s Law, which can be attributed to the field of optics, and is analogous to the refraction of a seismic wave across a boundary. This relationship is described as follows:

$$\frac{\sin\alpha_1}{\sin\alpha_2} = \frac{v_1}{v_2} \quad (3.1)$$

where α_1 and α_2 are the angles made with the normal to the boundary by the incident and refracted rays, and v_1 and v_2 are the seismic velocities of the incident and refracted rays, respectively. This relationship forms the basis for traditional 2D seismic refraction interpretation, which can be extended to multiple layers of increasing velocity with depth. Figure 3.2 provides a simple illustration of the principles fundamental to 2D seismic refraction procedures, where an incident wave is recorded at different times by geophones arranged in a straight line radiating outward from the source location. Figure 3.3 shows a typical distribution of arrival times for surface, body, and air waves within a travel-time plot recorded by 2D geophones during a seismic refraction survey.

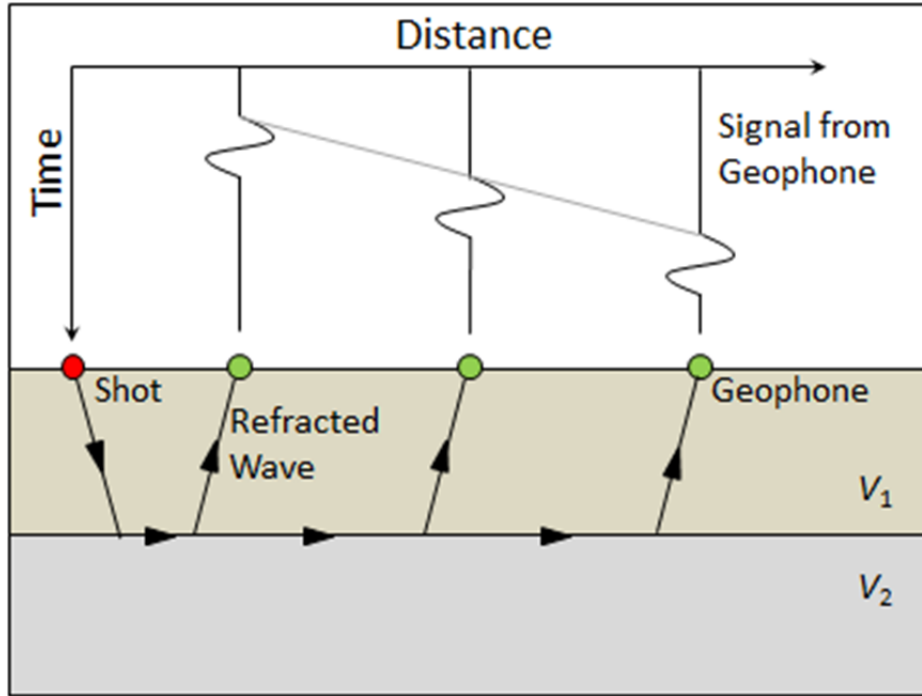


Figure 3.2. Schematic. Simplified seismic refraction process showing reflected waves and arrivals as recorded by geophones.

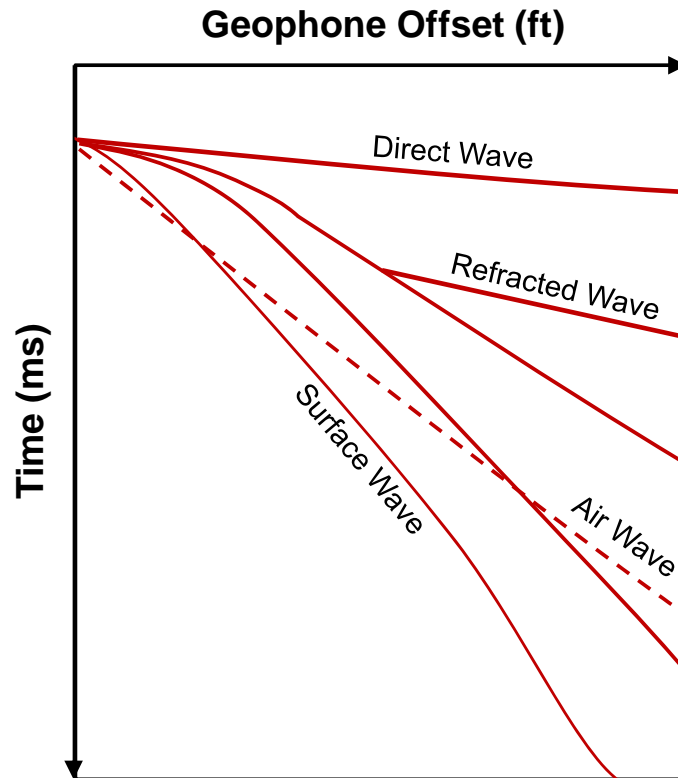


Figure 3.3. Graph. A comprehensive interpretation of body-, air-, and surface-wave events on seismic travel-time plots (after Park et al. 2001).

Pseudo 3D seismic processing marked the next step in seismic tomography and has been described by Sirles et al. (2006). Two case histories started by collecting seismic data using standard 2D seismic refraction field procedures, from which “data were processed using 2D tomography inversion, then calibrated 3D models were generated through interpolation.”

Additional clarification regarding the nature of propagating wavefronts and wave reflection and refraction is provided in Figure 3.4. For propagating p-waves, the waves of interest for 3D seismic surveys, raypaths describe the path traveled by the normal to the surface of the seismic wave as propagation occurs. For a wave traveling in either two or three dimensions, raypaths can either be straight or curved depending on the materials and therefore wave velocities encountered. Also, as shown in Figure 3.4, an incident p-wave will both refract and reflect at a boundary between materials having different seismic velocities. Depending on the type of incident wave, different refracted and reflected waves will be created. Kramer (1996) provides further discussion on the nature of wave reflection and refraction.

Sirles et al. (2006) defined a ray as “a region in the model that has the highest contribution to the first arrival time, and typically descends from the source at the ground surface to higher velocity layers before ascending to the surface receiver(s).” This definition relates to the predecessor to the software used for tomography generation as part of this study, GSR3D. A complete review of seismic wave propagation and ray theory has been provided by Červený (2001).

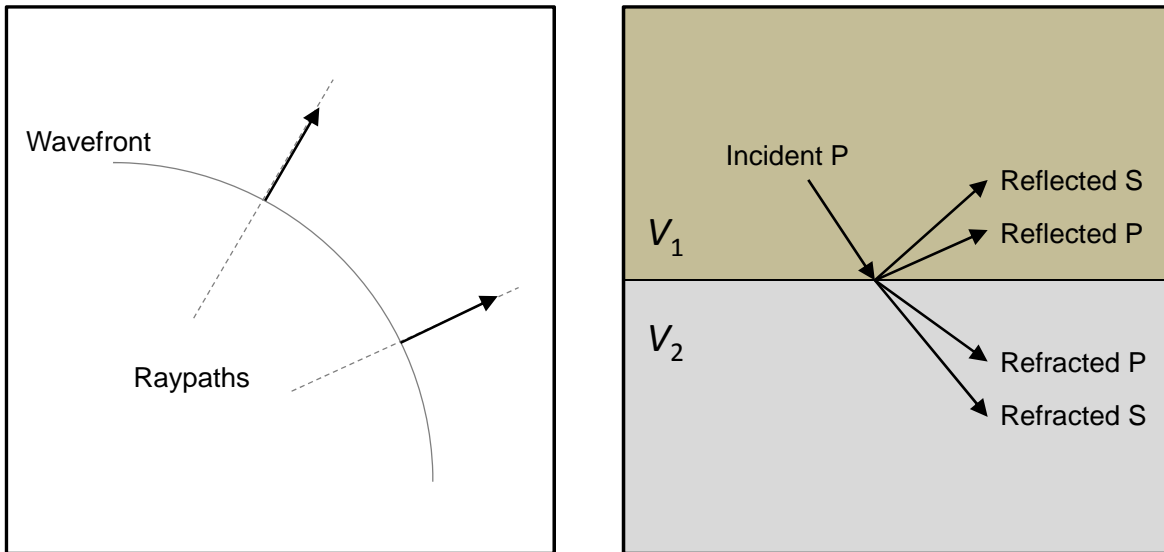


Figure 3.4. Schematic. (L) Illustration of raypaths normal to the surface of a propagating wavefront and (R) reflected and refracted waves resulting from an incident p-wave.

3.1.2. 3D Seismic Tomography

ASCE (1995) defines tomography as “an analytical technique for evaluating geophysical data such as the speed and amplitude of sound waves traveling through the earth, or electrical resistivity, radar frequency and signal strength.” The roots of tomographic imaging can be traced to the medical imaging profession, where computed tomography (CT) scans, computerized axial

tomography (CAT) scans and magnetic resonance imaging (MRI) have become commonplace terms in medical practice.

Whereas these types of medical tomography methods are often used to image bone or soft tissue structure in the human body, the term seismic tomography refers to a more specific area of tomographic imaging used to estimate engineering properties of different materials such as soils and produce graphical representations of their distribution. Propagating velocities of compression waves (p-waves) are the most common properties recovered directly through seismic refraction analysis. The term 3D seismic tomography therefore describes the use of seismic refraction data collection methods for three-dimensional analysis and quantification of seismic velocities.

The 3D seismic methods employed in this study are based upon wave propagation theory. In the three-dimensional domain, the seismic energy imparted by a source at the surface will travel through the ground along a wavefront. This wavefront will propagate through different materials, adjusting for the different velocities encountered by the wave. For 3D seismic tomographic methods, the arrival times of this wavefront can be measured at any point along (or below) the ground surface, instead of simply in a straight line at the surface as with 2D refraction methods, to more completely characterize the variation of seismic velocity in the material in question.

Fermat's principle was proposed by the 17th Century French mathematician Pierre de Fermat to explain the behavior of seismic raypaths at an interface. When applied to seismology and seismic tomography, the principle states that:

$$t = \int_A^B \frac{dl}{v} = \textit{minimum} \quad (3.2)$$

where t is the travel-time of the ray, A and B are two points along the travel path of the ray, dl is the elemental distance along a raypath, and v is the seismic velocity over that elemental distance. Fermat's principle states that of the many possible paths between two points, a ray will travel along the path that will result in the minimum possible travel time (Lowrie 1997).

Three-dimensional wave propagation methods generally begin by dividing a 3D initial velocity model into small grids. Raypaths are then traced between sources and receivers to develop calculated travel times. These calculated times are then compared to known or measured travel times obtained through the actual seismic survey. The following linearized inverse problem can then be solved for each cell:

$$(t_{\textit{calculated}} - t_{\textit{measured}})_i = \sum_{j=1}^n L_{ij} \delta \left(\frac{1}{v} \right)_j \quad (3.3)$$

where L_{ij} is the length of the i 'th ray in the j 'th grid cell and $\delta \left(\frac{1}{v} \right)_j$ is the change to be applied to the velocity model in the j 'th grid cell, sometimes referred to as the change in slowness, or inverse of velocity. The velocity model can then be updated iteratively following this procedure

until the solution providing a minimum difference between calculated and measured travel times is obtained, providing the final velocity model.

Three-dimensional first-arrival-time tomography methods were used by Zelt et al. (2006) to process 3D shallow seismic data collected as part of an environmental remediation investigation, where the 3D seismic refraction-based method used was found to be relatively simple, quick, and inexpensive, with less-subjective analysis and interpretation, when compared to 3D seismic reflection methods.

Another method which can be used to obtain 3D seismic tomography involves the use of subsurface source and receivers located in boreholes, also referred to as down-hole or cross-hole methods. This technique has been successfully used to investigate an active sinkhole causing property damage in a residential neighborhood (FHWA CFLHD 2003), detect abandoned coal mines beneath a retaining wall, and verify the effectiveness of jet-grouting beneath a bridge pier foundation (Hanson et al. 2000). Figure 3.5 illustrates typical source and receiver layouts between both surface and subsurface methods, which would allow for 2D tomography generation. The linear raypaths shown for the subsurface arrangement would only be accurate for a constant-velocity model where no refraction would occur. Additional geophone lines or boreholes would allow for 3D tomography to be created. Cross-hole sonic logging (CSL), which is a non-destructive evaluation method used to evaluate the integrity of drilled shaft foundations, can also be used to develop 3D seismic tomography. Haramy (2006) also showed that 3D CSL methods could be used to successfully determine seismic velocity differences before and after grouting of drilled shafts which were found to have defects.

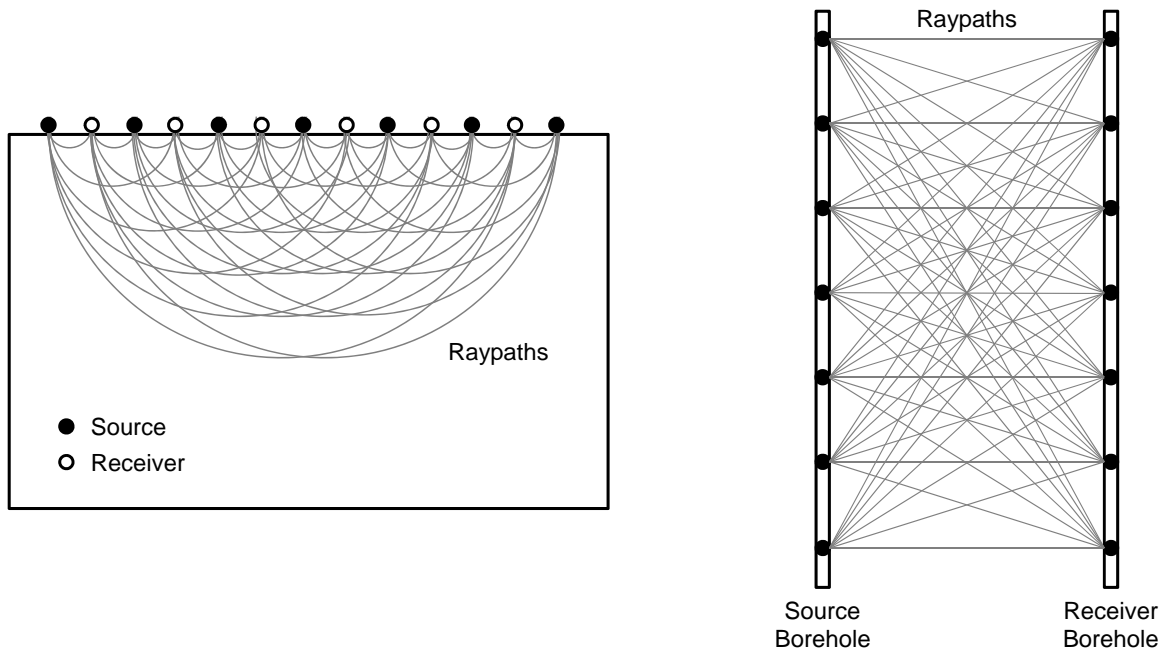


Figure 3.5. Schematic. Source and receiver locations along with raypath coverage for typical (L) surface seismic and (R) subsurface seismic surveys.

Data collection for true 3D seismic tomography investigations follows many of the same procedures as those used during conventional 2D seismic refraction. The most significant difference relates to the layout of the geophones and shot locations. During conventional 2D or pseudo 3D seismic surveys, geophones are arranged in a single line, and shots are recorded from locations in some arrangement surrounding or within that line. For true 3D seismic investigations, a grid of geophones and shot locations is established, so that a single shot is recorded by all geophones simultaneously, resulting in decreased required field data collection time and increased resolution and data confidence compared to pseudo 3D surveys, at the expense of increased overhead costs related to the additional equipment required to image the same volume of soil.

3.1.3. GSR3D Seismic Tomography Software

A recently-developed software package known as GSR3D, developed by Geostructural Seismic Research, Inc., was used to process the data collected at the two sites and produce three-dimensional tomographic images representing the seismic velocities before and after grouting. The GSR3D software package has been successfully proven for a variety of civil engineering applications, including the location of a collapsed tunnel, detection of abandoned coal mines, location of scour zones within an embankment dam, location of utility pipes beneath a concrete roadway, and determination of 3D bedrock topography.

This proprietary software integrates automatic signal processing techniques, numerical modeling procedures, and finite difference wave propagation methods to quickly obtain high resolution, accurate 3D ground images from shallow seismic data. Sirles et al. (2006) describes the numerical modeling approach that makes up the GSR3D analysis, combining the discrete element method with particle flow code (DEM-PFC). The predecessor to GSR3D was known as the *Geostructural Analysis Package (GAP)*, which received use in fields outside of geotechnical engineering, such as structural engineering. The GAP package has been used extensively to evaluate the structural capacity of drilled shaft foundations (Haramy 2006), but its potential use in the fields of chemical, thermodynamic, and groundwater flows have also been proposed (Sirles et al. 2006). This computational method allows for simultaneous processing of many source and receiver combinations in arbitrary configurations, located either along the ground surface or in boreholes.

The software estimates travel times by propagating waves across a model of constant initial velocity using wave front normal vector interpolation following a modified Eikonal method, which are then compared to the travel times determined from the seismic shot record. Sample picks of compression wave first arrivals can be combined with time, frequency, and velocity filters and a multi-dimensional B-Spline interpolation network (BIN) to determine first arrivals accounting for waveform shape, source/receiver distance, and adjacent picks, resulting in automatic and consistent travel time picks. Waves are then propagated from each source and each receiver to determine regions in the velocity model having the most significant effect on the travel time and rational functions of incremental resolution are generated from these regions for the tomographic inversion.

The arrival times for each element are added to the corresponding source arrival function for each ray to characterize the Fresnel zone. Differences in arrivals from the model were iteratively corrected using a corresponding Fresnel zone density function allowing for rapid convergence. Model elements are ordered in a compact tetrahedral packing consisting of spherical elements of equal radius connected by links of equal length. The model resolution is incrementally increased for each iteration and quickly converges to the solution of minimum travel time error with minimum velocity variation, providing consistent results. The resulting 3D tomograms can then be sliced and contoured from a variety of perspectives to allow for visualization of the velocity structure. Figure 3.6 illustrates a simplified flow diagram describing the processing routine followed during tomography calculation by GSR3D.

Boundary conditions for the tomography models generated by GSR3D cannot be specified by the user, and the results of different boundary conditions on the results were unable to be verified for this study. As waves which are propagated through the model do not have the ability to reflect along the model boundaries, there is no chance that the calculated arrival time can be influenced by these boundary reflections. The tomographic volume can therefore be considered as a region within an infinite elastic half space. Also, as the calculated seismic wave arrival times are determined from the propagation of seismic wavefronts and not their reflections, only the arrival of this wavefront will have an influence on the resulting tomography, and any other potential waves, such as shear waves that arrive at later times, are not considered.

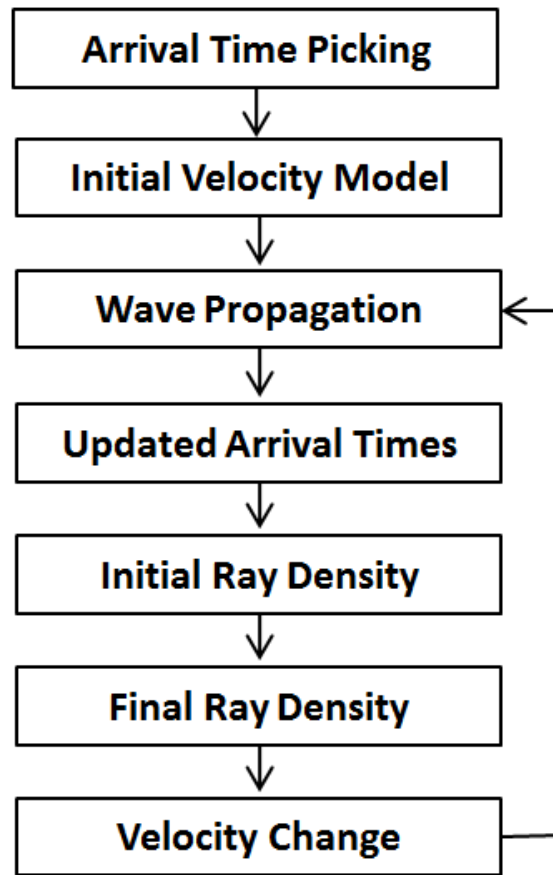


Figure 3.6. Flowchart. Simplified processing procedure utilized by GSR3D.

3.1.4. Assumptions and Limitations of GSR3D

An average value for the initial starting velocity of the model is determined based on the average distances between shot and receiver locations and the arrival times determined through the auto-picking process. This process is often referred to as straight-line average velocity determination. For regions having no raypath density, no procedure exists for updating the seismic velocities from this initial velocity approximation. Therefore, in many areas of the final tomography model, the initial velocity approximation may be reported. This is especially evident at the greatest depths and at the boundaries of the models, where it often appears that a velocity inversion (higher velocity layers above lower velocity layers) exist, which is not probable due to the known stratigraphy of the subsurface layers.

Auto-picker results and manual training picks do not always agree with complete accuracy. However, the benefits of decreased influences from fatigue when performing manual picking of shots can be said to outweigh the losses from the disagreement between auto-picker and manual training picks. Geometric data entered for the geophone and shot locations are automatically rounded to the nearest integer within the GSR3D software. Regardless of the accuracy maintained when performing surveys of geophone and shot locations, the tomographic processing will be performed using integer values for the x, y, and z coordinates. This rounding can potentially result in uncertainties in the calculated velocities. Resolutions reported by the program are also limited to integer values, which prevents the identification of grouted regions of nominal size less than 1 ft or 1 m, depending on which units are chosen when performing the calculations.

Edge effects, or regions along the boundaries of the tomographic volume having lower raypath densities, are reported in the same way as higher raypath density regions. This fact can potentially be misleading to users of this type of seismic tomography program who do not fully understand this limitation.

3.1.5. GSR3D Historical Case Study #1: Rocky Mountain National Park

One of the first studies involving the use of 3D seismic tomography for the assessment of compaction grouting effectiveness as part of roadway stabilization projects took place during the summer of 2007. Engineers with FHWA-CFLHD were tasked with rehabilitating a failed culvert that had been causing significant roadway settlement and cracking along Trail Ridge Road in Rocky Mountain National Park. The GSR3D program was investigated to determine seismic tomography before and after ground improvement at the site. Compaction grouting was used to stabilize roadway settlement caused by piping of fines from the subgrade due to a failed culvert. Before and after grouting, seismic data was collected using a sledgehammer impact on the ground surface as the input source while the refracted waves at different distances from the source were measured using geophones. The GSR3D program was used to interpret the arrival times of different waves at the different geophones. The method proved effective in producing pre- and post-grouting volumetric velocity difference images allowing for a more thorough assessment of ground improvement at the site. Further details relating to the site, the grouting operations carried out for the roadway remediation, and the seismic tomography investigation can be found in Haramy et al. (2009).



Figure 3.7. Photo. Photographs showing (L) differential settlement of roadway and (R) compaction grouting operations at Rocky Mountain N.P.

Some of the primary concerns in developing the compaction grouting program at this site resulted from the potential for damage to sensitive historic structures in close proximity to the injection locations. Maximum displacement limits were imposed for the existing stone guard wall and a dry-stacked stone armored slope below the roadway and surrounding the culvert outlet. For the armored slope, a maximum vertical movement of 40 mm was allowed, with the mortared stone guard wall restricted to a maximum vertical movement of 20 mm to reduce the potential for cracking. To reduce possible heave of the roadway surface, compaction grouting was performed prior to the removal and replacement of pavement. This first-known case of the application of seismic tomographic methods for verification of grouting for roadway stabilization projects was based upon the pseudo 3D, or 2.5-D, seismic tomography method, as described by Sirles et al. (2006). A single seismic line containing 24 geophones was deployed in four separate locations, during each of which shots were collected. The seismic data collected was later combined into a 3D volume representing a combination of the four smaller volumes resulting from each of the four seismic lines collected in the field, to finally produce the pseudo 3D volumetric seismic tomography images as shown in Figure 3.8. Further discussion of the data collection and processing methods used to develop this 2.5-D seismic tomography approach are provided by Sirles et al. (2006).

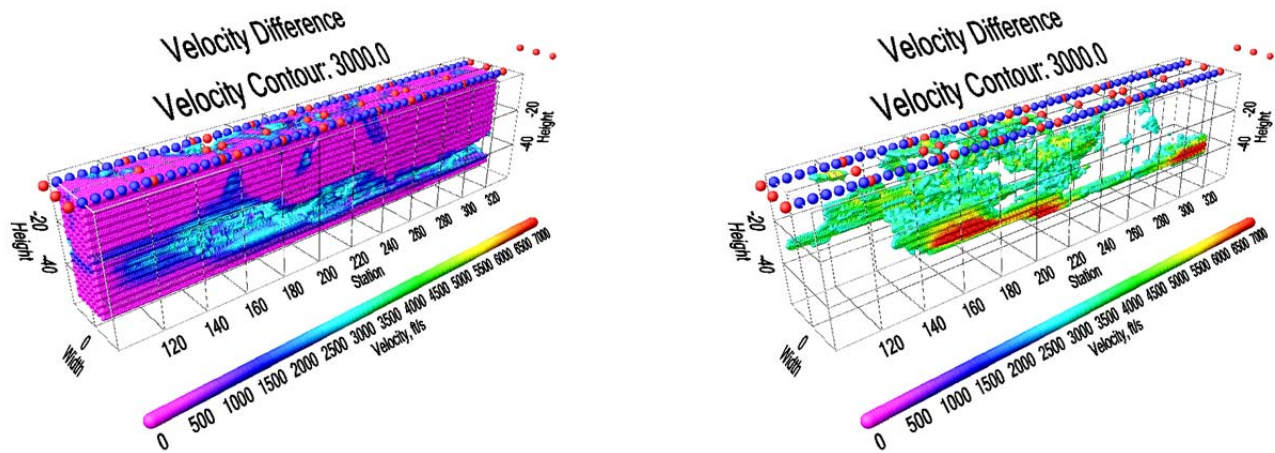


Figure 3.8. Graph. Pseudo 3D difference tomography from Rocky Mountain National Park, Colorado, compaction grouting site, showing seismic velocity differences (L) less than 3000 ft/s and (R) greater than 3000 ft/s, on a scale of 0 to 7000 ft/s.

From the results shown in Figure 3.8, the 3D difference tomography shows considerable increases in seismic velocities in the vicinity of the failed culvert. Records of the injected grout volumes, which show the highest grout injections near the midpoint of the volume, correlate well with the results of the seismic tomography. These results can be considered reasonable, as the highest degree of improvement could be expected near the midpoint of the volume where the failed culvert pipe was located, and the surrounding soils were believed to have been eroded and deteriorated. The existence of negative velocity differences in the resulting difference tomography is unknown, as the scales chosen for Figure 3.8 only displays positive velocity differences.

4. CASE STUDY 1: ZION NATIONAL PARK

The first site is located along the Zion-Mt. Carmel Highway, in Zion National Park, Utah, where excessive pavement subsidence and severe pavement cracking occurred. Initially, damage was attributed primarily to a large ancient landslide extending through three of the switchbacks approaching the Zion-Mt. Carmel Tunnel. On further investigation, roadway damage has been attributed to areas of very loose embankment material and open voids. Compaction grouting of this loose subsurface material was selected as the best remediation method to stabilize the subsiding embankment zones, and grouting was carried out following bottom-up procedures. Additionally, subsurface drainage improvements were completed in conjunction with excavation of the top 1 m (3 ft) of roadway and replacement with geosynthetic-reinforced fill. Two compaction grouting locations were chosen for conducting the 3D seismic tomography based on site access and high anticipated grout takes. Uncorrected SPT values ranging from 5 to 14 (very loose to medium dense) were documented at these sites prior to grouting.

During compaction grouting, dial gauges were used to visually monitor and record minimum and maximum injection pressures and a water manometer was used to detect ground heave. Grout takes were recorded by counting the number of strokes of the grout pump cylinder, which was calibrated to the cubic foot. Following grouting, the upper 1 m (3 ft) of the road surface was excavated to allow for replacement with reinforced compacted fill. This excavation revealed asphalt thicknesses as much as 1 m (3 ft) along the centerline and as much as 1.5 m (5 ft) or more along the shoulder. Previous boreholes showed asphalt thicknesses of only 0.13 to 0.25 m (5 to 10 inches), indicating more settlement had occurred at this location and there was a potential inversion of the subsurface density profile. Compaction grouting was performed on a staggered 1.2 m (4 ft) pattern to depths up to 3 m (10 ft). Figure 4.1 provides a typical construction detail for the compaction grouting layout, and Table 4.1 summarizes quantities.

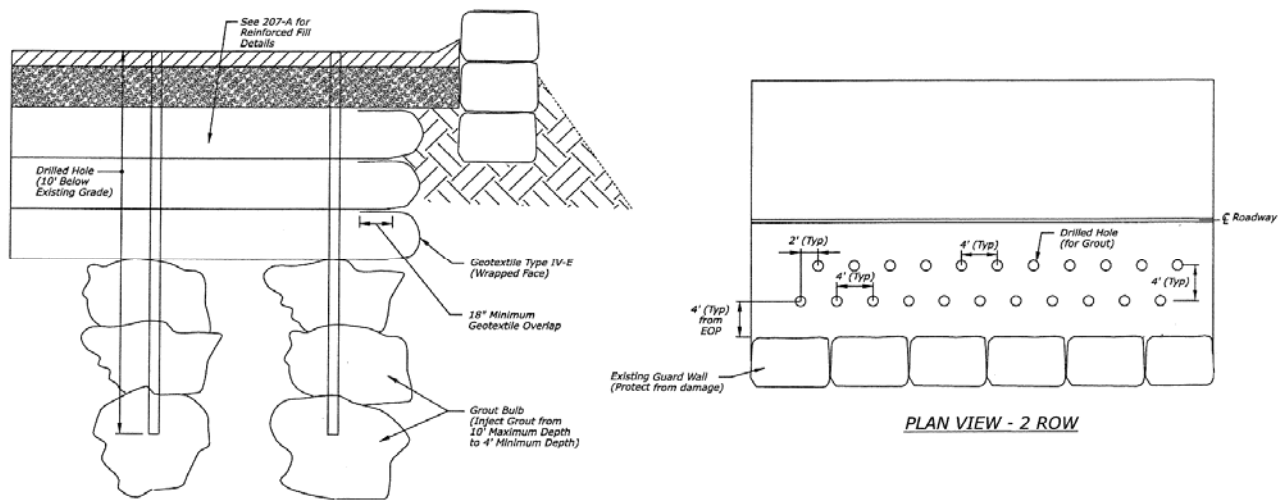


Figure 4.1. Schematic. Typical compaction grouting profile and layout at the Zion National Park.

Table 4.1. Compaction grouting summary for Zion National Park.

Location	Stationing	Number of Injection Holes ¹	Total Grout Casing	Total Grout Volume
			m (ft)	m ³ (yd ³)
1	172+54 – 174+10	79[8]	203(664)	3.2(4.2)
2	177+26 – 179+37	107[14]	204(670)	11.7(15.3)

¹ Number in brackets indicates number of holes where casing could not be advanced to minimum depth of 3 ft (1 m)

4.1. Soils and Site Conditions

As previously mentioned, the soils at the locations studied at Zion National Park can be broadly described as loosely consolidated poorly-graded fine sands with some gravel and large boulders up to 15 ft (4.6 m) in diameter. A complete review of the sites studied has been previously reported by Yeh and Associates, Inc. (2008; 2009), including geological background and the results of a subsurface investigation performed at this project location.

An important observation made at the site was an existing 18 in. (46 cm) corrugated metal pipe (CMP) culvert located at approximate stationing 178+00, aligned perpendicularly to the roadway alignment, which corresponds closely to the midpoint of grid #2. However, this culvert appeared to follow along the top of bedrock, and therefore, identifying this pipe in the tomography results was anticipated to be very unlikely, as the pipe would be difficult to differentiate between the bedrock boundary. As shown later in Chapter 6, the resolutions calculated by the GSR3D software for the tomography at grid #2 were 2 ft (0.6 m), which is larger than the diameter of this pipe.

Figure 4.2 also provides some illustration of the problems observed at the roadway surface in the vicinity of the grouting and seismic survey locations. In some areas of the roadway, large voids were present in the pavement, which, according to Park Service personnel, had to repeatedly be filled by Park maintenance staff to prevent the traveling public from exposure to an unsafe situation. In other areas, small holes were observed in the pavement ranging from approximately 2 to 5 cm in diameter, which upon closer inspection, connected to much deeper and larger voids immediately below the pavement, indicating a highly unstable base situation.



Figure 4.2. Photo. Voids beneath roadway surface daylighting at Zion National Park: (L) Large void opening resembling a pothole, more than 0.5 m (1.5 ft) in width; and (R) small hole in pavement surface observed to open to a much larger void beneath pavement.

4.2. Pre-Grouting Geophysical Investigation

For both sites, two 24-channel Geode seismographs manufactured by Geometrics were used to collect and process the information received from 48, 4.5 Hz vertical geophones. The seismographs were powered by 12V automotive batteries and data was viewed and stored using a battery-powered laptop PC. A 7 kg (16 lb) sledge hammer equipped with a “triggering” sensor was used as a seismic source. The hammer was impacted upon an aluminum strike plate with sufficient energy to produce good quality readings at every geophone, as determined by observation of the shot record immediately following every shot. A triggering sensor sent a signal to the data recorder to begin recording as soon as impact occurred.

At the Zion National Park sites, the 48 geophones were arranged in three lines of 16 geophones, with typically 1.8 m (6 ft) spacing between lines. Two different in-line spacings, 1.5- and 3-m (5- and 10-ft), were investigated to assess possible improvements in resolution achieved by the alternate spacings. At the Apache Trail sites, four lines of 12 geophones were used, utilizing landstreamers with 5-foot in-line spacing with either 3 or 4-foot spacing between lines.

Shot and geophone locations were surveyed to allow for relocation during the post-grouting survey. Activities including rock ripping, roadway pulverization, and heavy equipment traffic were occurring in the immediate vicinity of the planned survey at the Zion National Park site, requiring carefully-timed shots or multiple shots to achieve satisfactory seismic arrival times based on signal-to-noise ratios. An average of 70 in-line shots per geophone layout was obtained at Zion National Park, and 45 mid-line shots per layout at Apache Trail.

Zonge International, Inc. of Lakewood, Colorado was contracted as part of the Zion National Park investigation to provide geophysical data collection support. In addition, the Contractor provided manual picks of seismic first arrival times for each raypath between source and receiver for the pre- and post-grouting 3D seismic surveys, and final presentation of 3D seismic tomography processing results in a report format. Further discussion of the results contained

within the report from the Contractor is provided in Chapter 7, to which results obtained by this investigation are compared.

The road surface had been milled prior to arrival at the site, and loose granular material was found along the shoulder adjacent to the walls. Spike attachments were used on the geophones for the shoulder locations, where the spikes were pushed into the granular material and degraded asphalt. Tripod plates were attached to the geophones for the locations within lanes where the receivers could simply be set upon the road surface, with good agreement observed between signals from the spike and tripod plate attachments.

Table 4.2. Source and receiver summary for Zion National Park pre-grouting seismic survey.¹

Site	Sources (Shots)	Receivers (Geophones)	Raypaths
1.10	69	48	3312
1.5.1	66	48	3168
1.5.2	66	48	3168
2.10	69	48	3312
2.5.1	66	48	3168
2.5.2	65	48	3120

¹ Location of sources and receivers were not identical for Grid #1 between pre- and post-grouting surveys, due to retaining wall work at time of post-grouting survey.

4.2.1. Site #1 Grid Layout (172+54 – 174+04)

Layout of a rectangular coordinate axis for the first grid began with the placement of two stakes near an existing control point, at approximately 171+40, 19 ft Lt. A temporary stake numbered P1 was placed near an existing survey control point to serve as a basis for distance measurements to grid corners, and a second stake P2 was used to align P1 to visually locate the corner of the first grid along the roadway. This method was employed due to the fact that the only surveying equipment that could be secured in the field was a hand level and stadia rod. A tape measure was used to pull measurements from P1 to A1 and A2, the nearest corners of the coordinate grid established for grid #1. Point A2 was located near the inside corner of the masonry retaining wall adjacent to the roadway at this location.

A length of 150 ft (45.7 m) was then pulled using the tape measure along the inside face of the wall, which was nearly linear, from point A2 to point A4, the third grid corner. The fourth grid corner, point A3, was then located by pulling a 3-4-5 square triangle from the line connecting A2 to A4, resulting in a rectangular grid. The line connecting A1 to A3 served as the positive x-axis and the line connecting A1 to A2 as the positive y-axis, with the positive z direction measured upward normal to the roadway surface. The slope of the surface for the first grid was assumed to be constant, resulting in a planar geophone location layout. Appendix B provides diagrams of the layouts of geophones and source locations for the single 10-ft geophone spacing and both 5-ft geophone spacings at the first grid location. These three separate layouts were referred to as 1.10, 1.5.1, and 1.5.2. For each of the layouts, a total of 48 geophones were arranged in three

lines of sixteen geophones, with an intermediate line of geophone locations was established 6 ft (1.8 m) between the first and third lines.



Figure 4.3. Photo. Layouts of the (L) 10-ft (3-m) geophone spacing for grid #1 and (R) 5-ft (1.5-m) geophone spacing for grid #1 at Zion National Park, during pre-grouting seismic data collection.

The grid was marked out with spray paint at geophone and sourcing locations and masonry nails were driven into the remaining pavement at the named grid corners. A USGS benchmark was located at the west entrance to the Zion-Mt. Carmel Tunnel, approximately 1550 ft east of the previously mentioned control point. A hand level and stadia rod were used to establish elevations from the known elevation of this benchmark to the grid corners and control points.

4.2.2. Site #2 Grid Layout (177+26 – 178+76)

The layout for the second grid was more complicated than the first, due to the curved alignment of the roadway at the selected location. While the first survey location was along a fairly straight roadway segment, the second was located along a curve. Similar procedures were followed, with more care taken to record and lay out geophones and sourcing locations. A rectangular grid was established following the same procedures as those used for the first survey location, with distances to grid corners recorded based on the control points established and known fixed features at the site. Parallel lines were then marked every five feet in the x-direction along this grid. Geophones were then set up along a pattern that maintained either a 5- or 10-ft x-direction spacing, depending on the grid being surveyed, but the y-coordinates varied for each x-coordinate depending on the alignment of the roadway at that location. In other words, each geophone at a given x-coordinate was translated by the same distance in the y-direction, maintaining equal spacings of 6 feet in the y-direction as those used in the first grid layout. The single 10-ft in-line geophone layout and two 5-ft in-line geophone layouts were referred to as layouts 2.10, 2.5.1, and 2.5.2 for grid #2, following the same naming convention used for grid #1. Diagrams illustrating these layouts can also be found in Appendix B, and Figure 4.4 shows the curved alignment of the grid #2 and geophone layout for the 10-ft (3-m) geophone spacing.



Figure 4.4. Photo. Layout of the 10 ft (3.0 m) geophone spacing at Zion National Park, grid #2 during (L) pre-grouting and (R) post-grouting seismic data collection.

4.2.3. *Equipment and Data Collection*

Two 24 channel geode seismographs manufactured by Geometrics of San Jose, California were used to collect and process the information received from the geophones, as shown in Figure 4.5. Each of the seismographs was powered by a 12V automotive battery, and data output was recorded using a ruggedized laptop PC. Built into the seismograph operating software are signal observation tools to monitor each geophone, which was used to verify satisfactory operation of each geophone and recording of synthesized noise prior to data collection.



Figure 4.5. Photo. Twenty-four channel Geometrics Geode seismograph.

A 12 lb. sledge hammer equipped with a “triggering” device was used as a seismic source. The hammer was impacted upon an aluminum plate, both shown in Figure 4.6, with sufficient energy to produce good quality readings at every geophone, as determined by the contracted geophysicist. The trigger sent a signal to the data recorder to begin recording as soon as impact occurred. Shot records recorded by the seismograph were stored to the laptop hard drive, which were later transferred to another system for first arrival picking and tomographic analysis.



Figure 4.6. Photo. (L) Sledge hammer; and (R) aluminum strike plate.

Construction work took place between 8pm and 8am, with closure of the road beginning at the intersection of Scenic Drive and Zion-Mount Carmel Highway. Excavation involving frequent rock ripping, material placement, and heavy equipment traffic were all taking place in the immediate vicinity of the planned survey, preventing work from being performed the first night of the visit. Data collection efforts were completed for grid #1 the following morning, with traffic control arranged for one lane beginning at 8am. Flaggers alternated traffic in either direction while equipment was being set up along the grid and checked. Once data collection was ready to begin, flaggers were instructed to hold traffic in both directions. Authorization was given from the Project Manager that traffic could be held in both directions for up to 30 minutes at a time, but typical traffic delays during data collection lasted 10 to 15 minutes, after which traffic was allowed to pass.

Data collection at grid #2 proved to be much easier, as no construction activities were planned for the following night. Some effort was required to convince project management to agree to provide flaggers to keep the road closed, while allowing for any necessary access by construction

crew, to allow for data collection. A second project was underway east of the tunnel, inside the park, which was also operating on night shifts involving complete closure of the road. Once the necessary arrangements were made, data collection was able to proceed smoothly throughout the night.

Time requirements for the data collection can be summarized considering the conditions existing in the field at the time. Establishing the two grids, including six total geophysical layouts, was accomplished in approximately 5 hours using the manual tape-measure and hand-level methods described previously. For data collection for the three layouts at grid #1, where traffic control was maintained in the adjoining lane, approximately six hours were required. Data collection was accomplished at grid #2 in approximately half the time as was needed at grid #1 due to the removal of delays resulting from traffic and construction activities.

4.3. Observation of Compaction Grouting

The purpose of this site visit was primarily to observe compaction grouting being performed and to gather as much information as possible concerning methods and procedures followed, materials and grout mixes used, and any successes or difficulties encountered relating to this technique. This information will then be considered in upcoming revisions to the current compaction grouting (and general grouting) specification, otherwise referred to here as S270.

A 3D seismic refraction survey had previously been performed at this project site at segments 172+54 to 174+04 and 177+26 to 178+76 by CFL staff and Zonge Geophysics. These two locations are relatively straight sections of road, supported by historic stone masonry walls, that have been experiencing pavement subsidence and cracking, which is believed to be caused by the loose condition of the roadway fill and possible washing out of material beneath the roadway. The stone walls contain no provisions to allow for drainage of subsurface water that may accumulate behind the wall, and the presence of open void spaces is also suspected in these locations. Due to scheduling conflicts, a site visit could not be arranged to enable observation of compaction grouting at these specific locations. Several other locations along the Zion-Mt. Carmel Highway have experienced similar problems as the locations studied in the geophysical survey and have also been specified in the plans for compaction grouting. On the nights which the inspection occurred, compaction grouting was being performed from stations 114+96 to 118+65. Here the road begins at a straight segment which enters into a switchback progressing uphill and ahead station, supported by a historic stone masonry wall similar to those found at the locations studied in the geophysical survey.

Table 4.3. Grouting location summary for Zion National Park.

Station	to	Station	Side	Rows	Grouting Type	Geophysical Survey?	Observation of Grouting?
114+96	to	118+65	RT	1	Compaction	None	Yes
166+42	to	168+68	RT	2	Compaction	None	No
172+54	to	174+10	LT	2	Compaction	172+54 to 174+04	No
177+26	to	179+37	LT	2	Compaction	177+26 to 178+76	No
183+82	to	186+64	LT	2	Permeation	None	No

This location was the last location where compaction grouting was to be performed. During compaction grouting at the three other locations, less than expected grout takes (i.e., injected grout volumes) were observed. The Project Manager from CH2MHill, requested a site visit from the contracted geotechnical engineer from Yeh & Associates, to investigate some of these issues and make any possible recommendations. After speaking with the crew from DrillTech, and looking over the drilling and grouting logs from the evening of Yeh & Associates's visit, it appears as though Yeh & Associates requested compaction grouting be performed in the middle of segment 114+96 to 118+65, along the beginning and into the middle of the switchback. Yeh & Associates instructed DrillTech employees to try slight variations to their procedure, including "drying" and "wetting" of the grout mix, with no noticeable change in results. The contract documents specified a maximum slump of 1.5 in (3.8 cm), and during our observations, this mixture resulted in clogging of the grout hoses and couplings on several occasions, especially if held under high pressures at one location for too long. DrillTech employees commented that this requirement was a bit too "dry," and that a 2 to 3 in (5.1 to 7.6 cm) slump is typical, even ideal, for compaction grouting for the given conditions. While the Contractor's claim may have been true based on their experiences, no guidance has been found in the literature suggesting a grout slump greater than 2 in (5.1 cm) should be used for compaction grouting.

4.3.1. Equipment and Methods

An unusual technique was used to install the 2-in (5-cm) inside diameter (I.D.) steel casings, involving a sacrificial conical steel tip, inserted into the end of the casing and temporarily attached using one wrap of duct tape. These steel tips were said to have been manufactured by DrillTech at their shop. The 10.5-ft (3.2-m) casings with tips were driven to the required 10 ft (3.1 m) depth, unless refusal occurred, using a Hyundai 140W-7A excavator with a pneumatic driving attachment. The casings were then backed out of the borehole several inches using either an automatic hydraulic "casing puller" or a manually-operated lever-based remover. A steel rod a few feet longer than the casing was then inserted into the casing and rammed against the sacrificial tip to remove it from the casing. The rod was then held in place and the casing backed out a few more inches, checking that the rod remained in place while the casing moved to ensure removal of the tip. Casing installation advanced ahead of the grouting operations, and stopped when an adequately large group of casings had been installed. Casings locations were laid out using a tape measure, measuring from the inside of the stone wall and adjacent holes and marked out with spray paint.

Grout was mixed using a series of equipment specialized for grouting operations, trucked to the site from DrillTech's California yard. When looking over the grouting logs provided by CH2MHill prior to our arrival at the site, an equipment change was noticed. During the first night of compaction grouting, it was discovered that the equipment originally brought in by DrillTech was not performing adequately, as no grout takes were being recorded for the first several holes. DrillTech staff informed us that a replacement batch plant and pump were brought in from GeoGrout, Inc. and casings were again driven and compaction grouting re-performed at those hole locations. While the GeoGrout equipment seemed to perform adequately, further inquiry into this equipment change may be required. A truck-mounted generator provided electricity and a water tank fed water through a custom-designed water pump to both the batch plant and a water hose used mostly for tools and equipment cleaning. Mixing of cement, water,

and sand aggregate was accomplished using a trailer-mounted batch plant that supplied mixed grout to the concrete pump using an auger-type mixer. A Reed B20 concrete pump fed the mixed grout through high-pressure grout lines to a large-radius bend coupling which was then attached to the casing. A dial gauge was fitted to the bend and packed with grease that could be periodically flushed using a zerk fitting to prevent grout from entering the gauge.

The cement used in the grout mix was Commercial Grade Quickrete Type II-V, 94 lb. bags, that “complies with current ASTM C-150 and Federal Specifications for Portland cement.” The compaction grouting proposal originally submitted by DrillTech states, “compaction grout will be composed of a uniform mixture of fine aggregate, Portland cement and water. Use of natural or artificial clay-type substances as additives to improve flow or pumpability of the low mobility grout shall not be allowed. Fine aggregate shall consist of well-graded silty sand with 100% passing the 3/8 in (9.5 mm) screen and between 18% and 30% passing the #200 screen. Portland cement and/or flyash may be added to make up a deficiency in fines content. Material having a plastic index will not be used.” The actual proportion of cement used in the mix was unable to be verified in the field.

Monitoring of vertical displacement, or heave, was accomplished using both a water tube manometer and a laser-based system consisting of a Leica Rod-Eye Classic and Leica Rugby 100. Heave displacement was only checked when relatively large grout takes were observed. Lateral, or horizontal, displacements of the wall were never checked, and no reflective markers were ever observed as described in the DrillTech proposal. No cracking of the stone wall was ever observed.

4.3.2. Additional Observations

On the first night of our observation, the employee chosen to operate the pump switch and record the grouting logs informed us that he had just arrived on the project site, and had never operated this kind of equipment before. The result was that on the first hole being grouted, the pump was not shut off following proper procedures, and the coupling escaped from the grip of the grouters, and fell to the ground, breaking a dial gauge. No calibration stickers or serial numbers were observed on any of the dial gauges used. The calibration sticker found on the laser level was expired.

At the majority of holes grouted, maximum recorded injection pressure per the logs was 500 psi, while pressures of 650 psi or greater were commonly observed on the gauge. When driving some casings, difficult conditions were encountered, possibly due to encountering of bedrock or boulders. During driving of some holes, the casing was seen to move laterally, creating an oblong-shaped hole. When these casings were removed, mostly following successful grouting, they were usually significantly bent.

Several mistakes were noticed in the compaction grouting submittal from the Contractor (Drilltech). On Sheet D-03 of these plans, beginning station 114+96 was mistakenly labeled 114+69. In this segment, from 114+96 to 118+65, compaction grouting was intended to be performed using one row of grouting locations, while the proposal and what was actually constructed followed the two row procedure. This error resulted in driven casing quantities

roughly double the original estimate, with a yet unknown effect on the injected grout quantity. In the permeation grouting proposal submitted while at the site, sheet D-07 shows a single row of grouting locations instead of the specified two rows as in the plans.

Ground cracking extending between adjacent holes on a line was observed following casing driving and compaction grouting. The depths of these cracks are unknown. On some holes where larger grout takes were recorded, whether the grout was entering existing voids or these cracks was uncertain.

4.3.3. Comments and Suggestions from Contractor

The Contractor's Project Manager for DrillTech was kind enough to share some thoughts and experience concerning the grouting operations at Zion National Park, which are paraphrased below.

- A spherical zone of influence is created around the point of injection, having a diameter about equal to the depth of injection below the ground surface. This zone causes a "pitcher's mound" effect when grouting near the surface.
- At depths less than about 10 ft (3 m), insufficient overburden pressures exist to develop resistance to injection pressures during compaction grouting.
- Placing too many restrictions, or procedure-based specifications, on Contractors is a bad idea. If during grouting, attempting methods different than what is specified is believed to produce better results, the Contractor is bound to the conditions in the specifications. Sometimes Contractors end up having to continue using a procedure or grout mix they know is not working effectively or is not the most appropriate for the site conditions.

4.3.4. For Further Consideration

From some of the observations made on this trip, the need for further investigation into the use of slump measurements for grouting applications has become clear. For several reasons, the applicability of a slump measurement for ensuring a proper grout mix can be questioned. One reason has to do with the different stress conditions existing in the grout during slump testing and grout injection. During slump tests, gravitational forces are the only forces acting upon the slump cylinder. However, during injection, particularly during compaction grouting, much higher pressures act upon the grout, undoubtedly resulting in a different material behavior than under gravitational loading only. Whereas gravitational forces may not be of sufficient magnitude to induce shearing in the grout cylinder, the large forces encountered during injection are likely to produce a fluid condition in the grout. This argument calls into question the use of slump measurements alone. As pointed out by Warner (2004), an additional issue relating to the use of slump measurements has to do with the inclusion of fine-grained or cohesive soils, in the grout mix. Increasing the fraction of cohesive material would have the result of decreasing the apparent slump, which could mislead one into thinking that the mix had become "drier," or having lower moisture content, while moisture had in fact never changed. While the DrillTech proposal specifies a maximum amount of fines to be used in the grout mix (18-30% passing the #200 screen), no testing of this material ever seems to have been performed.

The other significant issue that became clear during this trip relates to the methods used during grouting to monitor injection parameters such as pressure, injection rate, and total grout take. The contractor monitored and recorded minimum and maximum injection pressures using a dial gauge. Grout takes were recorded by counting the number of strokes of the grout pump cylinders, which were said to have been calibrated. At each hole, the total strokes were counted, and the number divided by four to evenly distribute the take across the four separate stages. At one point when the remote pump switch line was severed, pump strokes were visually counted until the line could be reconnected. Continuous and real-time computer monitoring of these parameters would decrease the chances of human error in these situations, and show how injection parameters varied with time and depth.

4.3.5. Reinforced Fill (177+26 to 179+37)

At one of the segments being studied as part of the geophysical investigation, the excavation had been completed the night before we arrived, allowing some photographs to be taken and observations to be made. Perhaps most interesting about the excavation was the very deep areas of asphalt pavement that remained visible even after milling and 3 ft (1 m) of excavation. Greater than 2-ft (0.6-m) asphalt thicknesses were present at the centerline, increasing toward the stone wall, as shown in Figure 4.7. These observations were postulated to have the unexpected result of showing decreases in p-wave velocities for the reinforced fill zones once the post-grouting geophysical survey is performed. Nuclear density testing logs for the compacted fill placed at this location show placed wet densities ranging from 138 to 145 lb/ft³, at moisture contents of between 5.4 and 6.2%. Fill was placed in the excavation in 9 inch lifts separated by geotextile fabric as specified in the plans with multiple passes of a smooth drum vibratory roller compactor.



Figure 4.7. Photo. Asphalt thickness greater than 1 m (3 ft) observed at Zion National Park, site due to repeated maintenance patching to correct settlement.

4.4. Post-Grouting Geophysical Investigation

Nearly identical procedures as employed during the pre-grouting seismic survey were followed for the post-grouting survey, with a few notable exceptions. At each of the grids, the masonry

retaining walls which had been specified for removal and replacement in the plans were discovered to have been removed during the course of construction, but not yet completely reset.

As these walls were still in the process of being reset at the time of arrival to complete the post-grouting survey, and large trenches approximately one to two feet deep remained adjacent to the walls, minor modifications to the grid layouts had to be made in order to complete the data collection within the narrow time window available. Instead of 6 ft (1.8 m) spacings between geophone lines, 5 ft (1.5 m) spacings were used to narrow the grids. At grid #1, the alignment of the grid was skewed slightly to allow for the best possible relocation and coverage of the targeted soil volume considering the unexpected conditions at the site.

Data collection proceeded easily once the grids were relocated and modified as required, with similar access and scheduling challenges encountered during the pre-grouting survey. Similar time requirements for data collection were also noted between the pre- and post-grouting surveys.

(blank page)

5. CASE STUDY 2: APACHE TRAIL, TONTO NATIONAL FOREST

The second site studied as part of this research is located along the Apache Trail, within Tonto National Forest in Arizona. The Apache Trail traverses the Superstition Mountains and connects Apache Junction, on the eastern edge of the Greater Phoenix area, with Theodore Roosevelt Lake. Similar problems as observed at the Zion National Park site have plagued this road for many years, and a combined void-fill grouting and compaction grouting program was designed to stabilize areas showing evidence of void development from piping of material within loose roadway fill material and subsidence beneath both the road surface and adjoining retaining walls. One of the most sensitive concerns in performing compaction grouting on this project, and guiding the selection of associated performance criteria, was possible disturbance to historic dry-stacked stone retaining walls.

While traditional high-pressure, low-slump compaction grouting was originally specified in the plans as the primary method of filling potential voids and densifying zones of loose soil, concerns about possibly damaging the historic dry stacked retaining walls necessitated the inclusion of strict monitoring criteria, particularly for displacement of the wall faces and the maximum allowable grouting pressure. Similarly to the grouting at Zion National Park, casings were installed to relatively shallow depths from 2 to 17 ft (0.6 to 5.2 m). The first several holes that were attempted to be grouted using the compaction grouting technique were quickly advanced upstage without taking significant grout quantities. Following some changes, the greatest results were obtained by increasing the water-cement ratio of the grout and filling the holes strictly by gravitational pressure, or hydraulic head. A water to cement ratio of 0.77 by weight (1.17 by volume) was chosen, along with an equal weight of fly ash to cement, to which small amounts of retarding and thixotropic admixtures were added. Figure 5.1 provides a typical construction detail for the compaction grouting layout, and Table 5.1 summarizes grouting quantities.

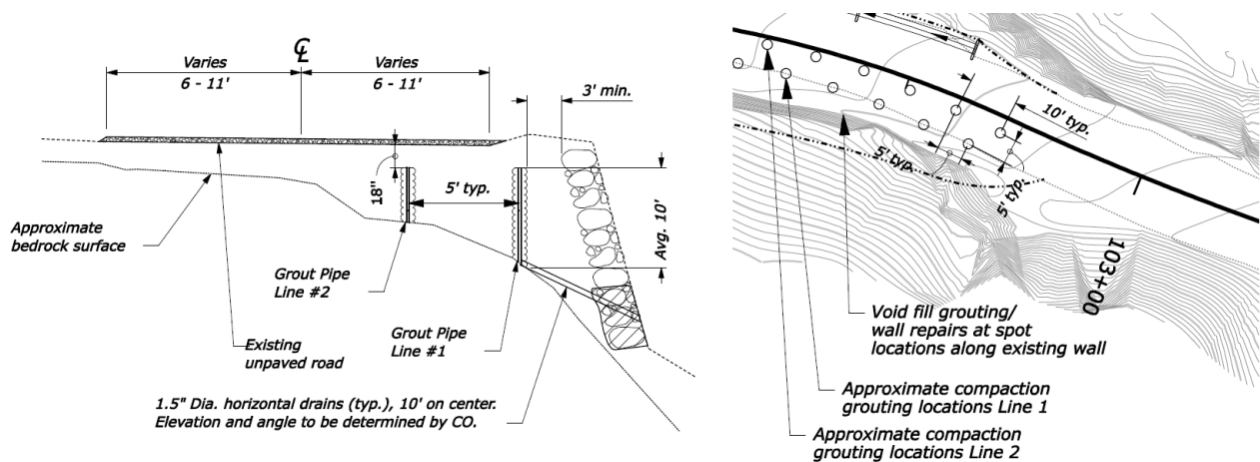


Figure 5.1. Schematic. Typical grouting profile and layout at Apache Trail Wall 1.

Table 5.1. Grouting summary for Apache Trail.

Location	Stationing	Number of Injection Holes ¹	Total Grout Casing	Total Grout Volume
			m (ft)	m ³ (yd ³)
Wall 1	100+00 – 102+71	27[6]	54(176)	14.5(19)
Wall 3	300+00 – 304+64	92[17]	197(647)	117(153)

¹ Number in brackets indicates number of holes where drilling was completed but no grout injected

5.1. Soils and Site Conditions

Conditions at the Apache Trail site were relatively similar to those encountered at Zion National Park, with the most significant variance being the different roadway surfaces in place. While at Zion National Park, asphalt pavement thickness ranging from several inches to several feet existed at the seismic survey locations, the roadway surface along the portion of Apache Trail studied consisted of dense, compacted decomposed granite material. Figures 5.2 and 5.3 provide some perspective into the terrain and conditions existing at the Apache Trail site. A more detailed analysis of the site conditions, including geotechnical evaluations of the roadway and stone retaining walls, has been reported by AMEC (2007) in a previous study.

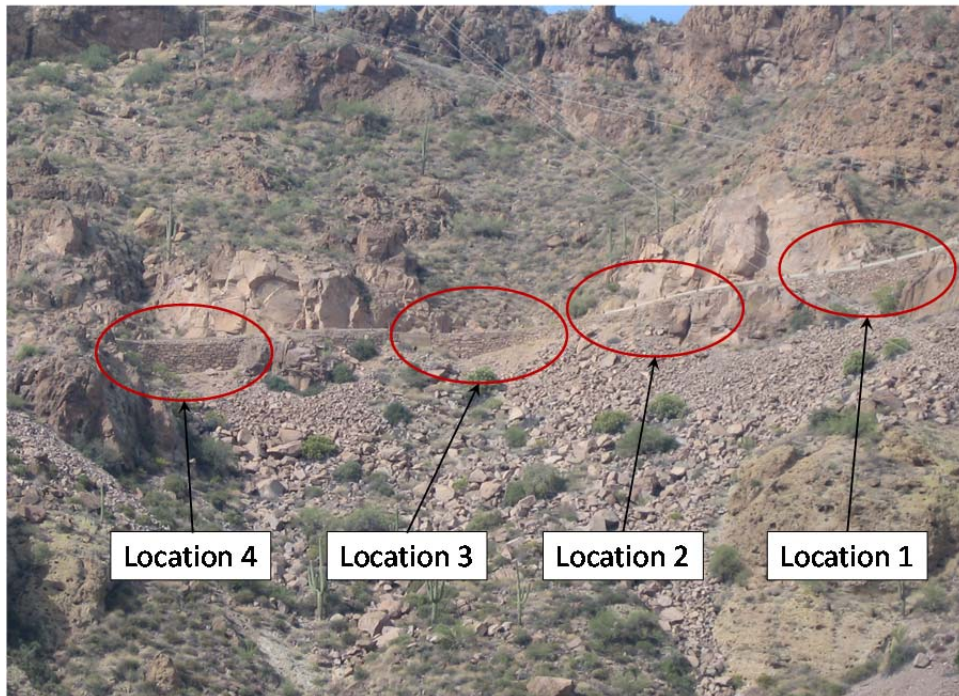


Figure 5.2. Photo. Panoramic photograph showing locations 1 to 4, from right to left, along Wall 3 at Apache Trail, with stationing advanced from approximately 300+00 at the right to 304+50 at the left.



Figure 5.3. Photo. Photographs of Apache Trail retaining walls: clockwise from top left: (1) Location 1; (2) Location 2; (3) Location 3; (4) and (5) Location 5, Wall 1; (6) large void daylighting at the roadway surface at Location 4.

5.2. Pre-Grouting Geophysical Investigation

Landstreamers, connected arrays of geophones designed primarily to be towed along the ground, were incorporated for the Apache Trail investigation as shown in Figure 5.4. These geophone arrays were chosen based on their flexibility in placement and relocation in the field, a choice that was supported by the good agreement found by van der Veen et al. (2001) between signals received using traditional geophones and landstreamers. The main advantages of using landstreamers for at this site were the significant reductions in time and effort required to place sensors and gather seismic data, as well as the ability to quickly move the line in the event that traffic was required to pass the narrow roadway. Four profiles of Geostuff landstreamers, consisting of twelve 4.5-Hz vertical geophones spaced 1.5 m (5 ft) apart, allowed for prompt relocation of receivers when moving between sites and clearing passing traffic. A minimum of 45 shots for each site were placed along the centerlines between adjacent landstreamers and off-end of the lines. Two 24-channel Geometrics Geode seismographs, as shown in Figure 5.4, were used for this investigation as well. Diagrams illustrating the layout of geophones and shots for each of the five locations are provided in Appendix B for further reference.

Due to the relatively shallow depths to bedrock at both sites and the close spacings of geophones, arrival times were relatively small. In these situations, the addition of a delay, or pre-trigger geophone signal record, provided a longer baseline signal to consider during data interpretation and resulted in easier to distinguish arrival times. The use of geophone tripod bases and landstreamers with geophones mounted to baseplates both allowed for successful identification of compression wave arrival times, often without requiring shot stacking. Background noise from nearby construction activities during data collection was addressed by stacking consecutive shot records from the same location when noise became significant.



Figure 5.4. Photo. (L) Laptop, seismograph, and battery setup; and (R) geophones deployed on landstreamers at Apache Trail.

Table 5.2. Source and receiver summary for Apache Trail.

Site	Sources (Shots)	Receivers (Geophones)	Raypaths
1	45	48	2160
2	45	48	2160
3	45	48	2160
4	45	48	2160
5	59	48	2832

Locations were chosen for this investigation based primarily upon the layout of the historic dry-stacked masonry retaining walls in the vicinity of the planned grouting operations. The grid layout chosen was centered at the midpoint of the tallest sections of these walls, and aligned as close as possible along the roadway surface near the walls. As the greatest depths of fill material were expected to exist at these locations, the greatest potential for grout takes was anticipated here, a hypothesis that had been supported by evidence gathered in previous studies of these segments of Apache Trail and the walls of concern.

5.3. Observation of Compaction Grouting

Due to scheduling conflicts, the frequently-changing construction schedule, and the need to plan any travel to this site well in advance, the author was unable to personally attend the compaction grouting operations. The grout mix that was finally chosen for the Apache Trail grouting can be found in Table 5.3. A thixotropic admixture and foam were added to this mix design, with amounts determined based on site conditions. The retarding admixture used was Eucon DS, manufactured by Euclid Concrete Admixtures, and the thixotropic admixture used was Rheomac VMA 362, manufactured by BASF. The grout mixture shown corresponds to a water-to-cement ratio of 0.77 by weight and 1.17 by volume.

Table 5.3. Grout mix used at Apache Trail.

Masonry Sand	1350 lb
Top Soil (Silt)	1350 lb
Cement	432 lb
Fly Ash	432 lb
Retarder	24 oz
Water	40 gal

Additionally, the grouting plan initially outlined in the plans specified three lines of grouting points along both Wall 1 and Wall 3. Due to higher than expected grout takes during grouting along lines 1 and 2 (line 1 being nearest to the outboard stone retaining wall), grouting line 3 was abandoned to avoid significantly exceeding the estimated grout and hole casing quantities.

5.4. Post-Grouting Geophysical Investigation

Identical procedures were followed during post-grouting data collection as were employed during the pre-grouting survey, with the exception that shot locations which were no longer

accessible due to the reduced two-person crew had to be abandoned. The choice to leave out these shot locations was determined in advance, and no significant reduction in the quality of the investigation was anticipated as a consequence.

6. RESULTS

Once the seismic data had been collected from the pre- and post-grouting investigations at each of the sites, and the geometries of the geophone and source locations determined from the surveying information, 3D seismic tomography images were developed using the GSR3D software package. Select pre- and post-grouting seismic tomography from the sites surveyed is provided in Appendix C, seismic difference tomography can be found in Appendix D, and ray densities are presented in Appendix E for each of the locations.

Figure 6.1 provides a schematic which helps orient the viewer as to the perspectives given for all tomography developed for this study. While different origins and directions of coordinate axes were chosen for the Zion National Park and Apache Trail relative to the adjacent retaining walls at the sites due to conditions in the field, the viewing perspective for the tomography is maintained consistently throughout this report with respect to viewing angle. This allows the viewer to better understand the conditions nearer to the retaining wall structures, which were of primary concern when performing grouting at these sites. Additionally, the most severe signs of settlement and roadway damage were observed along the outboard traffic lanes at these sites, which correspond to the nearer side of the tomography as presented here.

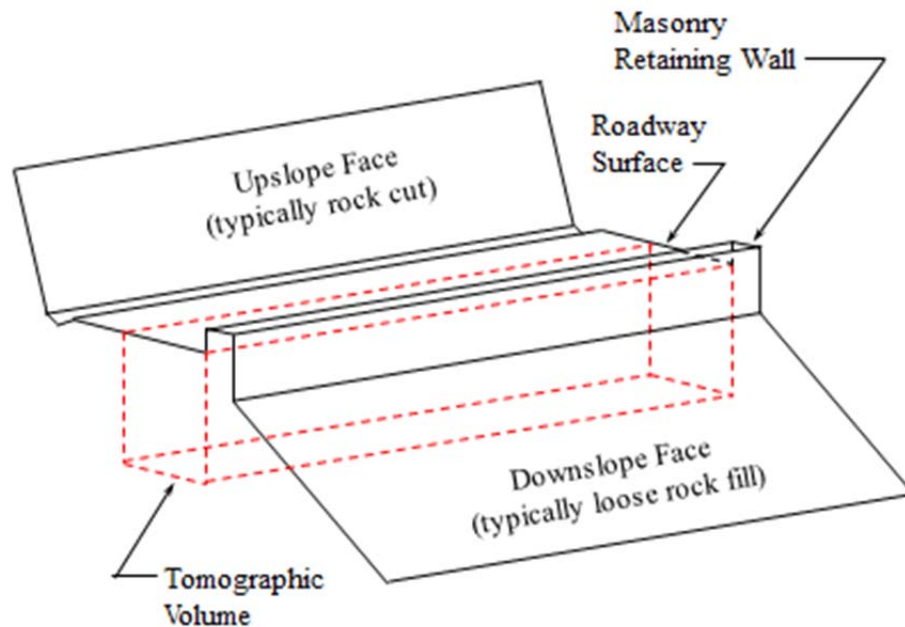


Figure 6.1. Schematic. Schematic illustrating the viewing perspective for the tomography generated for both Zion National Park, and Apache Trail sites, relative to the typical site conditions.

6.1. Zion National Park Results

Consistent procedures were followed for processing of the 3D seismic data collection during the field investigations for both Zion National Park and Apache Trail sites. In order to obtain the maximum benefit of the automated first arrival picker integrated within the GSR3D package,

while allowing for some degree of user influence in consideration of the picks, the full capabilities allowed by the software for entry of training picks into the autopicker feature was utilized. The following process was determined after several different procedures were investigated for determination of the first arrival times for the approximately 64,000 raypaths resulting from the pre- and post-grouting surveys at both sites. Figure 6.2 shows a typical shot record collected from the pre-grouting survey at layout 1.5.2 at Zion National Park. The seismic data collection and viewing software accompanying the seismographs included software called SeisImager2D which allowed for auto and manual picking of seismic first arrival times. This software was used to develop manual picks for selected shot locations, which remained consistent in relation to the position within grid layout for each of the layouts. These manual picks, resulting from one shot at each layout, were entered manually as training picks into the GSR3D program for use in the autopicking procedure.

Figure 6.3 shows overviews of the training picks used for generation of the 3D seismic tomography at the Zion National Park sites. A general trend can be observed in this figure, where significant increases in arrival times occurred following grouting for the 5-ft (1.5-m) geophone spacings, which may have resulted from decreases in seismic velocities following grouting. The opposite trend is generally observed for the 10-ft (3-m) geophone spacing layouts, where decreases in arrival times can be noted, which would suggest increased seismic velocities within the subsurface materials. It should be noted, however, that due to the circumstances encountered during data collection, as previously mentioned, the locations of shots and geophones for both grids were not able to be maintained completely between the pre- and post-grouting surveys, but the relative locations used for the training shots were held consistent.

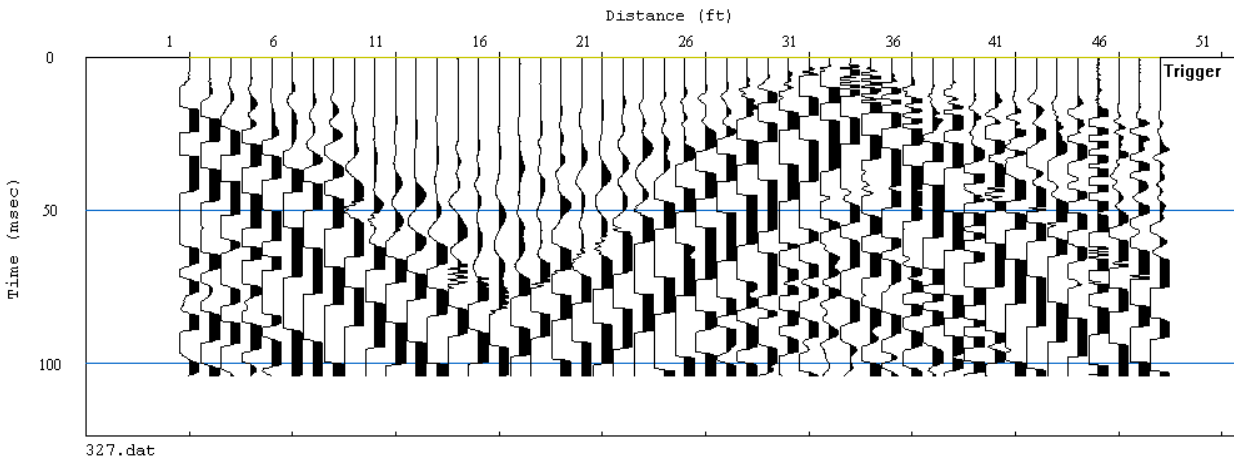


Figure 6.2. Graph. Typical shot record for 3D layout 2.5.1 at Zion National Park, with clearly distinguishable first arrivals.

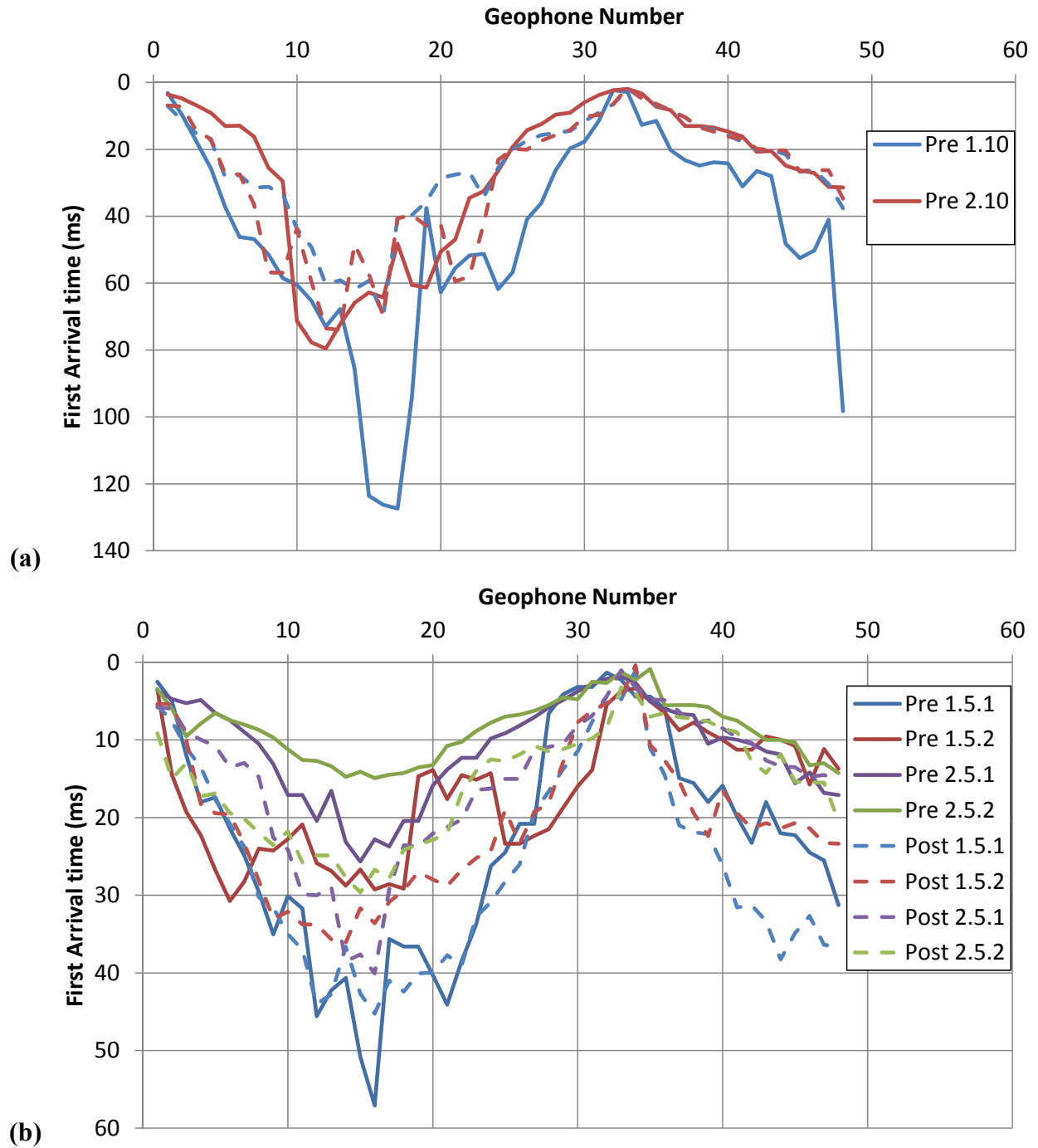


Figure 6.3. Graph. Manual training picks used for GSR3D autopicker for Zion National Park sites: (a) 10-ft (3-m) geophone spacing; and (b) 5-ft (1.5-m) geophone spacing.

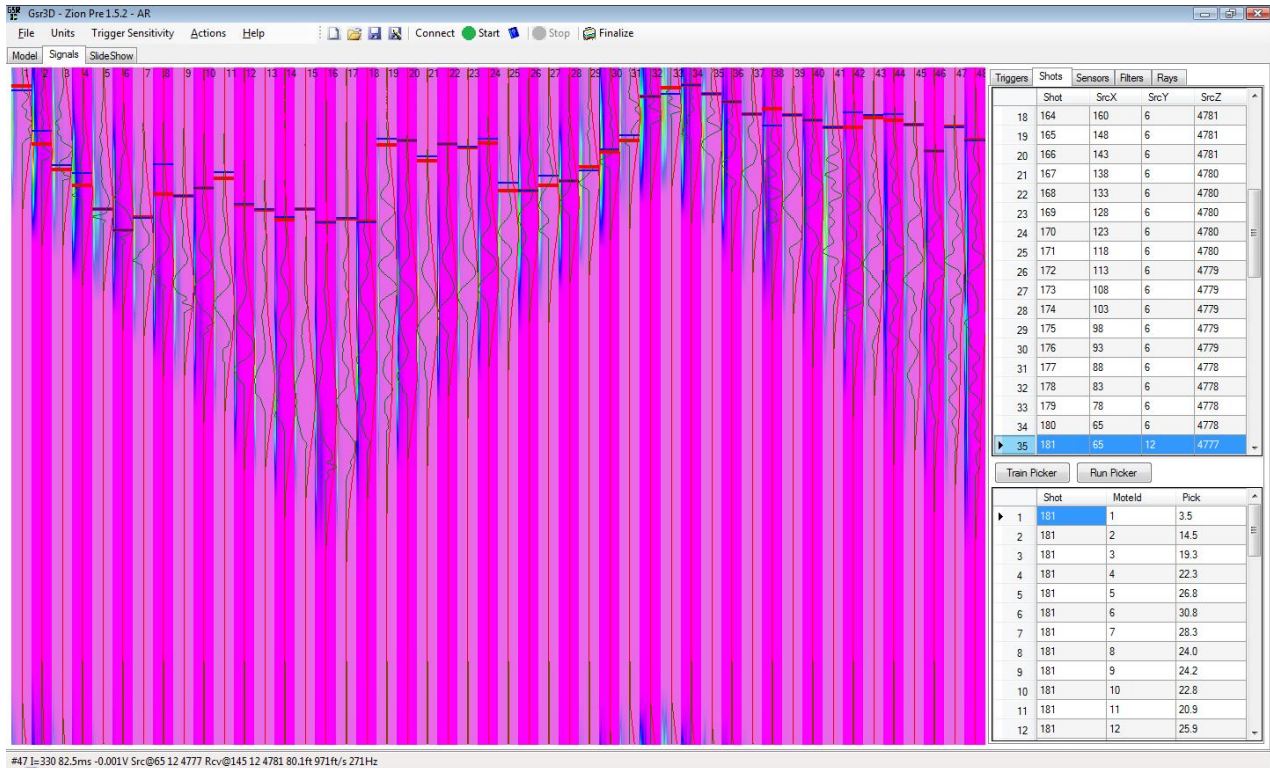


Figure 6.4. Screenshot. Typical GSR3D screenshot showing manual training picks (in red) and resulting trained autopicks (in blue) used processing of seismic data for Zion National Park pre-grouting location 1.5.2.

Red picks shown in Figure 6.4 were determined using SeisImager2D, and entered into GSR3D as example picks for one shot. The train picker and run picker commands were then executed within GSR3D, resulting in the final picks shown in blue. The shot record above is shown for the Zion National Park pre-grouting location 1.5.2.

Tomography calculated for the Zion National Park and Apache Trail locations was plotted using Matlab software, to allow for a variety of situations to be considered, and to determine the most effective means of presenting the results possible. The GSR3D software contains a fast, consistent, and automated tomography generation tool, which creates 3D perspective views and 2D slices of the velocity models calculated by the program, saving the images created to separate folders on the computer's hard drive. However, GSR3D does not typically allow for the computation of difference tomography, although the software does have this capability. To allow for the calculation and plotting of the difference tomography, as discussed in the next section, and to maintain consistency in the tomography presented in this study, the powerful 3D visualization and matrix computation abilities of Matlab were used to plot the pre- and post-grouting tomography instead. GSR3D creates a data file following tomography calculation that contains a table consisting of the nodes which make up the tomography. At each node, the value of the determined seismic velocity and ray density is reported along with the x-, y-, and z-coordinates of each node. This table could then be easily plotted using different Matlab functions to create the tomography for each location. A 3D scatter plot was chosen to represent the data, with spheres of equal radius centered at the node location, colored with respect to a specified colorbar, or scale, depending on the data being plotted.

Pre- and post-grouting tomography for the Zion National Park locations, showing only seismic velocities less than 500 m/s can be found in Appendix C. These representations of the tomography were found to provide a simple comparison between pre- and post-grouting tomography, while considering ray densities, as discussed later in this chapter. For most of the Zion National Park locations, less points below this threshold velocity can be observed following grouting, suggesting a decrease in the regions of lowest-velocity due to grouting. At some locations, unexpected increases in the number of points below the threshold velocity can be observed, which are attempted to be explained in later sections.

6.1.1. Difference Tomography

Difference tomography was calculated from the pre- and post-grouting tomography as follows:

$$v_{c,diff} = v_{c,post} - v_{c,pre} \tag{6.1}$$

where $v_{c,diff}$ refers to the seismic velocity difference and $v_{c,post}$ and $v_{c,pre}$ refer to the seismic velocities resulting from the post- and pre-grouting tomography, respectively. Upon examination of the data points calculated for the tomography at the Zion National Park sites, the discovery was made that data points did not exist at the same coordinates within the overlapping volumes between the pre- and post-grouting models. A simple Matlab routine was written to read the pre- and post-grouting tomography output, consider the locations of the data points in each, and compute the seismic velocity differences between points falling within a specified distance tolerance. For each site and instrumentation geometry, a variety of tolerances were considered to provide the most representative number of difference tomography points possible. A summary of the tomography output for each of the Zion National Park sites is provided in Table 6.1, and the difference tomography in Table 6.2. Reasonable numbers of data points were obtained according to this procedure for most sites, with the exception of sites 1.5.2 and 2.5.1, where higher disagreement between the locations of the pre- and post-grouting data points was found.

Table 6.1. Pre- and post-grouting tomography summary for Zion National Park.

Site	Pre-Grouting Tomography		Post-Grouting Tomography	
	Data Points	Resolution m (ft)	Data Points	Resolution m (ft)
1.10	34682	0.6 (2)	34639	0.6 (2)
1.5.1	82989	0.3 (1)	78936	0.3 (1)
1.5.2	86306	0.3 (1)	82158	0.3 (1)
2.10	54427	0.6 (2)	49181	0.6 (2)
2.5.1	16921	0.6 (2)	15833	0.6 (2)
2.5.2	17675	0.6 (2)	15907	0.6 (2)

Table 6.2. Difference tomography calculation summary for Zion National Park.

Site	Tolerance ft. (cm)	Minimum Tomography Data Points for Difference Calculation	Resulting Difference Tomography Data Points
1.10	0.75 (22.9)	34639	28313
1.5.1	0.50 (15.2)	78936	63045
1.5.2	0.60 (18.3)	82158	187755
2.10	0.50 (15.2)	49181	49156
2.5.1	1.00 (30.5)	15833	2617
2.5.2	0.50 (15.2)	15907	15896

6.2. Apache Trail Results

The same procedures were followed for this study for the processing of 3D seismic tomography for the Apache Trail sites as was used for the Zion National Park sites. Similarly, Figure 6.5 shows a typical shot record recorded for a location at Apache Trail, illustrating the addition of the pre-trigger geophone record, or delay, added to improve the determination of first arrival times. Figure 6.6 displays the manual training picks entered into the GSR3D program for the autopicking analysis, from which a general trend of decreased arrival times can be observed suggesting increases in seismic velocities.

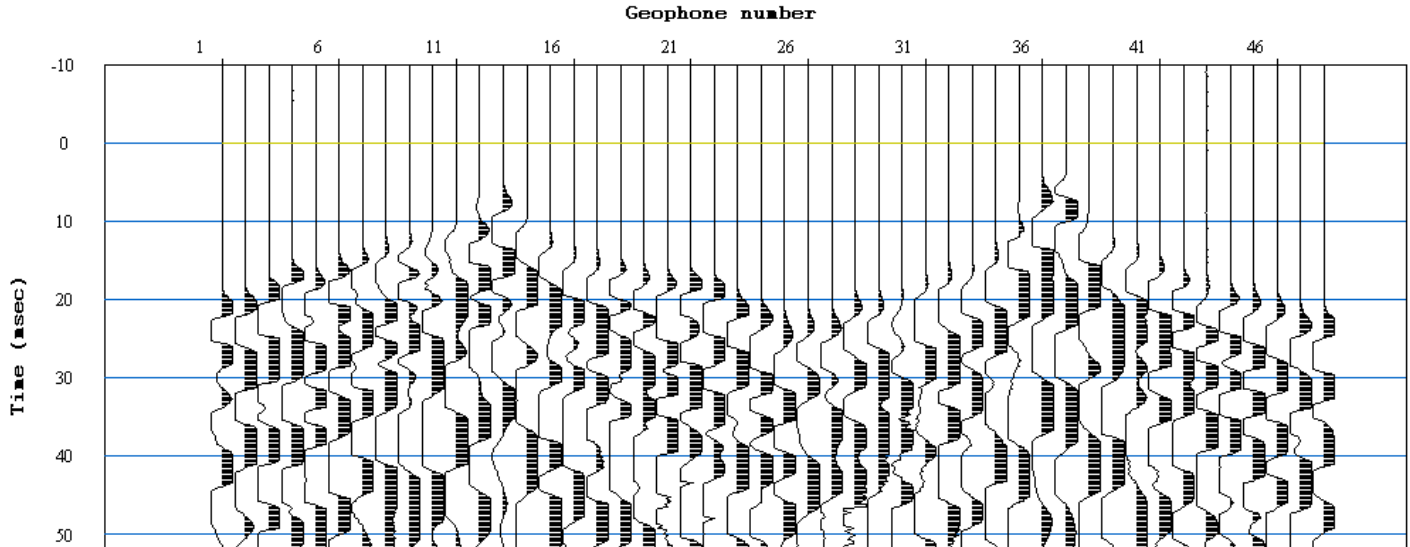


Figure 6.5. Graph. Typical shot record for 3D layout at Apache Trail, with clear first arrivals and pre-trigger delay interval shown.

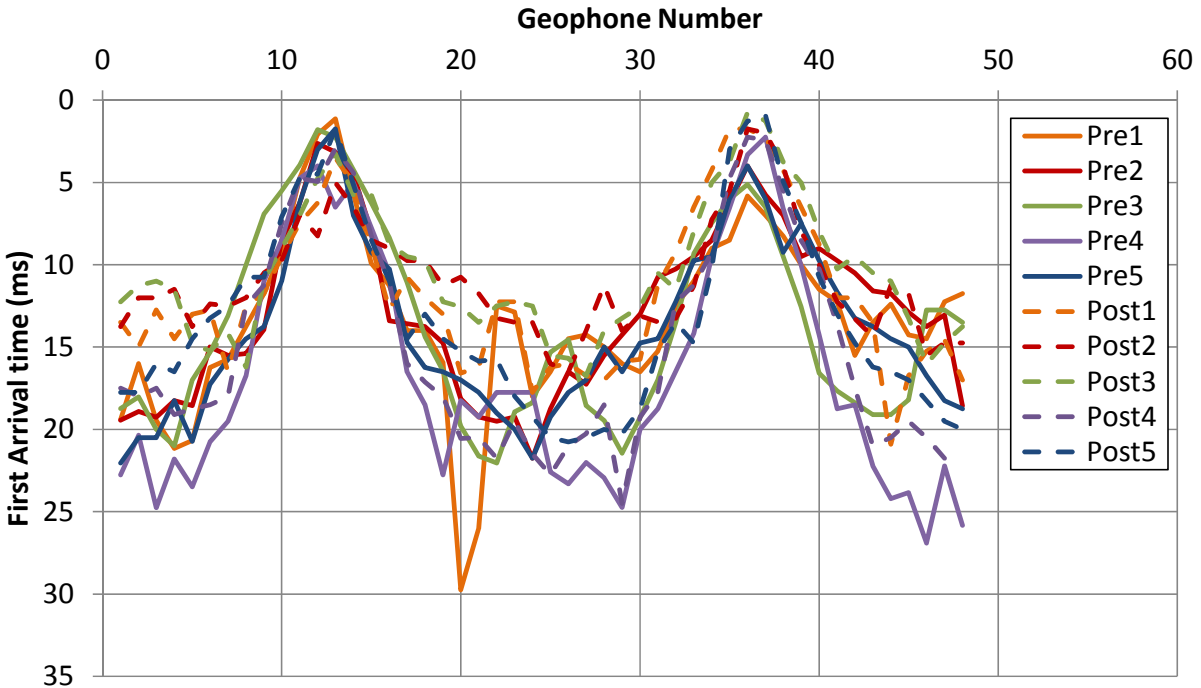


Figure 6.6. Graph. Manual training picks used for GSR3D autopicker for Apache Trail sites.

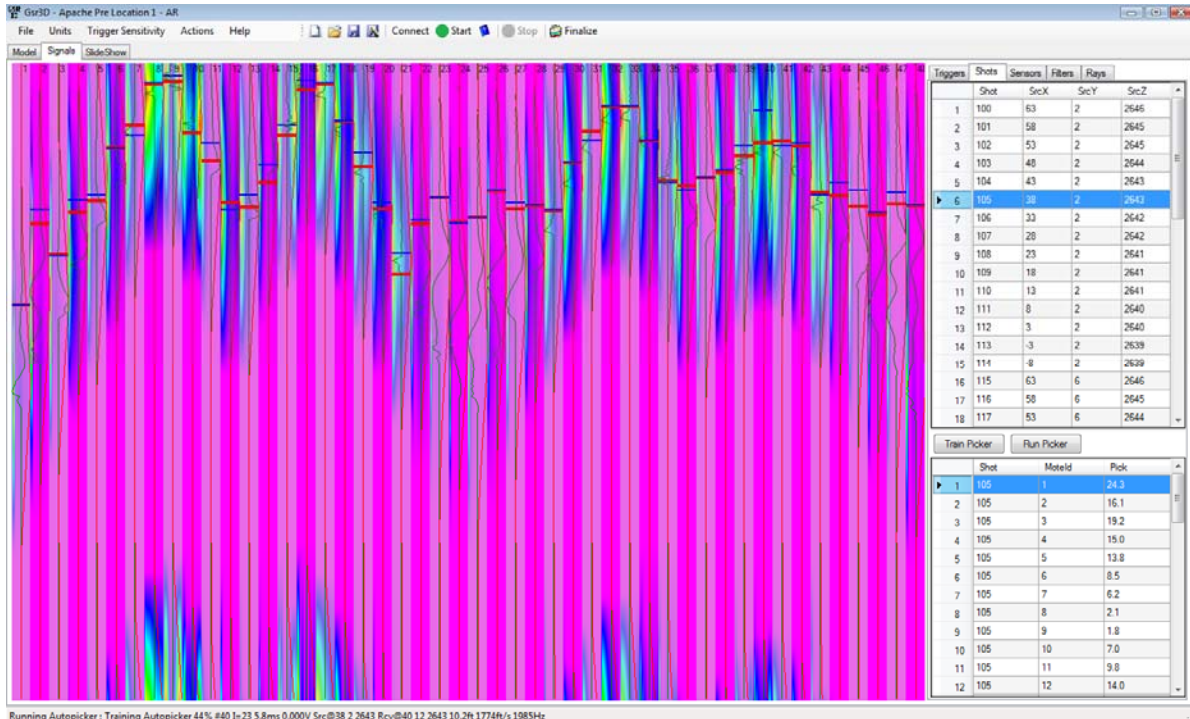


Figure 6.7. Screenshot. Typical GSR3D screenshot showing manual training picks (in red) and resulting trained autopicks (in blue) for Apache Trail pre-grouting location 1.

6.2.1. Difference Tomography

Values for difference tomography were calculated following the same procedures used for the Zion National Park sites, where a Matlab program was used to calculate the velocity differences between pre- and post-grouting tomography data points. However, unlike with the data resulting from the Zion National Park processing, very high agreement observed between the numbers of points and the locations of those points for the Apache Trail tomography. As a result, the velocity differences obtained can be plotted at the actual locations provided by the GSR3D software output, as summarized in Tables 6.3 and 6.4. Final model resolutions of 0.3 m (1 ft) were determined for all sites at Apache Trail, unlike at some of the sites as for the Zion National Park processing.

Table 6.3. Pre- and post-grouting tomography summary for Apache Trail.

Site	Pre-Grouting Tomography		Post-Grouting Tomography	
	Data Points	Resolution m (ft)	Data Points	Resolution m (ft)
1	33572	0.3 (1)	33587	0.3 (1)
2	33972	0.3 (1)	33972	0.3 (1)
3	33844	0.3 (1)	33844	0.3 (1)
4	33202	0.3 (1)	33202	0.3 (1)
5	35273	0.3 (1)	35241	0.3 (1)

Table 6.4. Difference tomography calculation summary for Apache Trail.

Site	Tolerance ft. (cm)	Minimum Tomography Data Points for Difference Calculation	Resulting Difference Tomography Data Points
1	0 (0)	33572	33571
2	0 (0)	33972	33971
3	0 (0)	33844	33844
4	0 (0)	33202	33201
5	0 (0)	35241	35241

Observations from the resulting difference tomography for the Apache Trail sites, provided in Appendix D, are more consistent than those determined for the Zion National Park difference tomography. A general trend that can be noted relates to the locations of velocity increases compared to locations of velocity decreases within the tomography. A larger proportion of the velocity increases appear to be found in the central regions of the tomography, compared to the velocity decreases, which appear to be found more along the boundaries of the tomography, where less certainty exists, as discussed further in the next section.

6.3. Ray Densities

Appendix E provides illustrations of the ray densities at each data point, or node, determined by the GSR3D software. Values for the ray densities determined represent the number of raypaths

traveling through a given node, following the final velocity iteration step. These images provide some valuable insight into the tomography generated by the software for the case studies considered here. Regions of the tomography model having higher ray densities can be said to have the greater confidence in the seismic velocity determined at those points, as they represent a summation of the individual probabilities that raypaths pass through a given node.

For the ray densities determined at the Apache Trail locations, good agreement between pre- and post-grouting ray densities can be observed, with the exception of Location 4. At this location, a significant region of high ray density occurs in the post-grouting plot but not in the pre-grouting plot. Interestingly, this same region corresponds well with the region of greatest velocity improvement in the difference tomography for Location 4 seen in Appendix D. This may be due to the presence of low-velocity material in this region prior to grouting, around which the seismic wavefront traveled, explaining the lack of raypaths. Following grouting, seismic waves may have been more likely to travel through this region, resulting in increased seismic velocities and ray densities. Potential correlations between increased ray densities and increased seismic velocities are not as apparent for the other locations at Apache Trail.

Another important observation that can be made for all of the Apache Trail locations relates to the correlation between regions found to have no ray density and decreased seismic velocity following grouting. While wavefronts would have been propagated through these regions, updating the seismic velocities at these points would have had little effect on the calculated wavefront arrival times. Therefore, it may be likely that these regions experienced little change in seismic velocity during the iterative process, resulting in final seismic velocities close to those determined for the starting model.

For the Zion National Park locations, some of the unexpected results from the pre-, post-, and difference tomography can potentially be explained by considering plots of the ray densities as shown in Appendix E. For two of the plots, post-grouting 1.10 and post-grouting 1.5.2, nonzero ray densities appear to have been reported for the entire final tomography model, which is not the case for any of the other plots. These abnormalities could have been due to an insufficient number of iterations of the model during processing, as well as the challenges posed by the shallow high-velocity layers present during data collection. For these two sites, the same observation between increased ray densities and increased seismic velocities can be observed as with Apache Trail Location 4, but even more noticeably.

For the remainder of the Zion National Park locations, reasonable agreement between the pre- and post-grouting ray densities can be observed. For these locations, however, the reported ray densities are relatively high and at shallow depths, which correspond to the shallow regions of high-velocity material determined in the pre- and post-grouting tomography and known to have existed in the field.

(blank page)

7. DATA ANALYSIS

Visualization of 3D seismic velocity and velocity difference tomography, whether by 2D slices or by 3D perspective views, can provide a useful graphical representation of the distribution, both in magnitude and spatially, of areas of concern for grouting and areas showing improvement as a result of grouting. These images alone do not provide engineers or technicians with useful quantitative understanding of these distributions, requiring an investigation into possible methods which could provide this type of information. Several methods are explored to determine their potential usefulness in communicating mathematical and statistical distributions of seismic velocities which make up tomography models like those studied in this investigation.

7.1. Improvement of a Target Velocity Range

One useful method for assessing the effectiveness of grouting operations using pre- and post-grouting tomography is to compare the proportions of the targeted soil mass falling below a velocity of concern both before and after grouting. For Example, Figure 7.1 shows pre- and post-grouting tomography results for Apache Trail Location 1, displaying only those points where the seismic velocity was determined to be less than a threshold value of 500 m/s. From visual observation of these two tomograms, an improvement can be observed due to the decreased number of points falling within the 0 to 500 m/s range. Similar tomography for seismic velocities less than a target velocity of 500 m/s are presented for both the Apache Trail and Zion National Park sites in Appendix C.

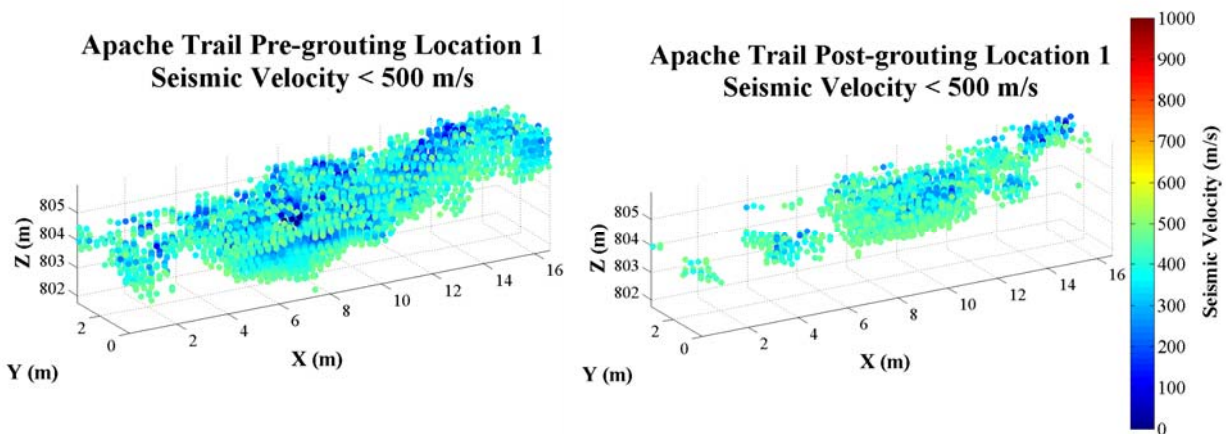


Figure 7.1. Graph. Pre- and post-grouting tomography for Apache Trail Location 1, showing data points having seismic velocities less than a targeted velocity of 500 m/s.

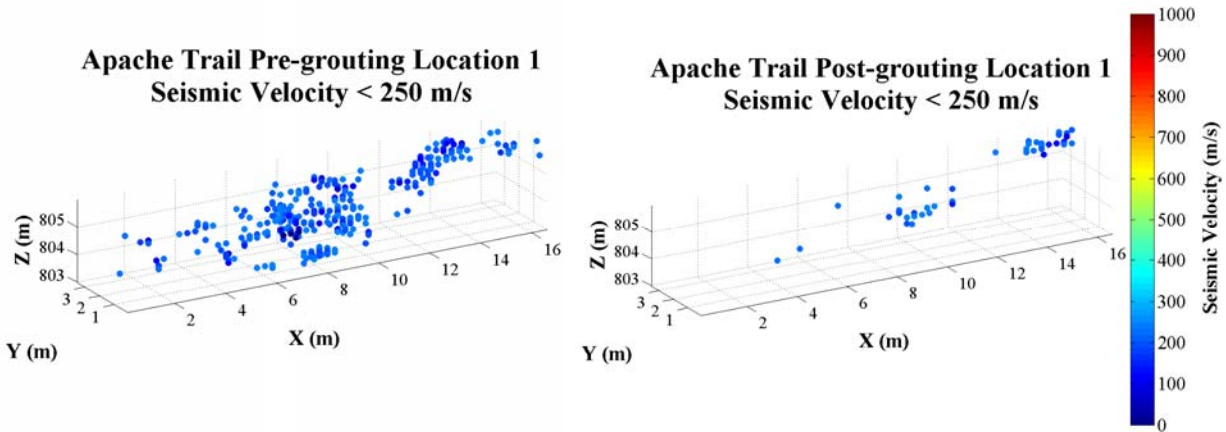


Figure 7.2. Graph. Pre- and post-grouting tomography for Apache Trail Location 1, showing data points having seismic velocities less than a targeted velocity of 250 m/s.

This concept can be quantified by assessing the percentage of points falling below a target seismic velocity before grouting and comparing the same percentage following grouting. An approach that would allow this degree of improvement to be quantified by the following relationship, where the effectiveness value, EV , can be described by Equation 7.1 below. Table 7.1 summarizes EV values for all sites considered as part of this study, showing a considerable range of values, both positive and negative. Negative values obtained from some sites indicate that more points were present after grouting that fell within the range of 0-500 m/s. This analysis could be repeated for a range of target velocities to investigate possible effects on the values of for different velocity ranges as well as potential trends.

$$EV = \left(\frac{\text{Points below Target Velocity}}{\text{Total Number of Points}} \right)_{Pre} - \left(\frac{\text{Points below Target Velocity}}{\text{Total Number of Points}} \right)_{Post} \quad (7.1)$$

Table 7.1. Effectiveness values for all sites, with corresponding target velocity range and recorded grout volumes.

Site	Target Velocity Range m/s	Pre-grouting (%)	Post-grouting (%)	EV (%)	Total Grout Volume m ³ (yd ³)
Zion 1.10	0-500	8.0	1.9	6.0	3.2 (4.2)
Zion 1.5.1	0-500	0.9	13.3	-12.4	1.6 (2.1)
Zion 1.5.2	0-500	3.4	2.2	1.2	1.6 (2.1)
Zion 2.10	0-500	1.8	11.4	-9.6	11.7 (15.3)
Zion 2.5.1	0-500	0.3	1.6	-1.3	5.6 (7.6)
Zion 2.5.2	0-500	0.3	4.5	-4.2	5.6 (7.6)
Apache Trail 1	0-500	8.4	3.7	4.7	18.1 (23.6)
Apache Trail 2	0-500	7.3	4.5	2.7	25.1 (32.8)
Apache Trail 3	0-500	10.7	4.8	5.8	25.8 (33.8)
Apache Trail 4	0-500	4.4	6.4	-1.9	22.2 (29.1)
Apache Trail 5	0-500	7.0	6.7	0.2	7.7 (10.1)

Table 7.2. Effectiveness values for all sites, with corresponding target velocity range and recorded grout volumes.

Site	Target Velocity Range m/s	Pre-grouting (%)	Post-grouting (%)	EV (%)	Total Grout Volume m ³ (yd ³)
Zion 1.10	0-250	3.5	1.1	2.4	3.2 (4.2)
Zion 1.5.1	0-250	0.3	0.3	-0.03	1.6 (2.1)
Zion 1.5.2	0-250	3.3	2.2	1.2	1.6 (2.1)
Zion 2.10	0-250	1.0	6.9	-5.9	11.7 (15.3)
Zion 2.5.1	0-250	0.1	1.0	-0.9	5.6 (7.6)
Zion 2.5.2	0-250	0.3	4.5	-4.2	5.6 (7.6)
Apache Trail 1	0-250	0.8	0.1	0.7	18.1 (23.6)
Apache Trail 2	0-250	0.2	0.3	-0.1	25.1 (32.8)
Apache Trail 3	0-250	2.0	0.2	1.8	25.8 (33.8)
Apache Trail 4	0-250	0.3	0.4	-0.1	22.2 (29.1)
Apache Trail 5	0-250	0.2	0.1	0.1	7.7 (10.1)

7.2. Seismic Velocity Difference Quantification

In order to provide a more quantitative measure of the degree of improvement resulting from the grouting operations completed at the study sites, several methods were considered. The potential application of any such analysis to a variety of sites, conditions, and tomography models needed to be considered, which lead to the investigation of the most straightforward methods possible that would achieve this goal. For example, due to the complications during the post-grouting seismic data collection at the Zion National Park sites, as mentioned previously, data points resulting from the tomography for the pre- and post-grouting surveys did not align at the same points. This prohibited individual data points from being assessed based on the seismic velocity difference relative to that point. Methods had to be developed which considered the seismic velocity difference relative to some initial measure of the seismic velocity distribution at the site. Equations 7.2 through 7.4 provide relationships that can be used in such situations.

The seismic velocity improvement factor, $SVIF$, can be defined in several different forms. Equations 7.2 through 7.4 describe three possible methods for describing this improvement factor, as follow

$$SVIF_a = \frac{\sum_{j=1}^n (\Delta v_{c,j})}{n} \quad (7.2)$$

where $\Delta v_{c,j}$ = change in seismic (compression, or p-wave) velocity at each data point
 n = number of data points

$$SVIF_b = \frac{\sum_{j=1}^n (\Delta v_{c,j})}{nv_{c,max}^{pre}} \times 100\% \quad (7.3)$$

where $\Delta v_{c,j}$ = change in seismic (compression, or p-wave) velocity at each data point
 $v_{c,max}^{pre}$ = maximum seismic velocity of the pre-grouting model
 n = number of data points

$$SVIF_c = \frac{\sum_{j=1}^n (\Delta v_{c,j})}{nv_{c,mean}^{pre}} \times 100\% \quad (7.4)$$

where $\Delta v_{c,j}$ = change in seismic (compression, or p-wave) velocity at each data point
 $v_{c,mean}^{pre}$ = mean seismic velocity of the pre-grouting tomography model
 n = number of data points

Assuming that following soil improvement measures, only increases, and no decreases, in compression wave velocity will be observed within a targeted volume, values obtained for the $SVIF$ will be greater than zero. Table 7.3 provides a summary of the values obtained for these three forms of the improvement factor relationship for all sites considered as part of this study, along with total grout takes (volumes) recorded within each site.

Table 7.3. Seismic velocity improvement factors for all sites, along with reported grout volumes injected at each site.

Site	$SVIF_a$ m/s	$SVIF_b$ %	$SVIF_c$ %	Total Grout Volume m^3 (yd^3)
Zion 1.10	454.8	7.7	45.7	3.2 (4.2)
Zion 1.5.1	-9.2	-0.2	-0.8	1.6 (2.1)
Zion 1.5.2	900.7	12.8	64.8	1.6 (2.1)
Zion 2.10	-411.1	-8.4	-33.2	11.7 (15.3)
Zion 2.5.1	-312.2	-11.4	-23.7	5.6 (7.6)
Zion 2.5.2	-424.3	-12.2	-25.8	5.6 (7.6)
Apache Trail 1	30.6	1.3	3.6	18.1 (23.6)
Apache Trail 2	212.1	9.7	26.8	25.1 (32.8)
Apache Trail 3	43.3	1.3	5.2	25.8 (33.8)
Apache Trail 4	-132.2	-2.6	-14.9	22.2 (29.1)
Apache Trail 5	0.8	0.05	0.1	7.7 (10.1)

7.2.1. Possible Explanations for Decreased Velocities following Grouting

Several possible explanations can be provided to account for the decreased seismic velocities observed following grouting which are not attributed to the tomography processing methods. Some of these potential reasons include:

- Vibrations and induced stresses caused by drilling and driving of borehole casings could have potentially disturbed the structure of the soil, including any cementation that might have previously existed within the soil.
- Excavation of thick layers of asphalt (as occurred at Zion National Park sites) and replacement with compacted fill near the surface, could have resulted in replacement with lower velocity (and less dense) material.
- Thick layers of asphalt present near the surface during pre-grouting geophysical data collection (as occurred during Zion National Park data collection) could have had an impact on quality of arrival times determined, although this interaction was unable to be decisively characterized in the analysis, resulting in higher than actual pre-grouting velocities.
- Changes in degree of saturation within the soils between pre- and post-grouting could have resulted in considerable changes in soil properties, especially values of shear modulus G which is directly related to seismic velocity. Saturation changes could have occurred due to precipitation or watering of the roadway surface which was occurring during construction operations for dust mitigation.
- Based on the fundamental relationships relating seismic p-wave velocity to shear modulus and density, changes in either of the latter two values as a result of grouting can have differing effects on the resulting value of the p-wave velocity for the soil in question. Shear modulus has been shown to be particularly sensitive to applied shear strains, which combined with the possibility of the development of large shear strains during compaction grouting operations, adds additional uncertainty to the final effect of grouting on the p-wave velocity for a soil.

7.3. 3D Spatial Analysis

The primary objective of the grouting carried out for the two case studies considered here was the stabilization of the loosest regions of the roadway subsurface, which correspond to the regions of lowest seismic velocity. One goal of a grouting verification program would be the identification of potentially loose or weak zones that remained following grouting. While the seismic velocity difference quantifications proposed provide an assessment of the average degree of improvement across the entire tomographic volume considered in the analyses, they are unable to account for potential changes in the distributions of these low-velocity regions following grouting.

An alternative approach to assessing the effectiveness of grouting programs by utilizing 3D tomography information is through three-dimensional spatial analysis methods. Spatial Analysis 3D is a user-friendly, graphical user interface (GUI) integrated with the MatLab environment that allows statistical and visual manipulations of real and simulated three-dimensional spatial point patterns (Eglen et al. 2008; Lofgreen 2011). Analyses included in Spatial Analysis 3D include those derived from the Delaunay tessellation method, including nearest neighbor and Voronoi domain analysis, autocorrelation analysis and its derived density recovery profile, as well as the related K, F, and G-functions. Spatial Analysis 3D was originally developed for the study of neuronal positioning within the central nervous system, but potential future applications in science, engineering, statistics, and mathematics had also been considered. The package was developed out of efforts to quantify the regularity and simulate patterning found in distributions of nerve cells across the retina, due to the dependence of retinal function on uniformity of nerve cell spacing.

Applying the tools available in Spatial Analysis 3D to the data available as part of this study, further quantification of the improvement made through the grouting processes considered can be made. For a set of data points in 2D, the Delaunay triangulation describes a set of lines connecting each point to its natural neighbors. A single point will have some variable number of natural neighbors, one of them being the shortest (or nearest) neighbor. A Delaunay tessellation is made up by a set of tetrahedra defined by the population of natural neighbors in the 3D case. The population of nearest neighbor distances thus becomes a useful means to describe the spatial relationship between elements in either a 2D or 3D population. Figure 7.3 shows nearest neighbor distance histograms for pre- and post-grouting tomograms having seismic velocities less than 250 m/s, where increases in the average, standard deviation, and maximum distances between points having seismic velocities less than 250 m/s are observed following grouting. These increases can be thought of as greater separations between the loosest or weakest areas of the subsurface following grouting.

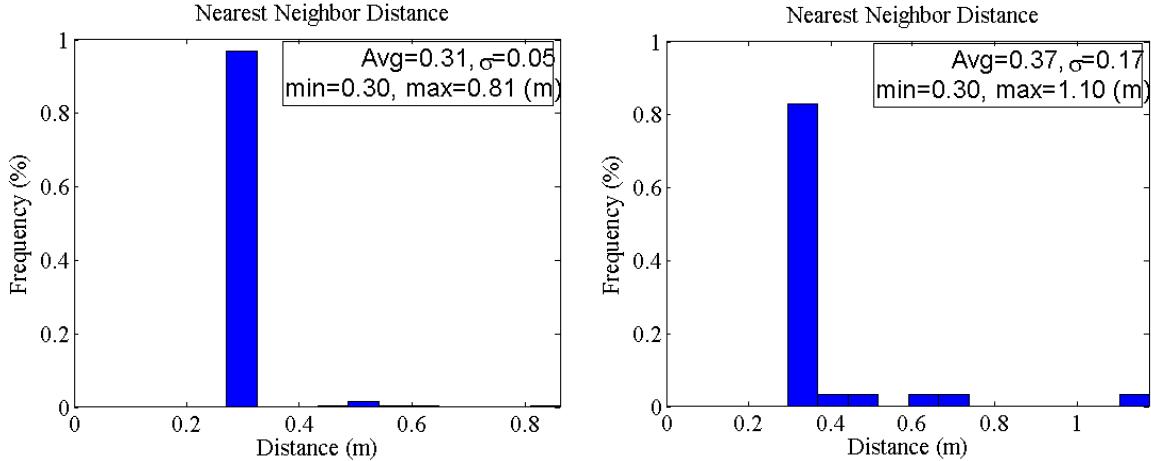


Figure 7.3. Graph. Nearest neighbor distance plots for Apache Trail Location 1 pre-grouting (left) and post-grouting (right) for seismic velocities less than 250 m/s.

The autocorrelation analysis provides a more robust three-dimensional representation of the spatial distribution of the points in data sets being considered. During the Autocorrelation calculation, each point is moved to the origin (0,0,0) and all other points are re-plotted with respect to this calculation. The tri-histogram plots shown in Figure 7.4 are one way to communicate the results of an autocorrelation analysis. The leftmost histogram, known as a density recovery plot (DRP), provides a normalized count of radial distances between points per unit volume considered. The *Spatial Analysis 3D User’s Guide* provides a further description of the tri-histogram plot:

When looking at the DRP, we are only concerned with the distance these points are from the origin, i.e. radius. There are two additional directions, however, that define the position of the points in such a plot relative to the origin, being azimuthal angle, theta, and elevation angle, phi. Together these three directions, radius, theta, and phi, make up the familiar spherical coordinate system.

For a randomly-spaced set of data, the density recovery plot would consist of bars of constant height for increasing distances from the point of interest. From the results of the autocorrelation analysis performed at Apache Trail Location 1 for seismic velocities less than 250 m/s, as shown in Figure 7.4, increased normalized densities of points can be observed following grouting, with little variation in the angles theta and phi. For this location, the results of both the nearest neighbor distance and autocorrelation analyses can be described as a tighter packing of the regions of lowest seismic velocity, and an increased spacing between those regions, following grouting at the location considered.

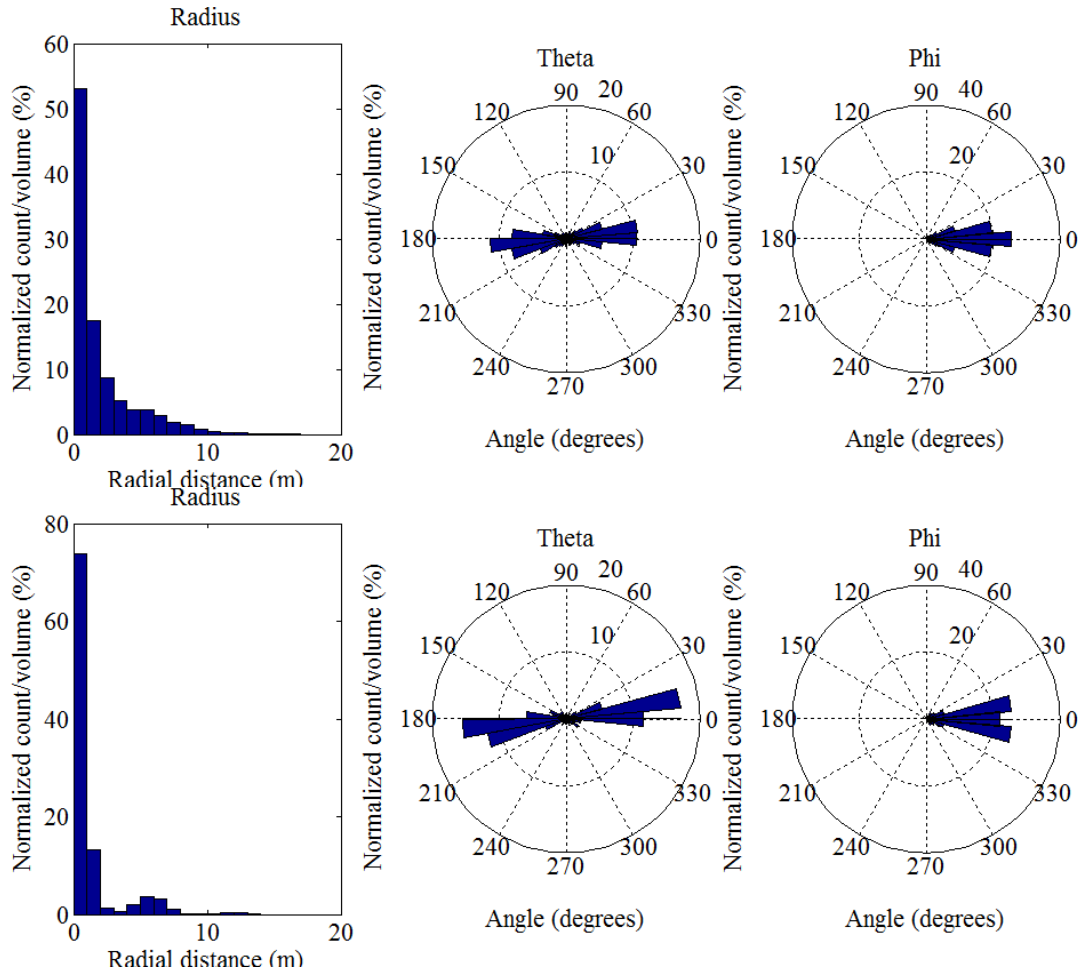


Figure 7.4. Graph. Tri-histogram plots for Apache Trail Location 1 pre-grouting (upper) and post-grouting (lower) for seismic velocities less than 250 m/s, showing a closer packing of points following grouting.

Tables 7.5 and 7.6 provide a summary of percent changes in values resulting from the nearest neighbor and autocorrelation analyses for both Apache Trail and Zion National Park sites, with percent change defined by the following relationship:

$$\% \text{ Change} = \frac{(\text{Post-grouting value}) - (\text{Pre-grouting value})}{(\text{Pre-grouting value})} \times 100\% \quad (7.5)$$

Values for the nearest neighbor distance and autocorrelation analysis at each of the sites studied are presented in Tables 7.4 and 7.5. From these values, inconsistencies in calculated percent changes are observed for the nearest neighbor distance analysis at the five locations considered at Apache Trail. Better agreement can be observed from the autocorrelation analyses, where consistent increases were found in point density due to grouting. Therefore, it can be said that for the regions of lowest seismic velocity at these sites, tighter packing of the points, corresponding to the increased densities and therefore smaller region sizes, were found after grouting, but the distances separating these regions of low velocity experienced inconsistent changes. This discrepancy may be due to the paths followed by the injected grout during the void-fill grouting operations. If a higher percentage of the injected grout migrated through an

opening or channel within the embankment, the result could potentially be a decrease in the size of the low-velocity region, without a corresponding decrease in the spacing between regions. For an ideal application of compaction grouting, increases in both nearest neighbor distances and autocorrelation analysis parameters would be expected, based on a uniform treatment of the soil volume.

Table 7.4. Summary of Spatial Analysis 3D nearest neighbor distance analyses for Apache Trail sites, with values shown for percent change from pre- to post-grouting for each parameter, for data sets having seismic velocities less than 250 m/s.

Site	Nearest Neighbor Distance Analysis (250 m/s Target Velocity), % Change			
	Average (m)	σ (m)	Minimum (m)	Maximum (m)
Apache Trail 1	19.4	240.0	0.0	35.8
Apache Trail 2	-14.9	-48.9	0.0	-39.2
Apache Trail 3	38.7	650.0	0.0	137.2
Apache Trail 4	-10.3	11.1	0.0	61.5
Apache Trail 5	0.0	-37.1	0.0	-52.4

Table 7.5. Summary of Spatial Analysis 3D autocorrelation analyses for Apache Trail sites, with values shown for percent change from pre- to post-grouting for each parameter, for data sets having seismic velocities less than 250 m/s.

Site	Autocorrelation Analysis (250 m/s Target Velocity), % Change			
	Density (m ⁻³)	Critical Density (m ⁻³)	Maximum Radius (m)	Reliability Factor
Apache Trail 1	0.075	0.209	1236	36.0
Apache Trail 2	0.174	0.209	933	83.2
Apache Trail 3	0.136	0.209	1013	65.0
Apache Trail 4	0.303	0.231	776	131.0
Apache Trail 5	0.130	0.275	1030	47.0

7.4. Comparison with 2D Seismic Refraction Results

As part of the previous geotechnical condition survey performed by AMEC Earth and Environmental, Inc. (AMEC 2007), several conventional 2D seismic refraction surveys were performed in the vicinity of the walls studied as part of this research. The purpose of these seismic refraction surveys was to evaluate the condition of the three walls identified for rehabilitation in the Fish Creek Hill vicinity of Apache Trail, to help evaluate subsurface backfill and foundation conditions. Both 5- and 10-ft (1.5- and 5-m) in-line geophone spacings were used during the seismic refraction data collection, some at the same locations. Four of these lines, as shown in Table 7.6, corresponded with the wall locations selected for 3D seismic tomography as part of this research.

Table 7.6. Summary for previous 2D and new 3D seismic surveys.

Wall Number	Corresponding 3D Site	Line Number
Wall 3	Apache Trail 1	L-9
Wall 3	Apache Trail 3	L-8
Wall 3	Apache Trail 4	L-10
Wall 1	Apache Trail 5	L-4

All surveys referenced in Table 7.6 utilized similar equipment and data collection procedures as those used in this study. Twelve geophones were used in a single 18.3 m (60 ft) long seismic line, with shots placed every 1.5 m (5 ft) between adjacent geophones. The commercially-available software SeisOpt2D was used to process the seismic refraction data. Refraction microtremor (ReMi) data was also collected along these lines, allowing for the inclusion of a shear wave velocity profile with the compression wave velocity results obtained through the 2D seismic refraction analysis. Further details relating to the surveys performed previously can be found in AMEC (2007).

The resulting distribution of p-wave velocities from the 2D seismic refraction analysis can be compared to a slice of the 3D seismic pre-grouting tomography results at the same location to consider potential similarities or differences. Figures 7.5 and 7.6 provide a comparison between the results of these two survey methods for Location 5 at Apache Trail, and Figures 7.7 and 7.8 provide the same comparison for Location 3. Similar trends in the distribution of p-wave velocities can be observed in the 2D and 3D tomography models. Several advantages and disadvantages can be extracted from the presentation of the different methods as well. For the case of the 3D tomography resulting from the GSR3D program, the higher resolution can allow for detection of anomalies such as high or low velocity regions within the soil volume as well as sloping ground surfaces. The output recovered from the SeisOpt2D analysis has the advantages of smaller numbers of velocity values to consider, as well as determination of the approximate depth of investigation resulting from the velocity inversion. For the GSR3D results, interpretation of the likely depth of reliable information is left to the user, which could potentially have unintended results in applications.

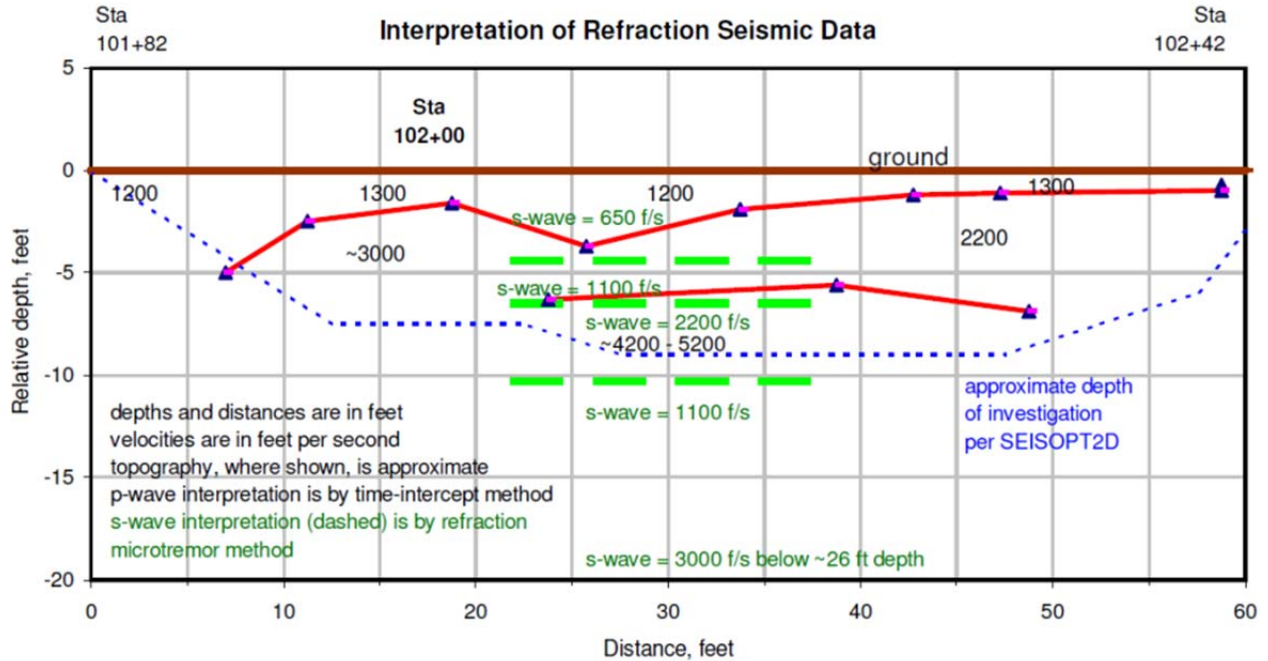


Figure 7.5. Schematic. Results from 2D seismic refraction analysis for Line 4 at Apache Trail, as performed previously by AMEC (2007) using SeisOpt2D, which corresponds to Location 5 of the 3D tomography study performed here.

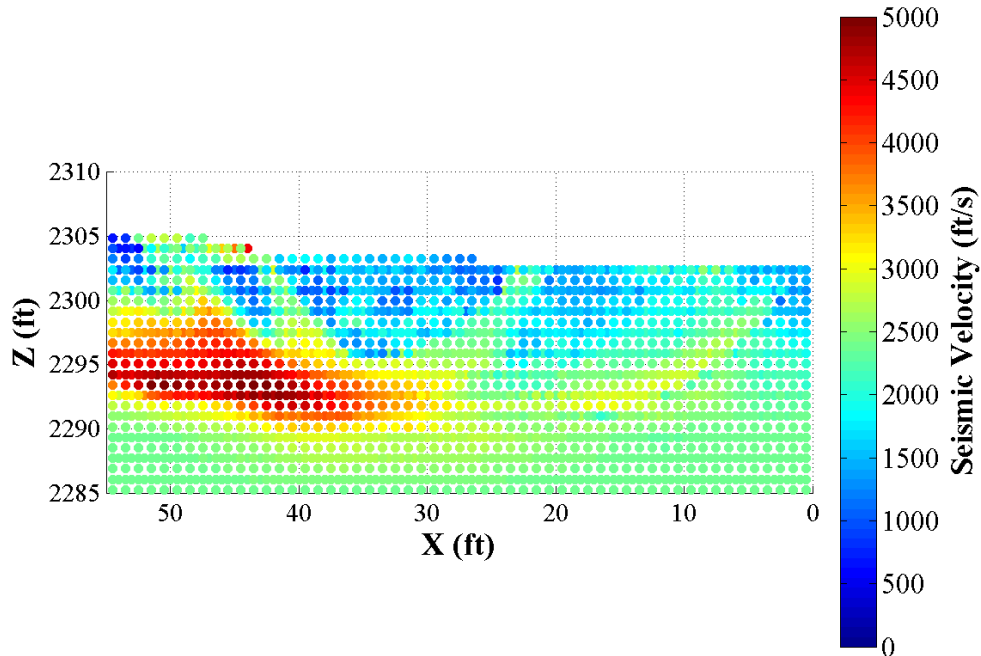


Figure 7.6. Graph. 2D slice of 3D seismic tomography results from Apache Trail Location 5, shown in the same orientation as the results from the 2D refraction survey. Slice shown for values of $-1 \text{ ft} < y < 1 \text{ ft}$ ($-0.3 \text{ m} < y < 0.3 \text{ m}$).

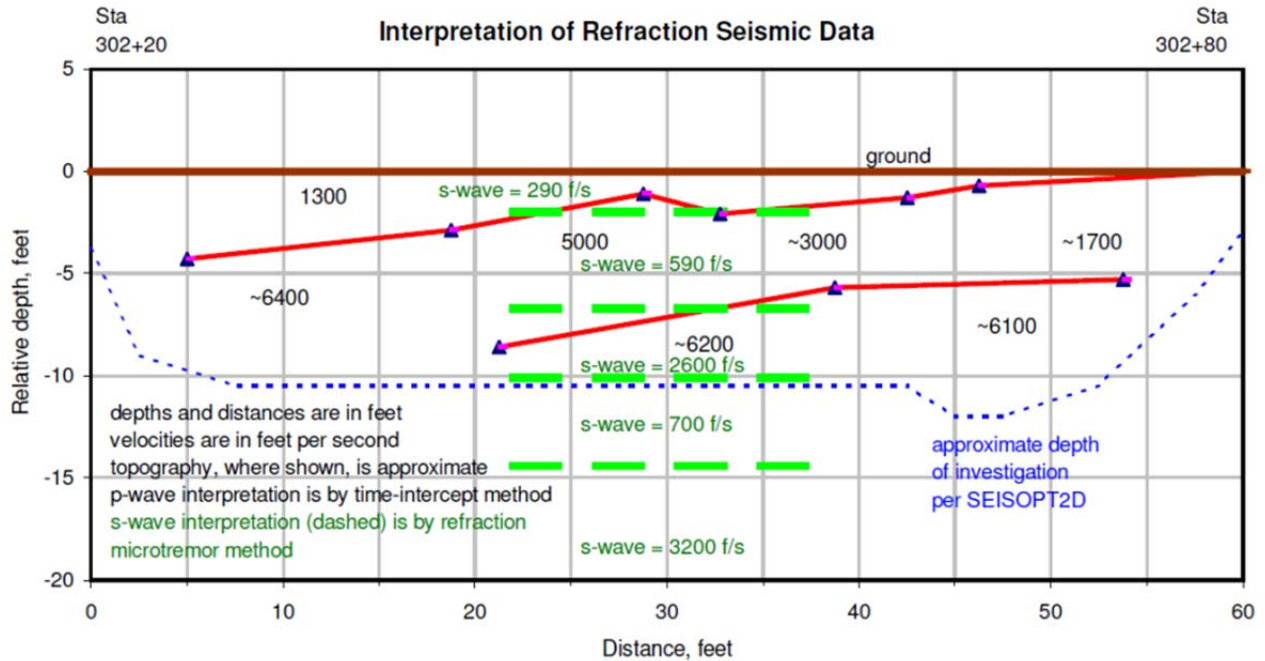


Figure 7.7. Schematic. Results from 2D seismic refraction analysis for Line 8 at Apache Trail, as performed previously by AMEC (2007) using SeisOpt2D, which corresponds to Location 3 of the 3D tomography study performed here.

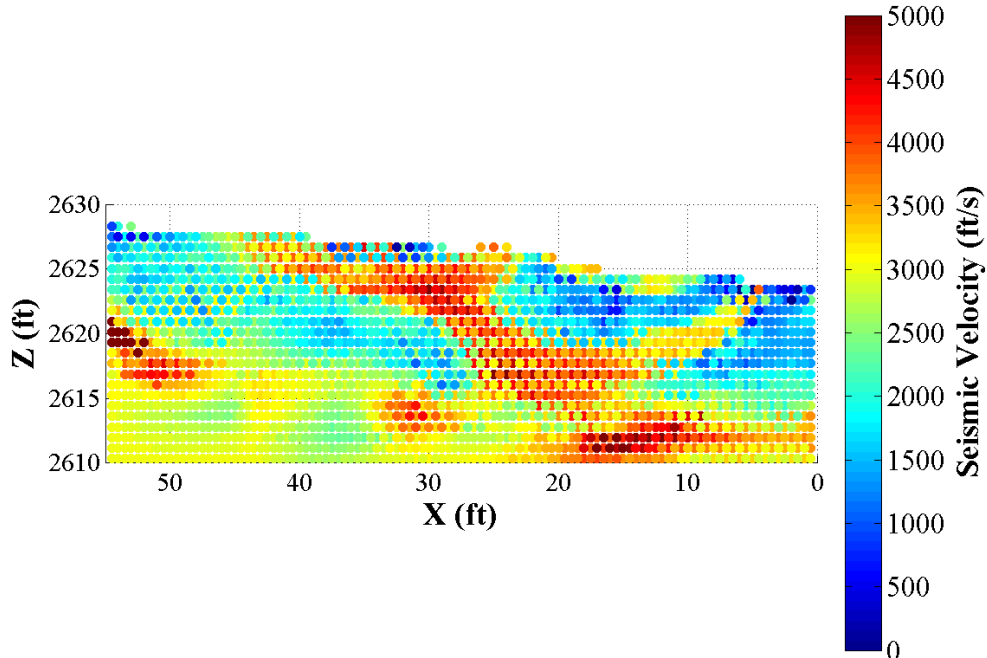


Figure 7.8. Graph. 2D slice of 3D seismic tomography results from Apache Trail Location 3, shown in the same orientation as the results from the 2D refraction survey. A slice is shown for values of $0 < y < 1.5$ ft ($0 < y < 0.5$ m).

7.5. Comparison with Consultant Findings at Zion National Park

As described in Chapter 4, Zonge International, Inc. was contracted to provide 3D seismic data collection services for the work performed at Zion National Park. In addition to data collection, Zonge was contracted to provide the raw seismic data collected, and the results of a 3D seismic tomography analysis for each of the sites studied. The details of their findings are provided by Zonge Project Report #10122 (Zonge 2011). This report summarized that while seismic data obtained was of good quality, first arrivals were obscured by the near-surface high-velocity layers present during both the pre- and post-grouting geophysical surveys. Two separate 3D seismic tomography processing software packages were investigated to process the data for this report, however, unexpected velocity decreases following grouting were observed using both processing methods.

Manual picking of each of the nearly 40,000 raypath arrival times was completed by the Contractor, with unsatisfactory signal traces discarded. GSR3D was the first program used for the seismic tomography processing, which was also the software used for the separate processing performed for this investigation. However, the Consultant chose to rely on the manual arrival time picks compiled for the collected data and manually enter those picks into the GSR3D software for the analysis, as opposed to the procedure followed for this investigation as described in Chapter 6. The second program investigated, GeoTomCG, is an alternative 3D seismic tomographic inversion program designed for civil engineering applications. The manual picks chosen by Zonge International, Inc. were again used in the processing of the pre-grouting, post-grouting, and resulting difference tomography. After consideration of the processed 3D seismic tomography obtained using both of these software packages, the Contractor also found unexpected decreases in seismic velocities throughout a majority of the tomography models following grouting operations. The Contractor noted that their determination of first arrival times for the collected data was significantly impacted by the interference of “pavement breaks,” which were due to the direct arrivals of the imparted seismic wave traveling through the high-velocity pavement layer at the ground surface. Observations included that the pavement breaks detected within the seismic data were sometimes of higher frequency and sometimes in an opposite direction as the direction of first movement. As a result, in some cases the pavement break magnified the first arrival of the refracted wave and in other cases obscured the arrival, leading to difficulties in obtaining the most accurate possible arrival times to be used in the 3D seismic processing, and likely contributing to the unexpected results obtained from their investigation.

(blank page)

8. RECOMMENDATIONS

Based on the experience gathered through this study, some general guidelines can be suggested for future investigations employing 3D seismic tomography surveys for pre- and post-grouting of roadway applications. One of the most critical recommendations that can be made would be to ensure to the highest degree of accuracy possible that locations of geophones and shots are the same for both pre- and post-grouting seismic data collection. Modern surveying instruments can be helpful in minimizing potential placement errors, especially in verifying the locations during post-grouting data collection. Due to potential site changes during construction, either related or not to grouting activities, benchmarks should be located a sufficient distance away from the survey site, or in a location determined to be safe from potential disturbance during construction activities. Adequate flagging and marking of benchmarks used for these purposes may avoid disturbance as well.

Based on the observations made for the pre-, post-, and difference tomography for the case studies considered here, a possible suggestion can be made to improve the difference tomography for investigations concerned with changes in seismic velocities before and after ground improvement. Choosing the same initial, or starting, velocity for the model for the generation of both the pre- and post-grouting tomography constructions could potentially reduce errors in velocity differences and result in a more accurate determination of seismic velocity difference tomography. For the software used in this study, the initial velocities are determined based on an averaging procedure between observed travel times and distances between shots and receivers, which could result in differences in the initial model velocities between pre- and post-grouting investigations. If these velocities are not updated in during the iterative procedure, seismic velocity differences would be observed. This situation would be of greatest concern in the regions of the tomography having the lowest ray densities, as mentioned previously.

An important question deserving of investigation is whether 2D seismic methods can be utilized more efficiently than 3D methods, and whether significant cost differences exist between the two. From the observations made during this study, 3D seismic tomography methods would be recommended for nearly all cases where 2D methods may be considered. Cost differences will likely only result from increased data collection requirements for 3D. For example, traditional 2D seismic refraction typically employs 12 geophones, 1 seismograph, and from anywhere from 5 to 15 or more shot locations per line. Compared to the 48 geophones, 2 seismographs, and 45 to 69 shot locations per grid used in this study, a greater investment in time and equipment can be observed for the 3D seismic tomography method as used here. However, 3D methods can be utilized using smaller quantities and densities of data. Software has been available for the processing of 2D data for many years, and has experienced many improvements and decreases in cost over that time. While currently, costs associated with 3D seismic tomography processing may be higher than those associated with 2D processing, this cost gap may close between the two approaches as additional programs and versions become available.

Table 8.1. Considerations for and potential limitations to performing 3D seismic tomography for grouting verification of roadway applications.

Site Conditions	Saturated soil limitations Pavement thickness (can be variable across a site) Depth to bedrock Adjacent structures, especially historic or sensitive
Environmental	Background noise due to weather (wind), construction or public traffic Impact of noise and vibrations generated during data collection on environment
Access	Maintenance of traffic during data collection Changing site layout, including roadway elevation, due to construction operations
Documentation	Photographs and detailed notes describing shot and receiver locations should be used extensively in addition to surveying
Data Processing	Method of first arrival picks (consistency)
Labor and Equipment	Attempt to use same technicians, engineers, and equipment for pre- and post-grouting seismic investigations

8.1. Changes to Design of 3D Seismic Tomography Grouting Verification Programs

General guidelines for layout of 3D seismic refraction grids can be proposed based on the experiences gathered during this study. Maintaining straight and parallel lines for all seismic line layouts, regardless of grout injection points or roadway alignment, is highly suggested not only to ease equipment layout but also avoid unnecessary confusion or mistakes made during the data processing stage. While sloping ground surfaces do not create any particular challenges to the 3D seismic processing methods explored here, maintaining geophone and shot locations in a relatively planar orientation may provide for the most simplified data collection possible, especially at sites with difficult terrain. The benefits obtained from the use of “downslope” shots, those shots collected at the base of the retaining walls like those found at the study sites considered here, may not outweigh the added time, cost, and safety risks associated with their collection. While 3D seismic tomography processing software such as GSR3D is capable of considering geophone and shot locations at different elevations, maintaining consistency and simplicity in geophone and shot layouts, with consideration of site specific conditions, is recommended for future investigations.

8.2. Cost Comparison between Sites

Costs for verification of grouting operations based on the methods utilized here will vary widely. Consideration should be given to the most sensitive or critical locations, where grouting operations may be of greatest concern, to select the locations where these verification techniques should be performed. From the experiences gained through this study, costs should not vary considerably for different geophone spacings used, as long as the capacity of the equipment selected (seismic takeout line geophone interval, for example) is not exceeded. For larger geophone spacings, additional time will be required between shot collections due to the larger

distances between shots, and accompanying travel between locations, which could potentially be offset by including fewer shots in the survey at the expense of decreased raypath densities.

Significant savings can potentially be realized by using 3D seismic tomography methods as opposed to conventional methods such as CPT or SPT when the locations being considered for verification are remote or difficult to access. In these cases, mobilization costs for the large or specialized drilling and sampling equipment required for these conventional methods may significantly outweigh those for a seismic investigation.

8.3. Effect of Different Geophone Spacings

One goal of the investigation at the Zion National Park sites was to assess the influence of in-line geophone spacing on the effectiveness of the verification methods used as part of this study. Both 5- and 10-ft (1.5- and 3-m) in-line geophone spacings were used to investigate possible benefits of using smaller geophone spacings to conduct shallow 3D seismic surveys. Due to the unexpected difficulties encountered at the Zion National Park sites, providing any conclusive recommendations relating to this question proved more difficult than anticipated. The large regions of decreased velocities observed for many of the Zion National Park tomography models, and the resulting uncertainties associated with those decreases, raised concerns about attempting to provide any definite conclusions as to the influence of geophone spacing on the quality of the results.

Considering that for the sites studied, as nearly identical numbers of geophones and shots were employed, for smaller geophone spacings, higher raypath densities could be expected within the soil volume. This would provide increased resolution and confidence in the final tomography model, as long as confidence in signal and first arrival time quality was certain. Alternatively, the effective depth of a seismic investigation can be said to increase as the largest dimension of the geophone spread increases. Therefore, for any project considering the use of either 2D or 3D seismic methods for verification of grouting in the future, tradeoffs will have to be made between the number of geophones and shots used, and the resolutions and depths of the tomography desired.

From the results of this study, some observations can be made between the smaller 5-ft (1.5-m) and larger 10-ft (3-m) in-line geophone spacings used at the Zion National Park locations, with consideration given to some of the unexpected results obtained. A possible advantage of the larger spacings, increased effective depth of investigation, was not observed, as similar depths of reported ray densities can be noted between the different spacings. The depths of the reported ray densities at the Zion National Park locations also corresponds closely with the known shallow depths to bedrock at the site, which will to a large extent limit the effective depth of a seismic investigation. For sites with much deeper soil profiles, some advantage may be obtained by utilizing larger geophone spacings, allowing for longer overall geophone line spreads.

Differences in resolutions between the two spacings were found at one of the grids but not at the other. For grid #1, the larger spacing was found to have a 2-ft (0.6-m) resolution while the smaller spacing resulted in finer 1-ft (0.3-m) resolutions. For grid #2, no difference in resolution was determined for the different spacings, with 2-ft (0.6-m) resolutions determined for both

spacings. Further investigation of the potential benefits of alternative geophone spacings for use in these types of shallow 3D seismic applications is warranted, with the hopes of understanding with more certainty the most efficient geophone spacings and layout to be used for future investigations of this type.

8.4. Improvements to Quality Assurance and Quality Control Programs

Potential modifications can be made to contracting procedures and plans and specifications relating to 3D seismic tomography verification of grouting operations to produce the highest quality product for the owner as the result of grouting and verification. Real-time monitoring of injection parameters can be required to be submitted, at a reasonable expense to the contractor performing the work, who may already possess the necessary equipment to collect this data. Better involvement of project managers and geotechnical engineers during compaction grouting operations can ensure that any changes made to the grouting plan during the course of the work are consistent with the overall intention of the grouting program. Prequalification of geophysical contractors can be used in the verification process to ensure the collection of high quality seismic data, consistency in field procedures followed, and reliable tomography processing and presentation. Performance-based payments, in lieu of quantity-based payment structures are also a potential option to be considered in this respect.

Changes to performance-based specifications can be considered for 3D seismic tomography applications, where one potential method could consider load ratios and pay factors based on quantitative relationships between pre- and post-grouting tomography, such as the volumetric improvement factors proposed here. The load ratio can be defined as the actual value determined for a particular material property, such as asphalt strength or seismic velocity increase, divided by the desired value of that property following the completion of work. The load ratio can also be substituted by a range of desired material properties resulting from the work performed corresponding to the associated pay factors. Table 8.2 shows one possible structure to such a system, which could be used to adjust payments for work performed based on the results of 3D seismic tomographic analysis of the site, and can be weighted for different circumstances. Such a system would provide grouting contractors financial incentive to create the greatest amount of improvement possible.

Table 8.2. Pay scale for potential inclusion into performance-based specifications for grouting work.

Seismic Volumetric Improvement Factor (SVIF_a), m/s	Pay Factor
SVIF < -100	0.90
-100 < SVIF < -50	0.95
-50 < SVIF < 50	1.00
50 < SVIF < 100	1.10
SVIF > 100	1.20

As a way to assist engineers in determining whether 3D seismic tomography-based verification methods should be considered for a given project, a basic framework can be proposed to aid in scoring the sensitivity and potential risks of the project. Such a framework is provided in Tables 8.3 and 8.4. This system can potentially be utilized as a starting point for determining applicable verification methods for different grouting projects, and can easily be modified to consider different scoring criteria or weighing in the scoring process.

Table 8.3. Scoring rubric framework for grouting programs.

	Criteria	(1)	(2)	(3)	Points
1	Traffic volume	ADT < X	X < ADT < XX	XX < ADT	
2	Risk to public	Low	Medium	High	
3	Risk to critical lifeline infrastructure	Low	Medium	High	
4	Prequalified compaction grouting contractor	Yes	Yes	No	
5	Historical significance of adjacent structures	Low	Medium	High	
6	Cost of compaction grouting to removal and replacement of soil	Low	Medium	High	
Total Score					

Table 8.4. Verification method hierarchy for grouting programs.

		Score	< 3	3-6	7-10	11-14	15-18	>18
Potentially Applicable Verification Method	Manual injection parameter logging		•	•	•	•	•	•
	Ground heave criteria		•	•	•	•	•	•
	Grouting intensity number (GIN)		•	•	•	•	•	•
	Geotechnical field testing (CPT, SPT)					•	•	•
	Test injections with excavation					•	•	•
	Continuous injection parameter monitoring					•	•	•
	3D seismic tomography					•	•	•

8.5. Use of Pre-Grouting Tomography for Design of Grouting Plans

Pre-grouting tomography can potentially be utilized by geotechnical engineers during the grouting design. From the pre-grouting tomography, areas having the lowest seismic velocities

can be identified, and grouting operations can be concentrated in the areas most needing improvement. Additionally, areas showing the highest seismic velocities can be avoided in some cases, to prevent these areas from being discovered in the field during grouting and expending unnecessary time and resources. In situations where bedrock is much shallower than grouting would allow, drilling and driving of casing for unnecessary injection holes can be avoided, reducing costs and maximizing the grouting effectiveness. This method can be achieved as long as the turn-around time required for processing the pre-grouting tomography is relatively quick. Generally, as long as sufficient flexibility is provided in the contracts and specification for the grouting work, the locations of injection holes can be modified prior to the commencement of work, especially if sufficient information is made available in time to warrant modification. This process would, however, require the pre-grouting and post-grouting tomography to be processed and analyzed separately.

8.6. Future Work

One potential question that has arisen as a result of the work performed for this investigation is whether 3D seismic refraction techniques can be applied to other ground improvement methods such as dynamic or vibro-compaction, or other underground construction operations, as a way to reliably verify effectiveness. While the answers to these questions exist outside the scope of this study, many potentially useful extensions of the technology and data analysis methods explored here can be made in additional areas of ground improvement.

A variety of technologies currently exist for developing 3D seismic tomography using subsurface sources or receivers (downhole and crosshole seismic). Many of the challenges characteristic to surface-based 3D tomography methods employed in this study, such as those related to surface layer interference during data collection, are not found in the subsurface-based methods, which often produce higher-quality data due to the decreased influence of environmental factors. Instead of relying upon arrival times to be recovered from refracted waves, down-hole and cross-hole methods can utilize the propagation of direct compression waves to characterize the spatial variation in wave velocities in three dimensions. The methods explored here for the analysis of pre- and post-grouting data analysis are applicable to any 3D seismic tomography results regardless of the data collection and processing methods used to develop that tomography.

One potential area for development of future grouting verification technology relates to real-time monitoring. Several challenges must be overcome before real-time 3D seismic tomography techniques can be practically applied to compaction grouting programs. Many ground improvement methods attempt to achieve densification, or rearrangement, of soil particles, which generally requires energy to be transferred into the soil. This process, whether through vibro-methods, injection of grout, or otherwise, introduces energy into the ground mass, which can influence the seismic wave data collection process. Conflicting noise can result not only from the direct application of the ground improvement, as in dynamic compaction for example, but also from the energy imparted by supporting activities such as equipment or worker movement, which would exist during any real-time seismic data collection efforts.

Further study can also be made into the qualitative methods that can be used to assess the volumetric improvements due to grouting activities, potentially employing more advanced

statistical methods than those utilized here. Recommendation is also given to any future work to attempt to secure pre- and post-grouting geotechnical field testing data, such as CPT or SPT, to correlate with the results of the 3D seismic tomography. Another potentially useful investigation could combine the methods employed here with physical verification methods such as test injection and excavation sites. This would allow the results obtained from the post-grouting tomography to be compared with the actual locations and distributions of injected grout in the ground. Forward modeling techniques can also be employed to include known velocities into the starting model for specific regions at the start of tomography generation. The velocities and locations for these regions can be obtained through a variety of methods including drilling and sampling during an SPT investigation, correlation with CPT results, or known locations of structures such as retaining walls, foundations, or utilities. While the retaining walls adjacent to the sites considered in this study were not likely to have had an influence on the resulting tomography due to their location outside of the tomographic volume, in some cases, the presence of such structures within the model boundaries would have a considerable influence on the results, which could be considered through the use of forward modeling.

Lastly, based on the observations made during this study, potential relationships between changes in ray densities and changes in velocities before and after grouting could be better understood through further investigation. A useful starting point for such an assessment could involve a redetermination of the tomography for the sites considered here, based on identical initial velocity models for pre- and post-grouting cases. Maintaining a constant initial velocity for the tomography may have significant influence on determined velocity differences, especially velocity decreases, and could potentially increase the overall confidence in the difference tomography through a better knowledge of the relationship between ray densities, initial velocities, and velocity differences.

(blank page)

9. CONCLUSION

Successful use of 3D seismic tomography for assessment of grouting programs for roadway applications does not come without some considerable practical challenges. Potential roadway applications should thoroughly investigate asphalt depths and reconsider seismic use if these depths are significant. Limitations inherent to traditional 2D seismic refraction, including those related to saturated soils, must also be considered for these investigations. However, the three-dimensional wave propagation method used has been shown to have considerable advantages compared to traditional 2D seismic refraction analysis, especially for characterization of volumetric improvement resulting from grouting operations. Large amounts of information can be retrieved relatively quickly and processed efficiently when data quality is good, allowing for subsurface characterization in ways that are unachievable by conventional point-based, intrusive testing methods. As for any other tool available to engineers, considerable emphasis should be given to the adequate use of engineering judgment during the interpretation of any results obtained. Familiarity with not only grouting operations and soils and site conditions, but also geophysical and seismic data collection and tomographic processing procedures, are essential prerequisites for successful interpretation of results such as those presented here.

Grouting programs that follow traditional compaction grouting procedures involving the high-pressure injection of grout have shown more promise for this method due to the volumetric improvement created within the soil mass as well as the grout volumes created during the ground improvement process, but confirming this potential through this study proved challenging due to unexpected condition encountered in the field. Where grouting is used to fill voids alone or permeate locally through loose soil, the ability of this 3D seismic tomography to communicate the resulting improvement has been shown to be limited, as dimensions of voids filled with grout may be less than the resolution of the tomography. The greatest potential for 3D seismic tomography lies in complementing traditional quality assurance testing to allow for a more complete understanding of the degree of improvement resulting from grouting, which may be feasible for only the most sensitive or high-risk projects.

The fundamental basis of 3D seismic tomography technology has been proven through a variety of case studies and conditions to be a viable and useful extension of geophysical methods to civil engineering applications. Significant interest has been noted throughout this study by researchers, contractors, and designers in further developing 3D tomographic methods for innovative uses. At one time, the rate at which such technologies could advance was largely limited by available computing power and electronic equipment. Today, however, many of those restrictions have been removed through the rapid advancement of computer technologies, abilities, and ease of use. Further advancement of these methods will therefore rely largely on the creativity of geophysicists and engineers, together with the support and encouragement of upper-level management, toward achieving further advancements in understanding and development of this field.

(blank page)

REFERENCES

- Abdelrahman, G.E., Abdelbaki, M.S., Baligh, F.A. (2003). "Compaction grouting in sand." *Civil Engineering Research Magazine*, Al-Azhar University, Vol. 25.
- American Society of Civil Engineers (1995). "Verification of grouting." Geotechnical Special Publication 57. Michael J. Byle and Roy H. Borden, eds. ASCE, Reston, VA.
- American Society of Civil Engineers (2010). "Compaction grouting consensus guide." *Standard ASCE/G-I 53-10*. ASCE, Reston, VA. 79 p.
- AMEC Earth and Environmental, Inc. (2007), "Geotechnical Conditions Surveys and Engineering Evaluations, Fish Creek Hill Retaining Walls, State Route 88, Milepost 222-226, TRACS No. H6920 01D, Maricopa County, Arizona," February 12, 2007, AMEC Project 6-117-001048. Tempe, AZ.
- Anon. (1987). *Specifications and Application Handbook, 10th Edition*. Komatsu, Akasaka, Minato-ku, Tokyo, Japan.
- Anon. (1988). *Caterpillar Performance Handbook, 19th Edition*. Caterpillar, Peoria, IL.
- ASTM D5777-00. Standard guide for using the seismic refraction method for subsurface investigation.
- Baker, W., Cording, E., and MacPherson, H. (1983). "Compaction grouting to control ground movements during tunneling." *Underground Space*, 7: 205-212.
- Baez, J.I. and Henry, J.F. (1993). "Reduction of liquefaction potential by compaction grouting at Pinopolis West Dam, SC." *Geotechnical Practice in Dam Rehabilitation*, GSP No. 35, ASCE, Reston, VA: 493-506.
- Bandimere, S. (1999). "LMG geotechnical/structural information requirements," *CIGMAT Conference Proceedings*, March 5, 1999.
- Boulanger, Ross W. and Hayden, Robert F. (1995). "Aspects of compaction grouting of liquefiable soil." *J. of Geotechnical Engineering*. 121(12): 844-855.
- Brown, D.R. and Warner, J. (1973). "Compaction grouting." *J. of Soil Mech. And Found. Div.*, ASCE. 99(8): 589-601.
- Bruce, D.A. and Dugnani, G. (1994). "Innovations in American grouting practice." *International Symposium on Anchoring and Grouting Techniques*. 7-10 December 1994. Guangzhou, China. 21 p.
- Červený, V. (2001). *Seismic Ray Theory*. Cambridge University Press, Cambridge, UK. 713 p.
- El-Kelesh, A.M. and Matsui, T. (2008). "Calibration Chamber Modeling of Compaction Grouting." *Geotechnical Testing Journal*. 31(4): 295-370.

-
- Eglen, S.J., Lofgreen, D.D., Raven, M.A., and Reese, B.E. (2008). "Analysis of spatial relationships in three dimensions: tools for the study of nerve cell patterning." *BMC Neuroscience*. 2008 Jul 21. 9:68.
- FHWA CFLHD (2003). "Application of geophysical methods to highway related problems." Contract No. DTFH68-02-P-00083. September 2003. 742 p.
- Geraci, J. (2007). "Time-history compaction grouting data obtained through instrumentation." *Grouting for Ground Improvement: Innovative Concepts and Applications*. GSP No. 168. ASCE, Reston, VA: 1-12.
- Graf, E.D. (1969). "Compaction grouting technique and observations." *J. of Soil Mech. And Found. Div., ASCE*. Vol. 95.
- Graf, E.D. (1992). "Compaction grout." *Grouting, Soil Improvement and Geosynthetics*, Geotechnical Special Publication 30. ASCE, Reston, VA: 275-287.
- Hanson, D.R., Haramy, K.Y., and Neil, D.M. (2000). "Seismic tomography applied to site characterization." *Use of Geophysical Methods in Construction*, Geotechnical Special Publication 108. ASCE, Reston, VA: 65-79.
- Haramy, K.Y. (2006). "Structural capacity evaluation of drilled shaft foundations with defects." MS Thesis, University of Colorado at Denver, Denver, CO. 389 p.
- Haramy, K.Y., Henwood, J.T., and Szyrakiewicz, T. (2009). "Assessing the effectiveness of compaction grouting using seismic methods." *Contemporary Topics in Ground Modification, Problem Soils, and Geo-Support*, GSP No. 187, ASCE, Reston, VA: 241-248.
- Hardin, B.O. and Drnevich, V.P. (1972). "Shear modulus and damping in soils: design equations and curves." *J. of the Soil Mechanics and Foundations Division, Proceedings of the American Society of Civil Engineers*. July: 667-692.
- Hausler, E.A. and Sitar, N. (2001). "Performance of soil improvement techniques in earthquakes." *Proc. of the 4th Int'l Conf. on Recent Advances in Geotechnical Earthquake Engr. and Soil Dynamics*, San Diego, Paper 10.15.
- Holmquist, D.V., Thomas, D.B., and Simon, K. (2003). "Subsidence mitigation using void-fill grouting." *Advances in Grouting and Ground Modification*, GSP No. 104, ASCE, Reston, VA: 1103-1114.
- Kramer, S.L. (1996). *Geotechnical Earthquake Engineering*. Prentice Hall, Upper Saddle River, NJ. 653 p.
- Kleyner, I. and Krizek, R. (1995) "Mathematical model for bore-injected cement grout installations." *J. of Geotech. Engr.* 121(11): 782-788.
- Lofgreen, D.D. (2011) *Spatial Analysis 3D User's Guide*. Accessed 21 April 2011. <http://www.nri.ucsb.edu/Labs/breese/SA3D.html> 98 p.
-

-
- Lowrie, W. (1997). *Fundamentals of Geophysics*. Cambridge University Press, Cambridge, UK. 355 p.
- Miller, E.A., and Roycroft, G.A. (2004). "Compaction grouting test program for liquefaction control." *J. Geot. and Geoenv. Eng.*, 130(4): 355-361.
- Mitchell, J.K., Baxter, C.D.P. and Munson T.C. (1995). "Performance of improved ground during earthquakes." *Soil Improvement for Earthquake Hazard Mitigation*. Geotechnical Special Publication No. 49, ASCE, Reston, VA: 1-36.
- Mitchell, J.K., Cooke, H.G. and Schaeffer J. (1998). "Design considerations in ground improvement for seismic risk mitigation." *Proceedings of Geotechnical Earthquake Engineering and Soil Dynamics III*, Seattle, 1, 580-613.
- Muller, R., and Bruce, D.A. (2000) "Equipment for cement grouting: an overview," *Advances in Grouting and Ground Modification*, GSP No. 104, ASCE, Reston, VA: 155-172.
- National Cooperative Highway Research Program (2006). *Use of Geophysics for Transportation Projects, Synthesis 357*. Transportation Research Board: Washington, D.C. 108 p.
- Nichols, S.C. and Goodings, D.J. (2000). "Physical model testing of compaction grouting in cohesionless soils." *J. of Geotech. and Geoenviron. Engr.* 126(9): 848-852.
- Nichols, S.C. and Goodings, D.J. (2000). "Effects of grout composition, depth and injection rate on compaction grouting," *Advances in Grouting and Ground Modification*, Geotechnical Special Publication No. 104, ASCE, Reston, VA: 16-31.
- Orense, R.P. (2008). "Liquefaction remediation by compaction grouting." *2008 NZSEE Conference Proceedings*, Wairakei, New Zealand, 11-13 April. Paper No. 50.
- Park, C.B., Ivanov, J., Miller, R.D., Xia, J., Ryden, N. (2001). "Seismic investigation of pavements by MASW method—geophone approach." *Proceedings of the SAGEEP 2001*, Denver, RBA-6. <http://www.kgs.ku.edu/Geophysics2/Pubs/Pubs/PAR-01-03.pdf>; Accessed 18 March 2011.
- Rucker, M.L. and Ferguson, K.C. (2006). "Characterizing unsaturated cemented soils profiles for strength, excavatability and erodability using surface seismic methods," *Unsaturated Soils 2006*, Geotechnical Special Publication No. 147, Miller, G.A., Zapata, C.E., Houston, S.L. and D.G. Fredlund, eds., ASCE, Reston, VA: 589-600.
- Rutledge, F.A., Mauldon, M., and Smith, C.J. (2005). "Geophysical primer for geotechnical engineers." Center for Geotechnical Practice and Research, Virginia Polytechnic Institute and State University. Blacksburg, VA. June, 2005. 124 p.
- Schmertmann, J.H. and Henry, J.F. (1992). "A design theory for compaction grouting." *Grouting, Soil Improvement and Geosynthetics*, Geotechnical Special Publication 30, ASCE, Reston, VA: 215-228.
-

-
- Schuyler, J.N., and Gularte, F. (2008). "Automated tiltmeter monitoring of bridge response to compaction grouting." *Proc. of SPIE's 7th Annual Int'l Symposium on Smart Structures and Materials*. March, 2000. p. 1-8.
- Seed, H.B. and Idriss, I.M. (1970). "Soil moduli and damping factors for dynamic response analyses." EERC Report No. EERC-70-10, Berkeley, CA.
- Sirles, P., Rock, A., and Haramy, K. (2006). "Advancements in subsurface modeling using seismic refraction data." *19th EEGS Symposium on the Application of Geophysics to Engineering and Environmental Problems*. 19 p.
- Spaulding, C., Masse, F., and LaBrozzi, J. (2008). "Ground improvement technologies for a sustainable world." *GeoCongress 2008: Geosustainability and Geohazard Mitigation*, Geotechnical Special Publication 178, ASCE, Reston, VA: 891-898.
- Strauss, J., Dahncke, D., and Nonamaker, F., (2004). "Compaction grouting to mitigate settlement beneath approach fills, CA SR73 at Laguna Canyon Road." *Geot. Engr. for Transport. Projects, Proc. of Geotrans 2004*, ASCE. 1876-1883.
- United States Army Corp of Engineers (1995). "Geophysical exploration for engineering and environmental investigations." Report EM 1110-1-1802. 31 August, 1995. Washington, D.C., 208 p.
- United States Army Corp of Engineers (2008). "Grouting technology." EM 1110-2-3506, 30 May 2008. Washington, D.C., 640 p,
- van der Veen, M, Spitzer, R., Green A.G., Wild, P. (2001). "Design and application of a towed land-streamer system for cost-effective 2D and pseudo-3D shallow seismic data acquisition." *Geophysics* 66(2): 482-500.
- Warner, J., Schmidt, N., Reed, J., Shepardson, D., Lamb, R., and Wong, S. (1992). "Recent advances in compaction grouting technology." *Grouting, Soil Improvement, and Geosynthetics*, GSP No. 30, ASCE, Reston, VA: pp. 252-264.
- Warner, James. (2003). "Fifty years of low mobility grouting." *Advances in Grouting and Ground Modification*, GSP No. 104, ASCE, Reston, VA: 1-24.
- Warner, J. (2004). *Practical Handbook of Grouting*. John Wiley and Sons, Inc., Hoboken, N.J., 700 p.
- Warner, J. (2007). "Proper grout rheology assures quality work." *Grouting for Ground Improvement: Innovative Concepts and Applications*. GSP No. 168. ASCE, Reston, VA: 1-12.
- Warner, James. (2010). "Grouting fundamentals and current practice." *31st Annual Short Course on Grouting Fundamentals and Current Practice*. Colorado School of Mines, Golden, CO. June, 2010.
-

-
- Weaver, K.D. (2000). "A critical look at use of "rules of thumb" for selection of grout injection pressures," *Advances in Grouting and Ground Modification*, GSP No. 104, ASCE, Reston, VA: 173-180.
- Welsh, J.P. and Burke, G.K. (2009). "Advances in grouting technology." *Hayward Baker Library*. <http://www.haywardbaker.com>. Accessed December 4, 2010.
- Wong, H.Y. (1974). "Discussion of compaction grouting, by Douglas R. Brown and James Warner." *J. of Soil Mech. And Found. Div., ASCE*. 100(5), 556-559.
- Yang, X. and Zou, J. (2009). "Estimation of compaction grouting pressure in strain softening soils." *J. Cent. South Univ. Technol.* 16: 653-657.
- Yeh and Associates, Inc. (2008) "Final Geotechnical Report: Zion-Mount Carmel Highway Switchbacks Landslide, Zion National Park, Utah, UT PRA ZION 99(1)," May 6, 2008, YA Project Number 27-354, Denver, Colorado.
- Yeh and Associates, Inc. (2009), "Addendum to Geotechnical Investigation Report: Zion National Park Landslide, UT PRA ZION 10(5) & 10(6), Zion National Park, Utah," April 8, 2009, YA Project Number 28-220, Durango, Colorado.
- Zonge International, Inc. (2011). "Geophysical Survey Report, Zion National Park, Springfield, Utah." Zonge Project #10122, March, 2011. Lakewood, CO.

(blank page)

APPENDIX A – LOCATION MAPS AND PLAN DRAWINGS



Figure A.1. Map. Location map of Zion National Park project site.

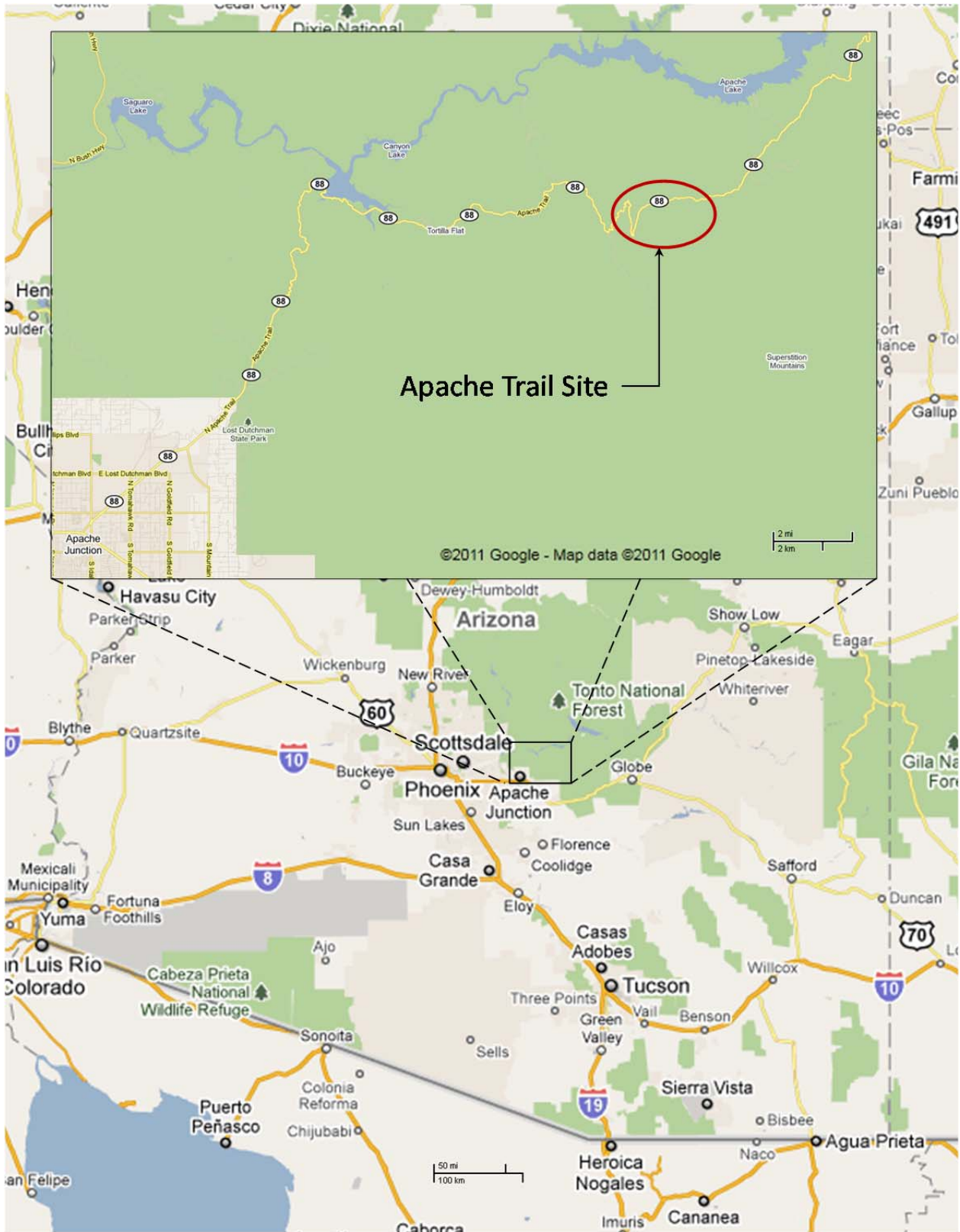


Figure A.2. Map. Location map of Apache Trail project site.

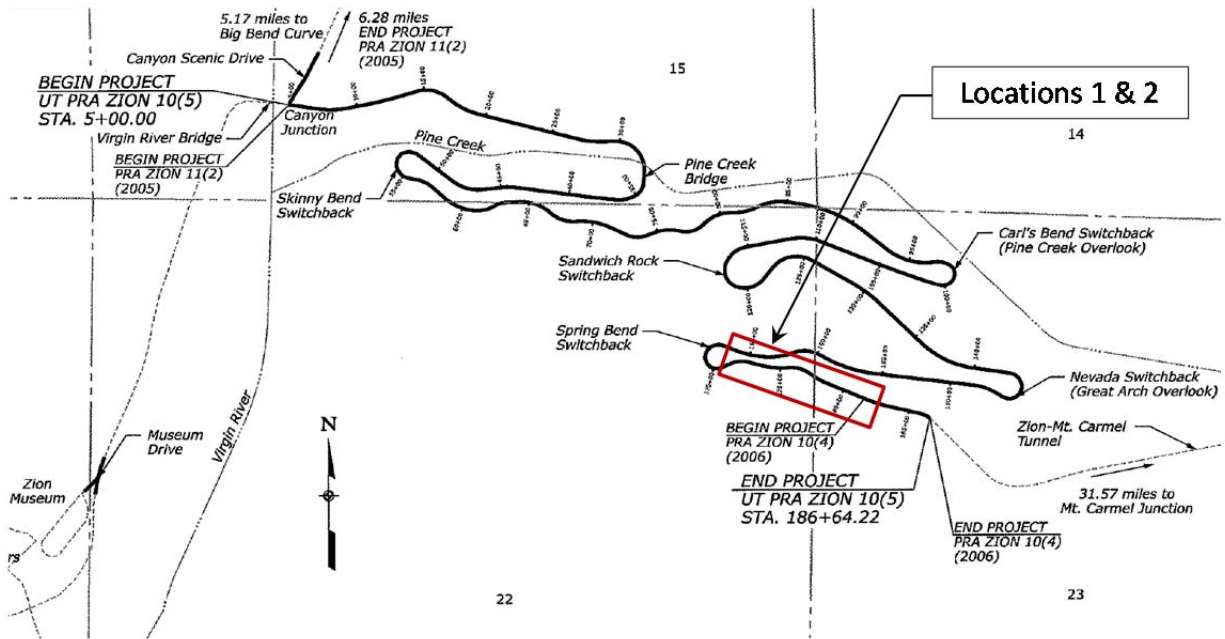


Figure A.3. Schematic. Plan drawing detail of Zion National Park project site.

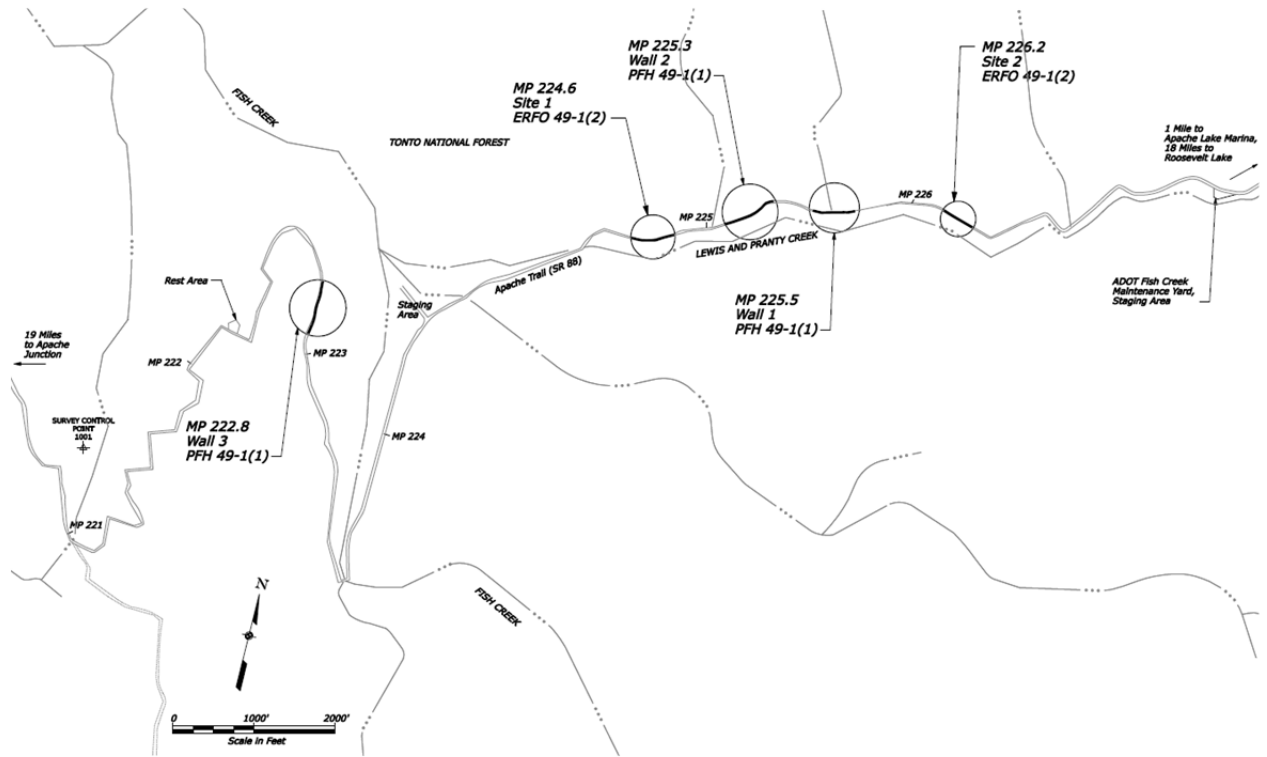


Figure A.5. Schematic. Plan drawing detail of Apache Trail project site.

APPENDIX A – LOCATION MAPS AND PLAN DRAWINGS

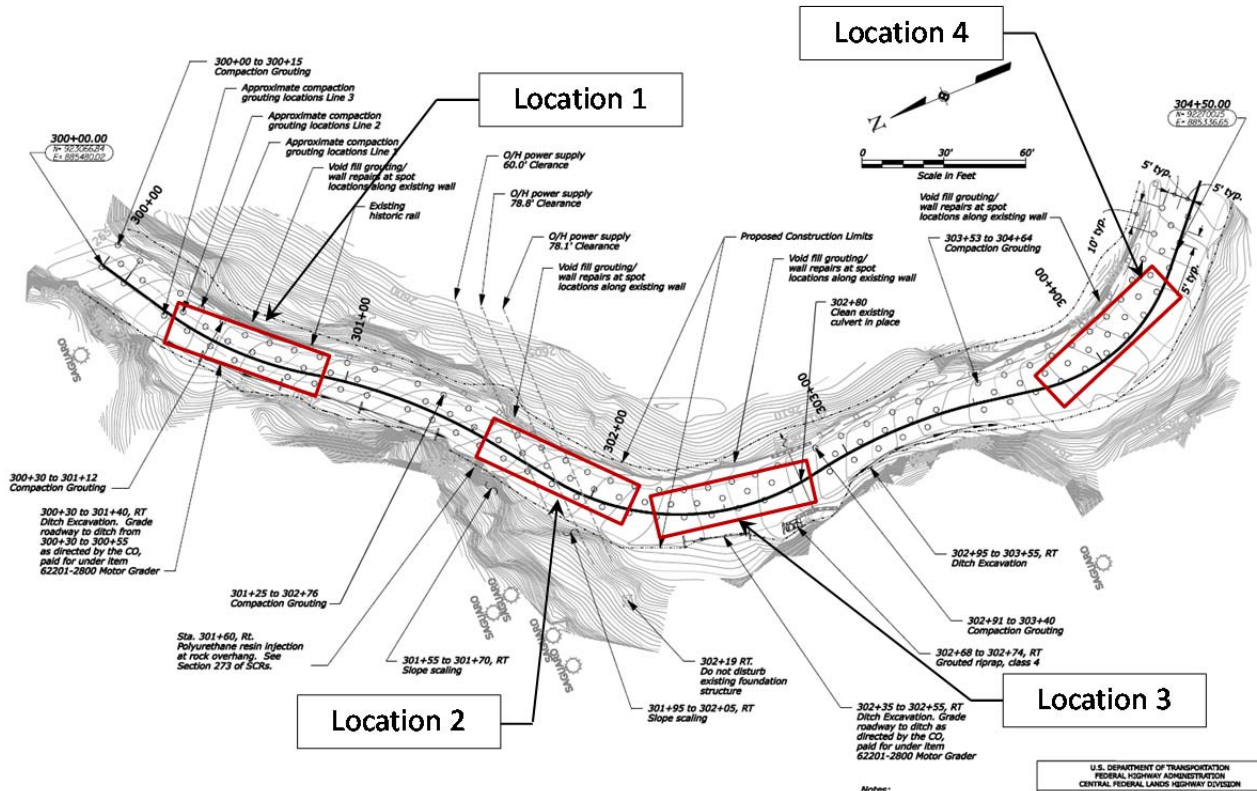


Figure A.6. Schematic. Plan drawing detail of Apache Trail Locations 1 through 4.

APPENDIX A – LOCATION MAPS AND PLAN DRAWINGS

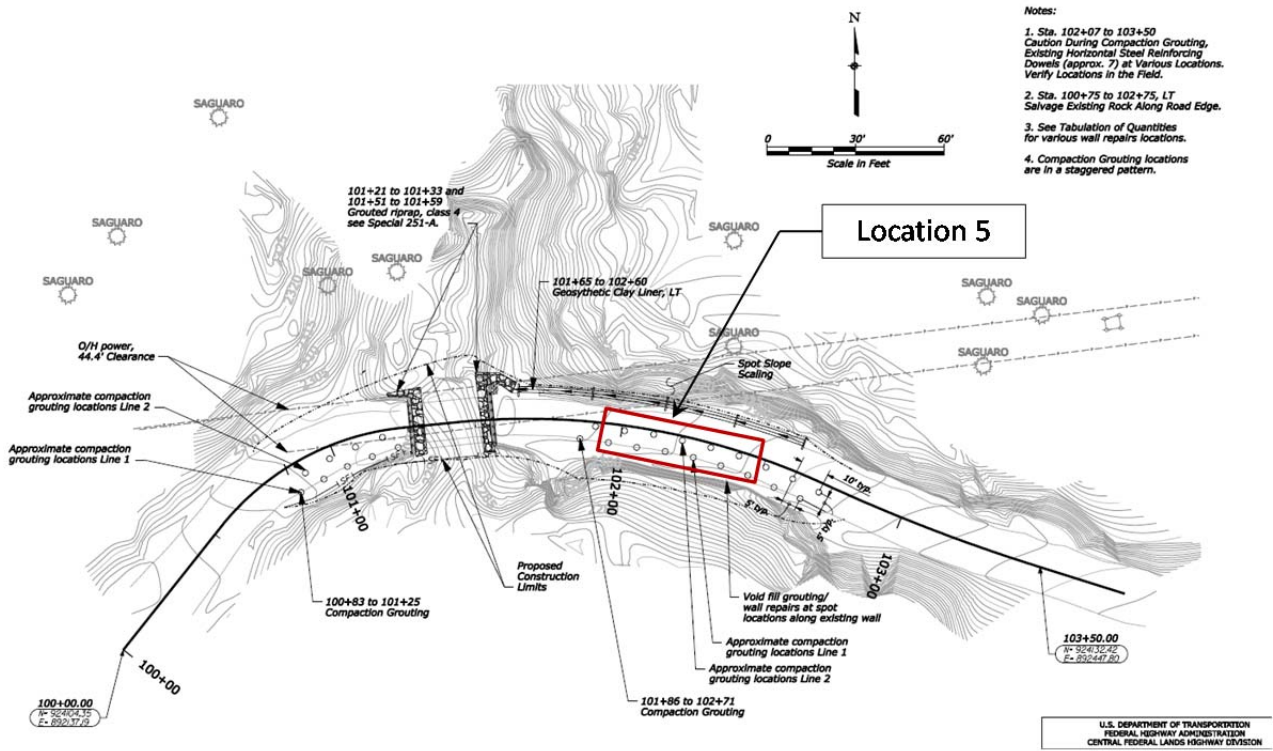
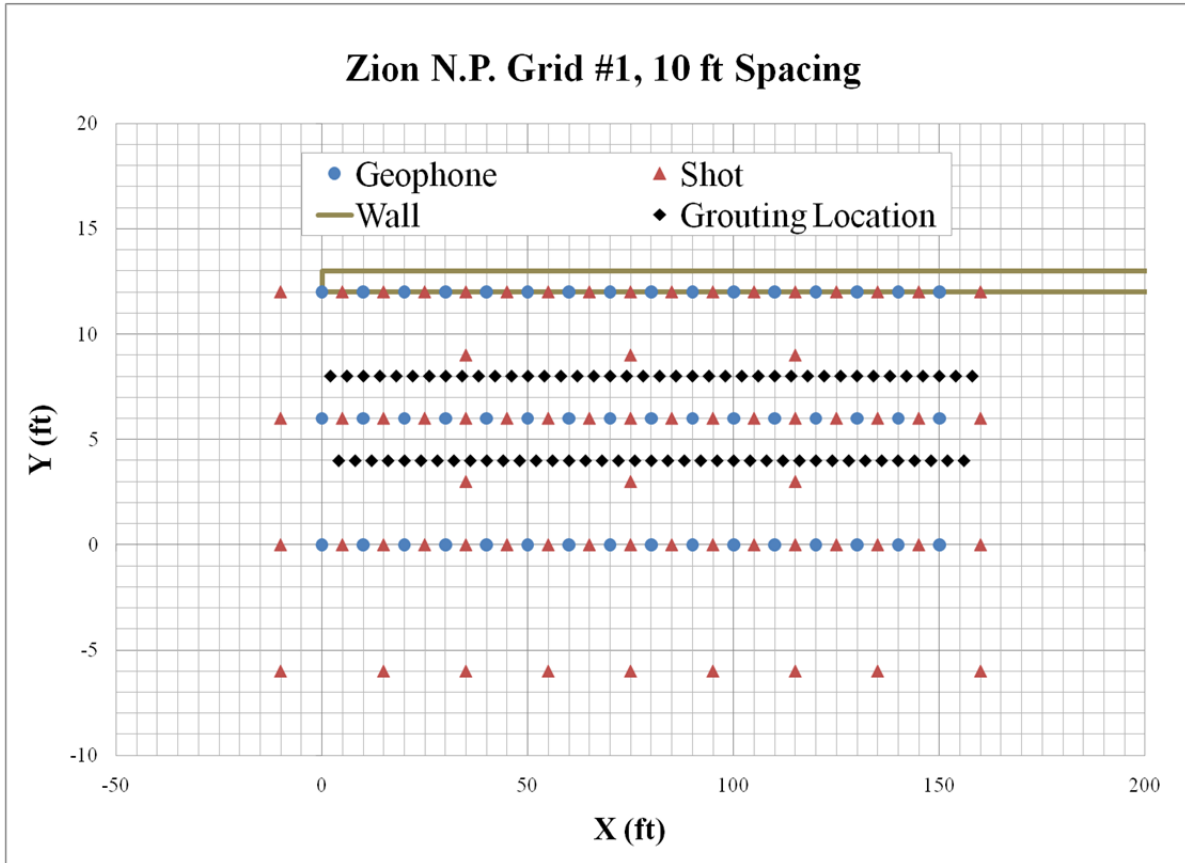
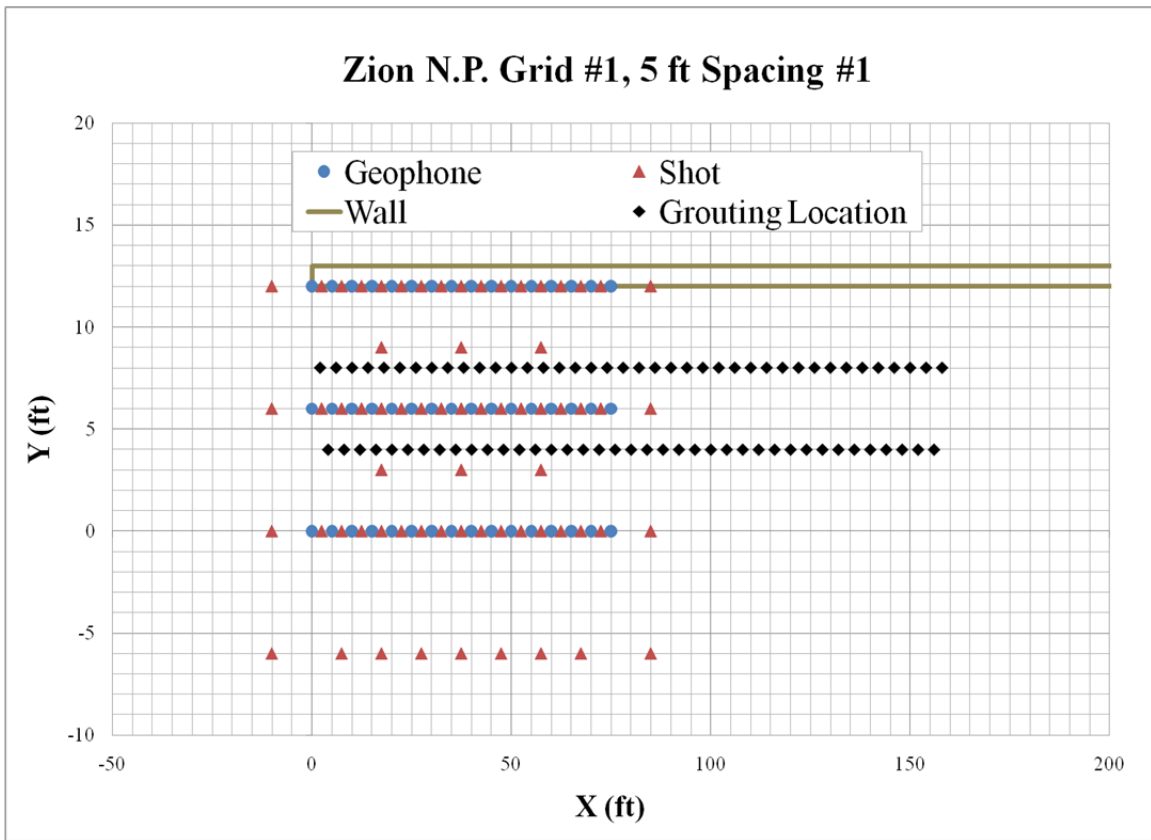
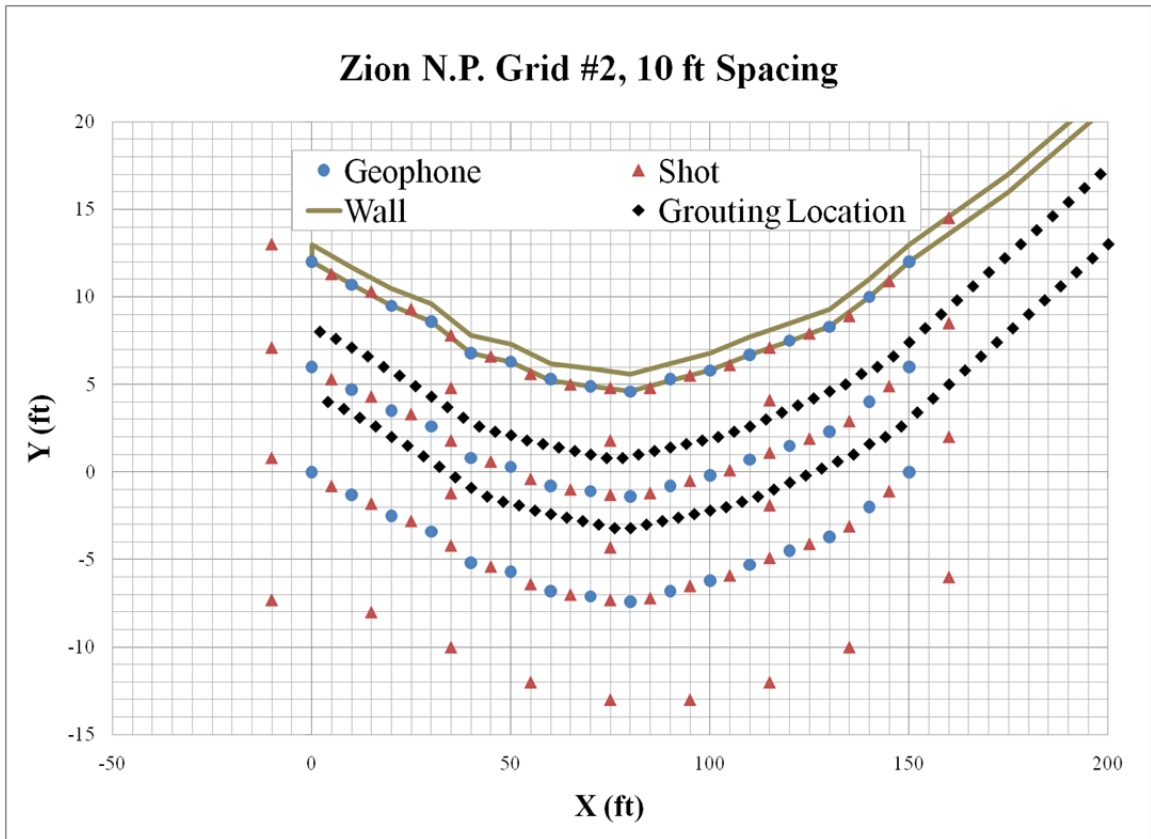


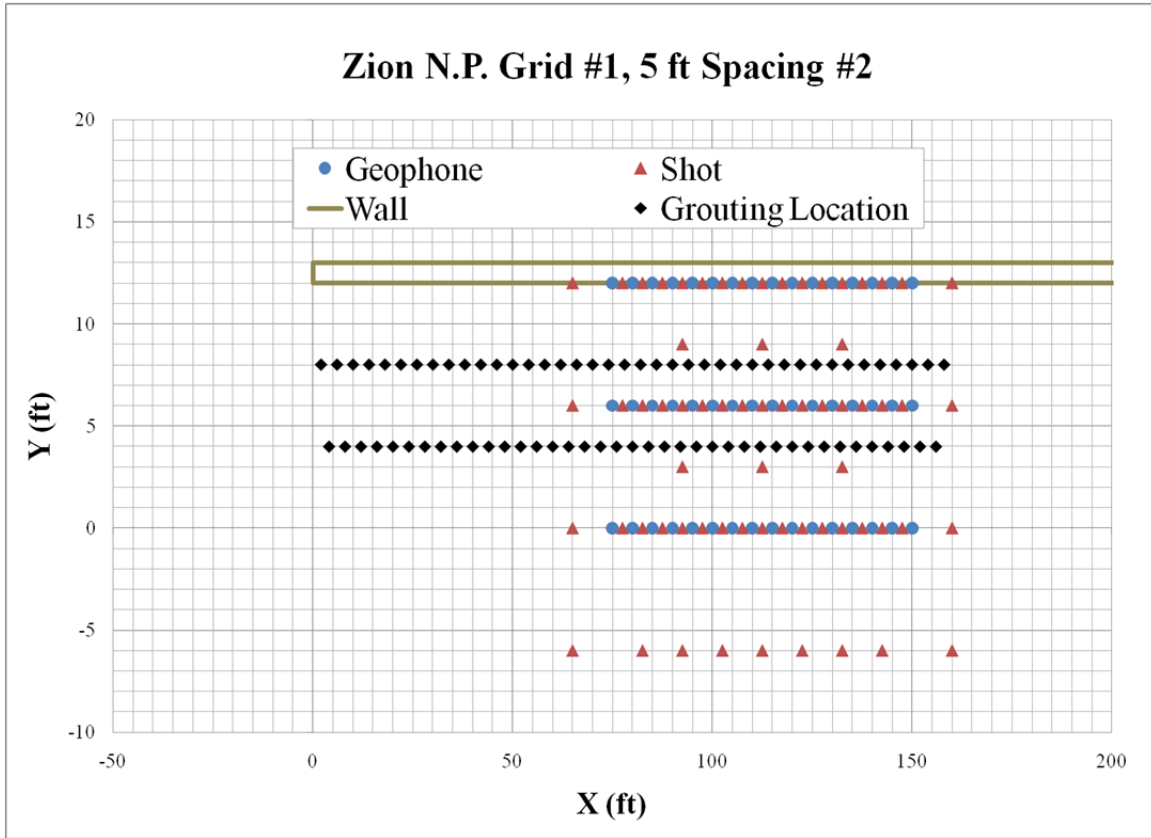
Figure A.7. Schematic. Plan drawing detail of Apache Trail Location 5.

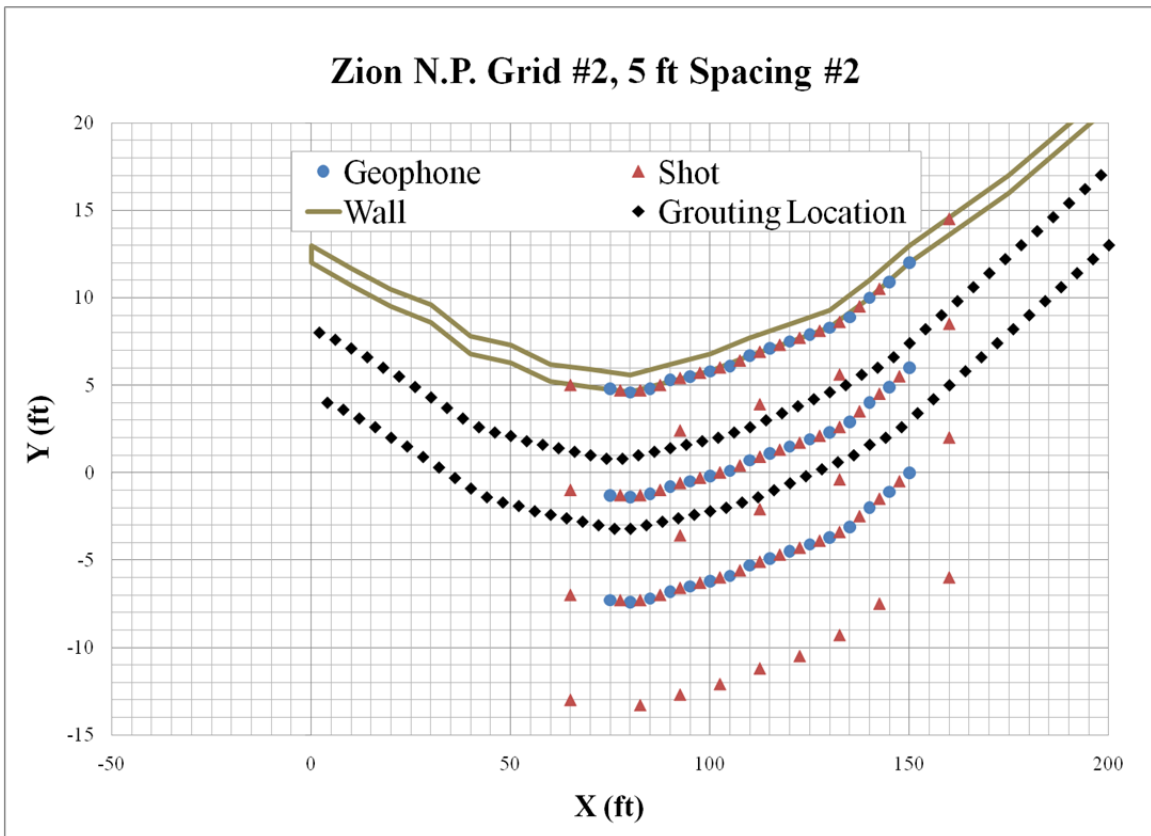
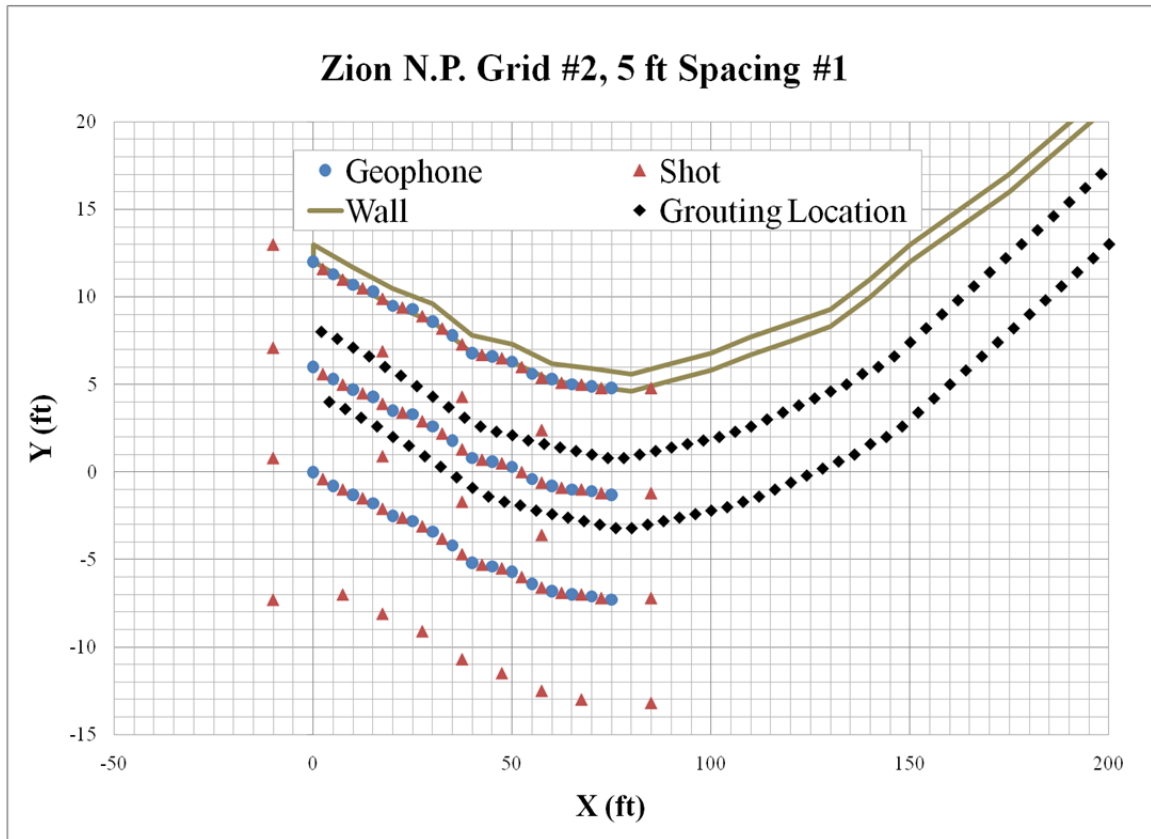
(blank page)

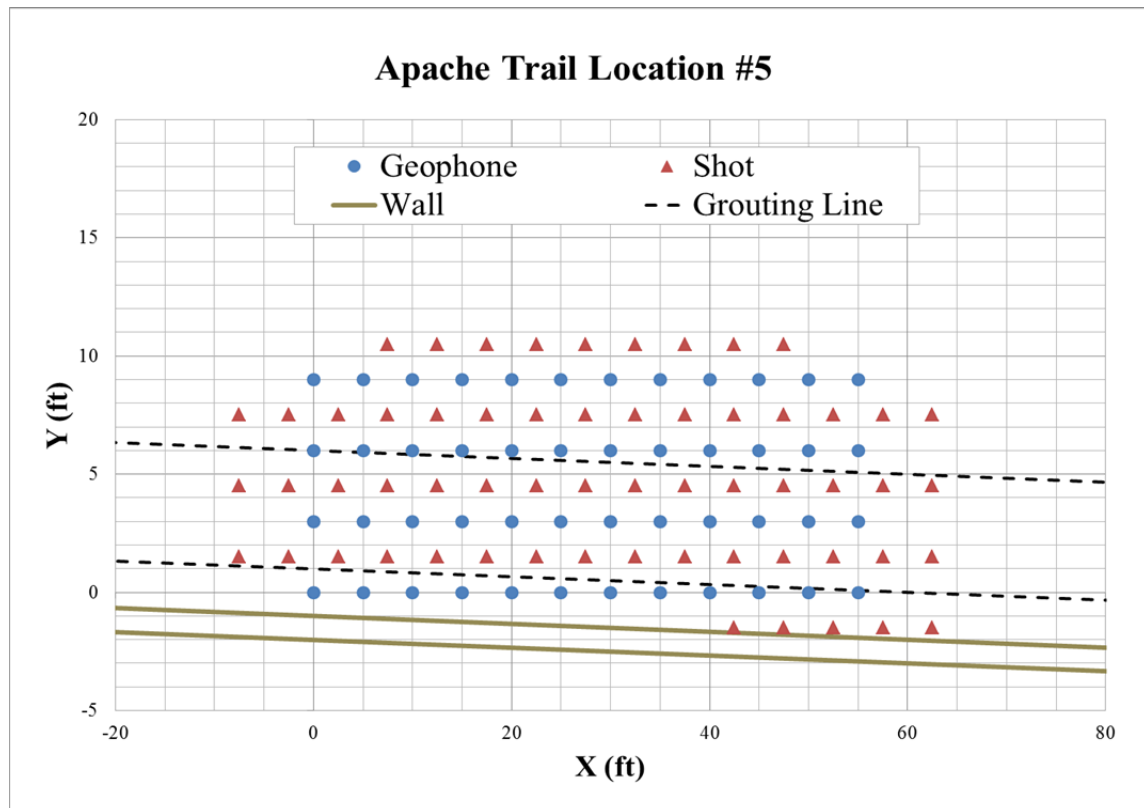
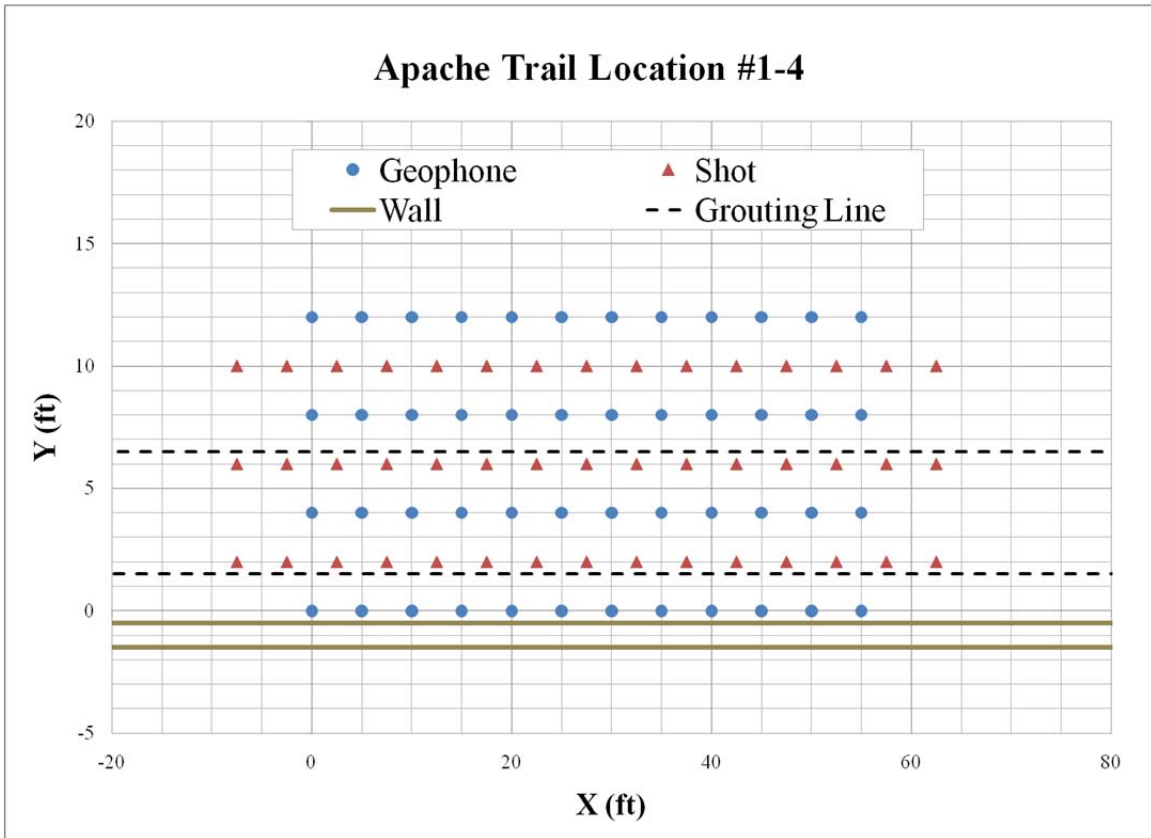
APPENDIX B – DATA COLLECTION LAYOUT DIAGRAMS





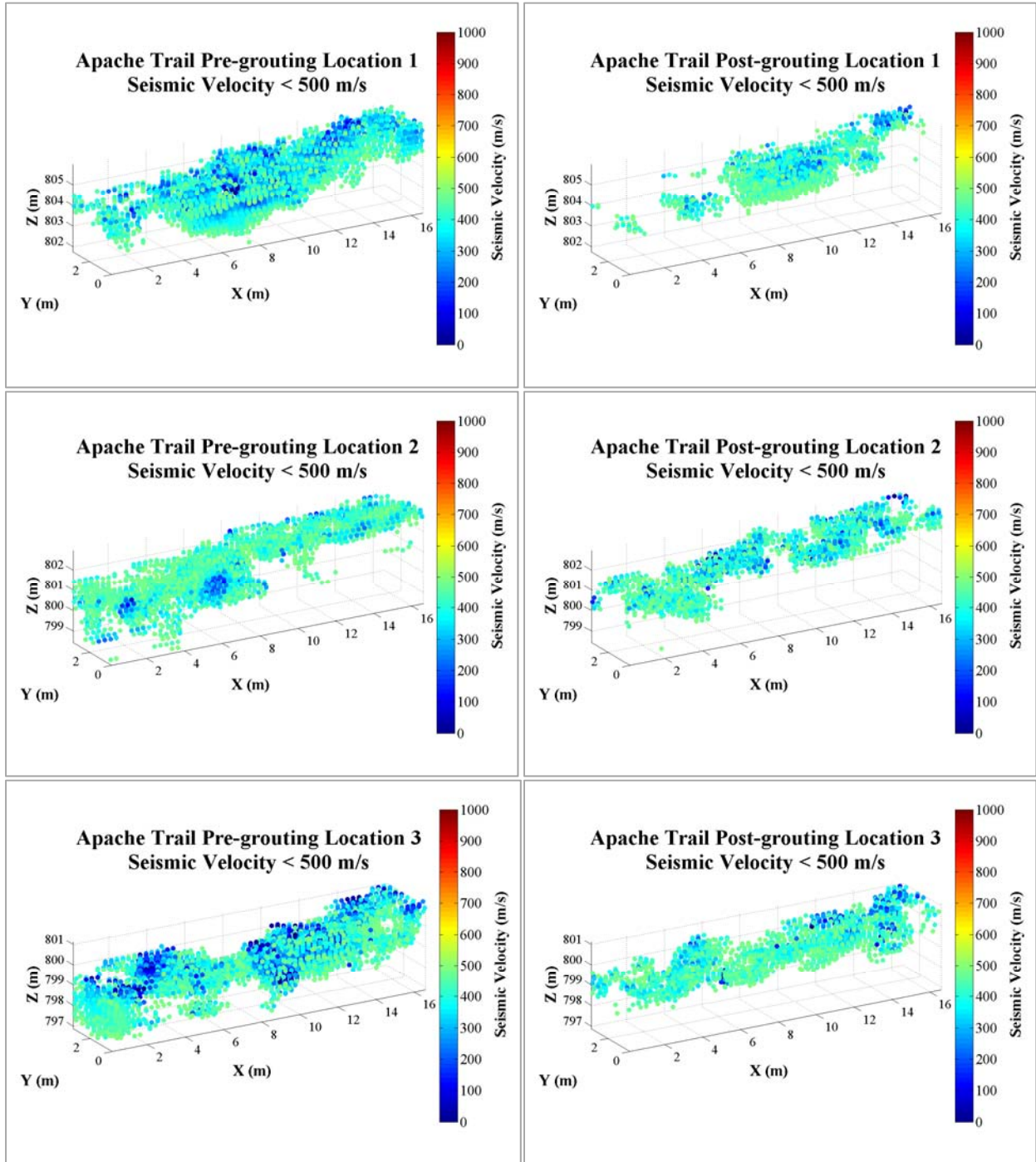


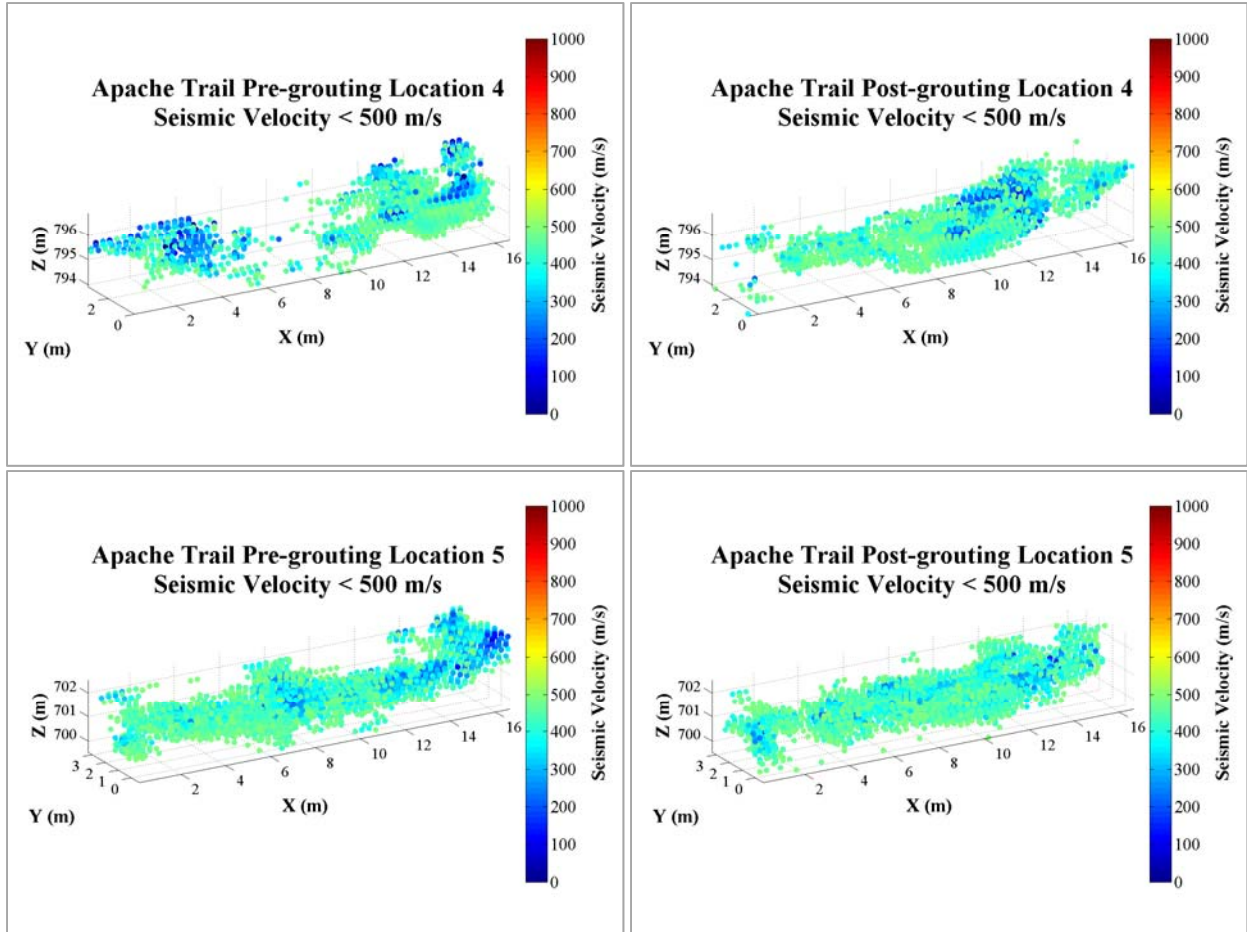


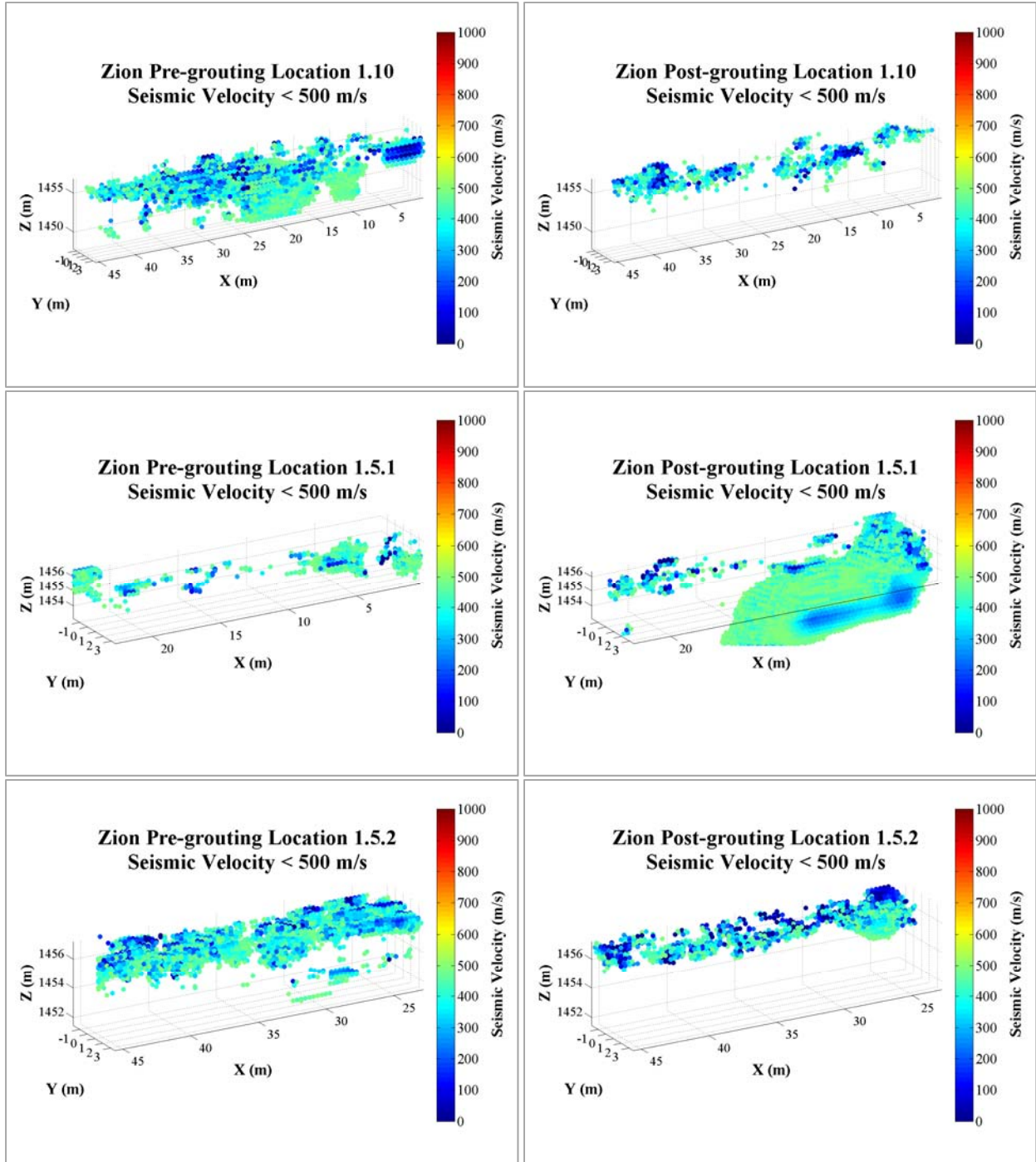


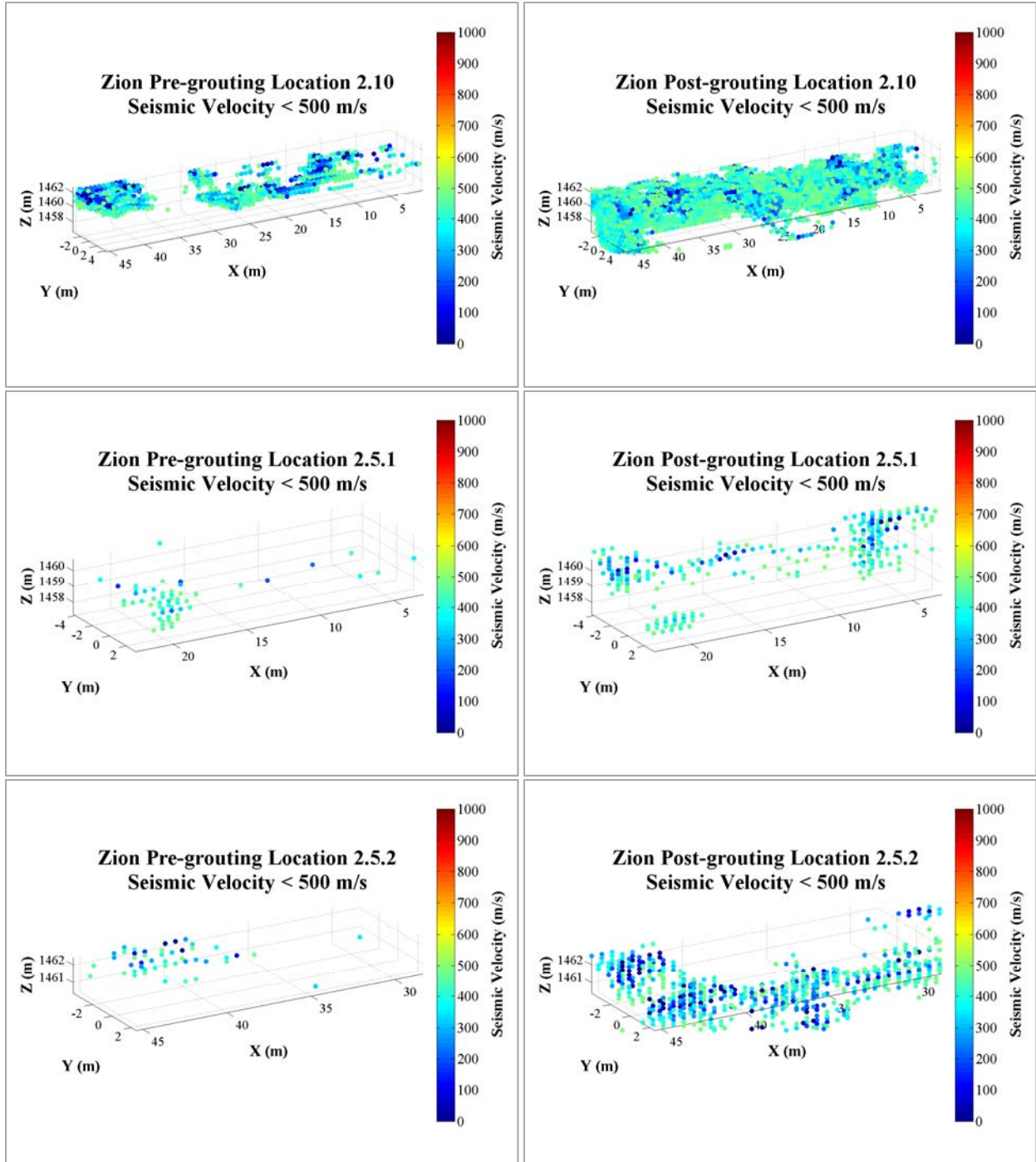
(blank page)

APPENDIX C – SEISMIC TOMOGRAPHY

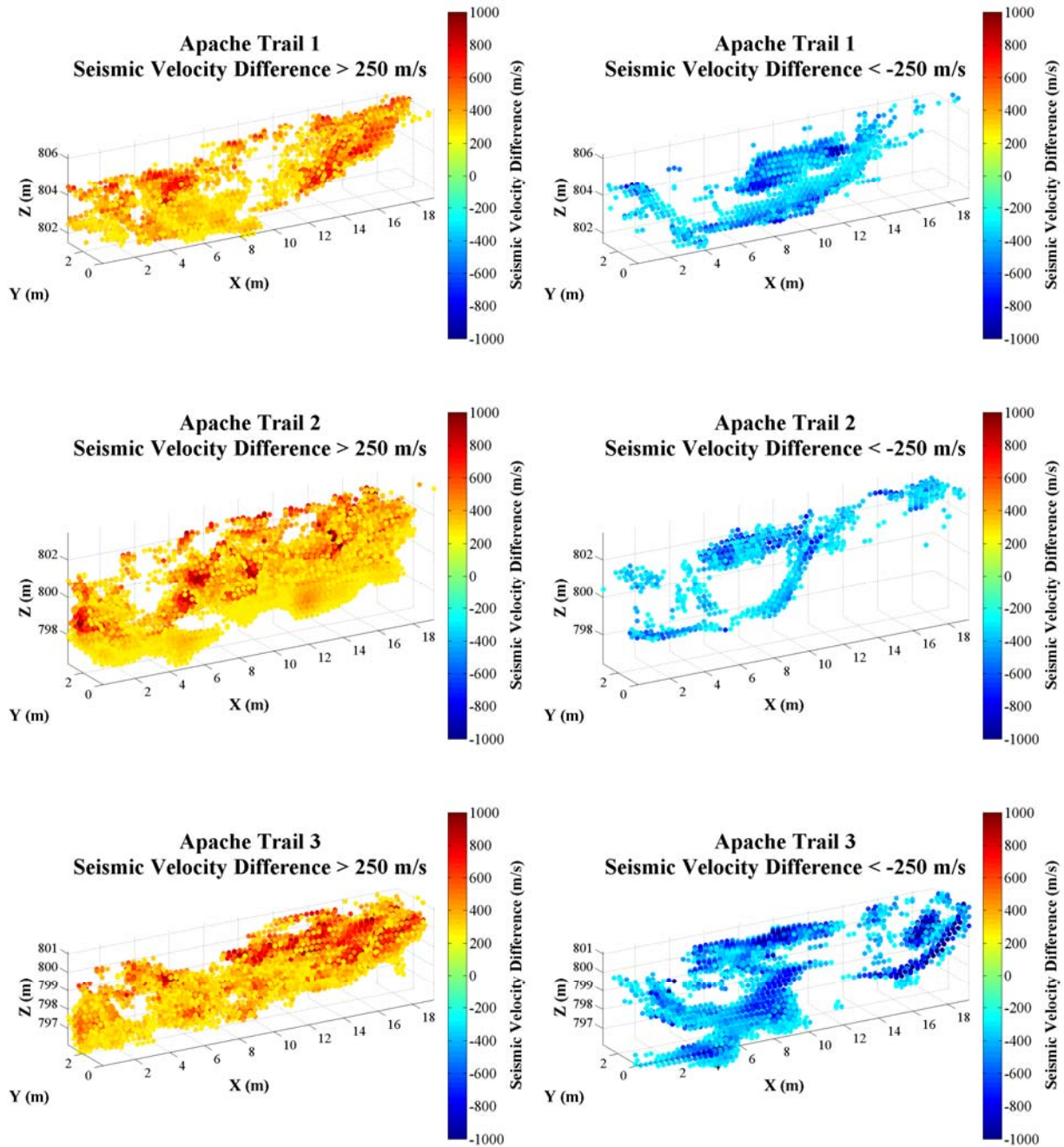


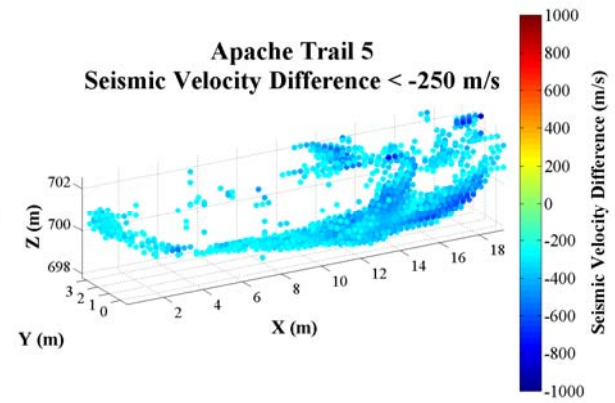
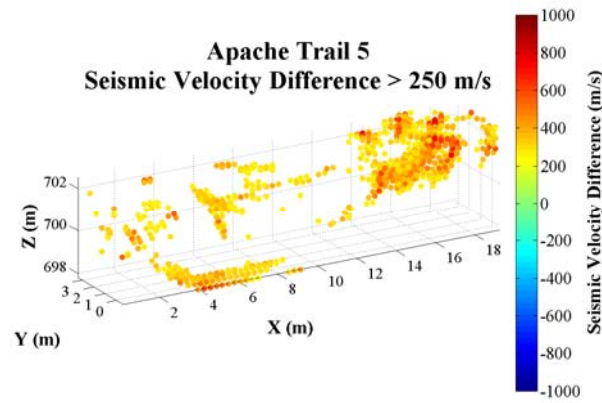
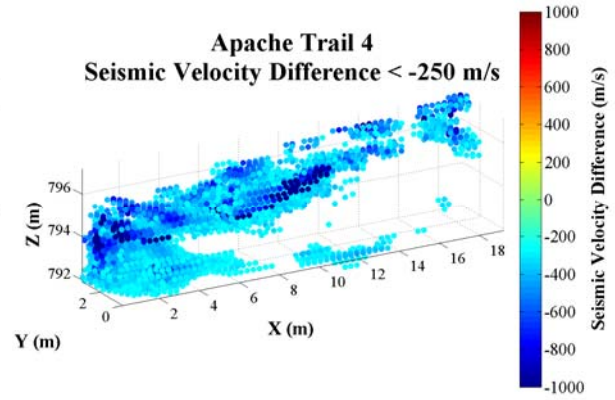
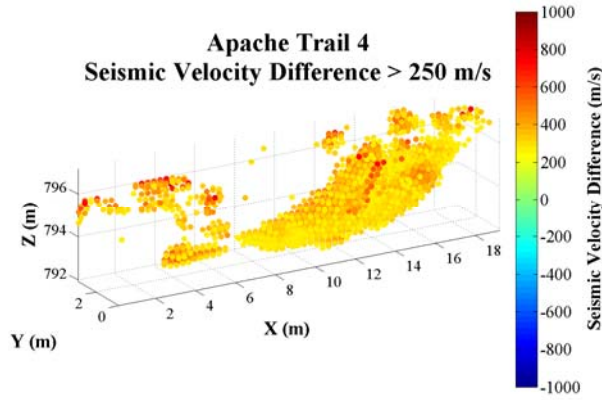


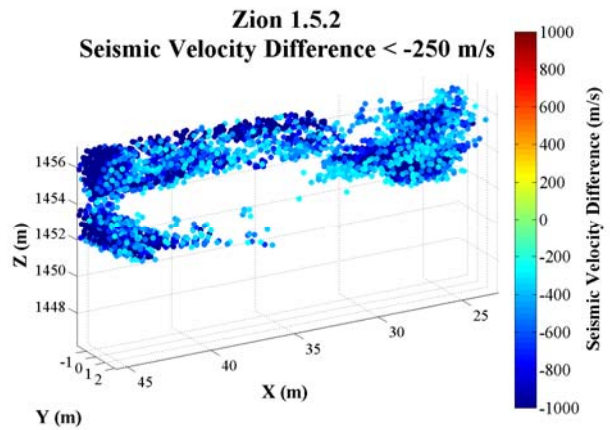
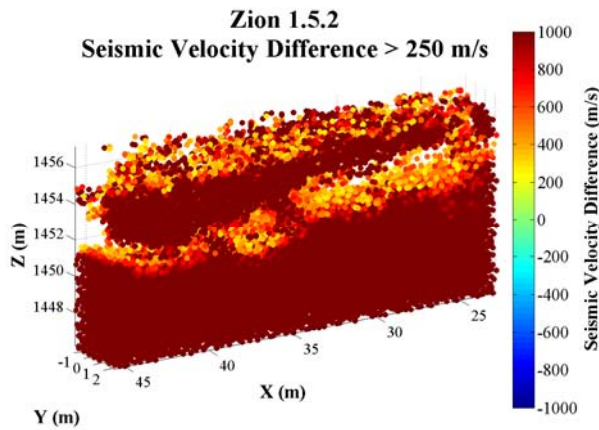
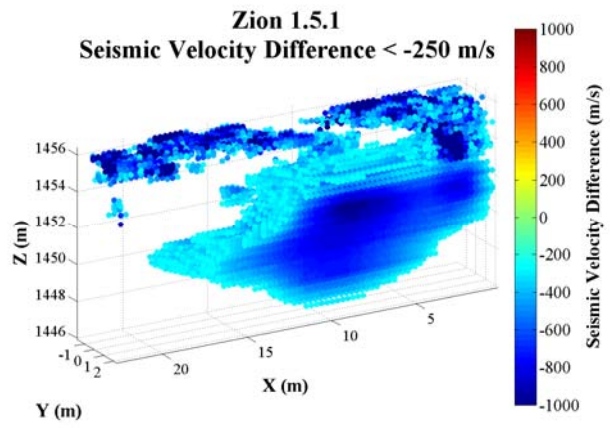
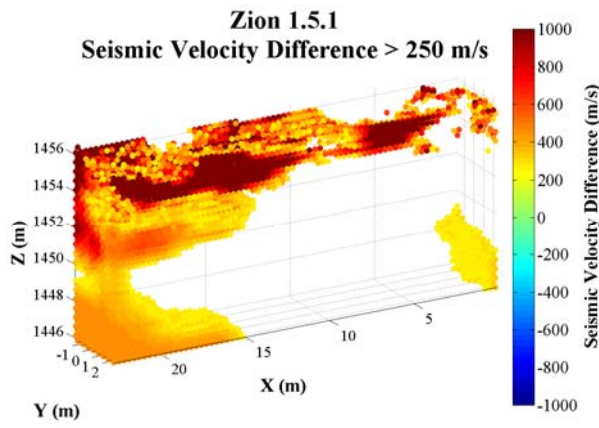
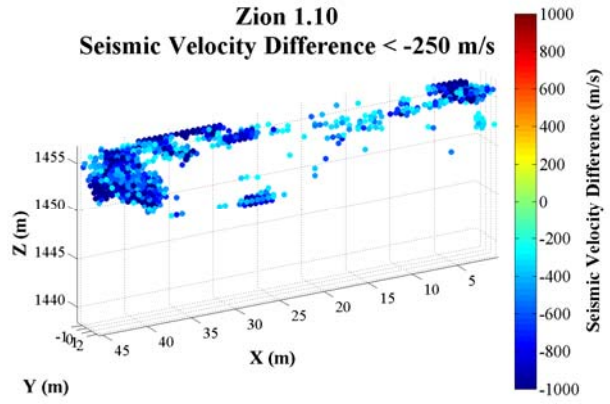
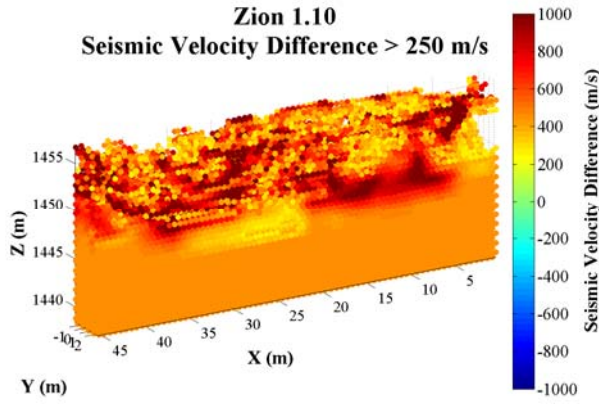


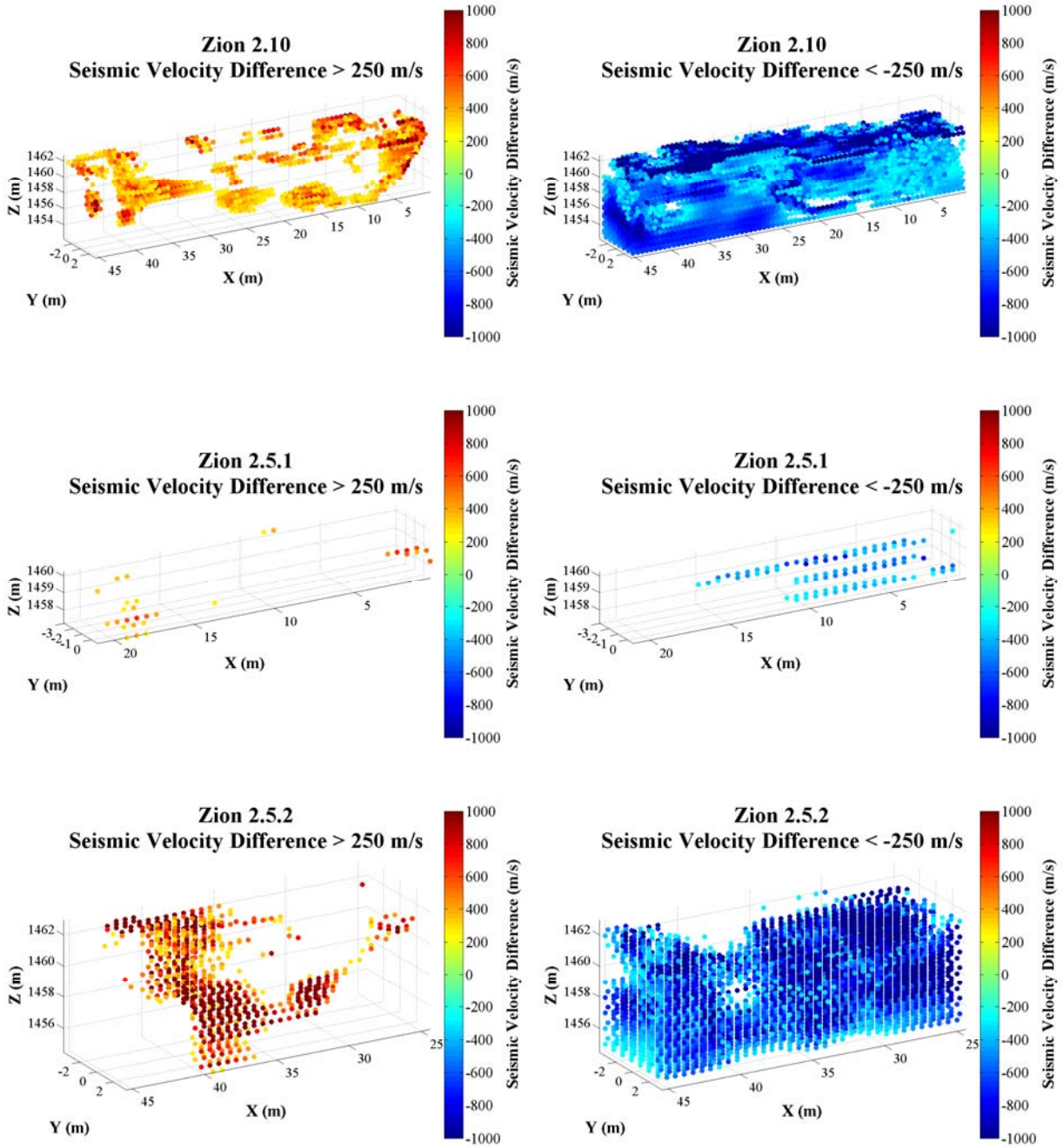


APPENDIX D – SEISMIC DIFFERENCE TOMOGRAPHY

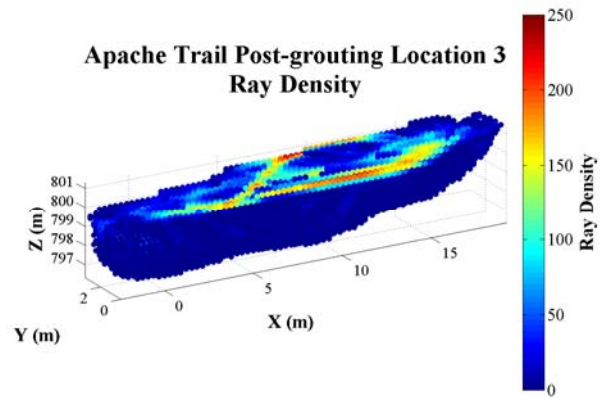
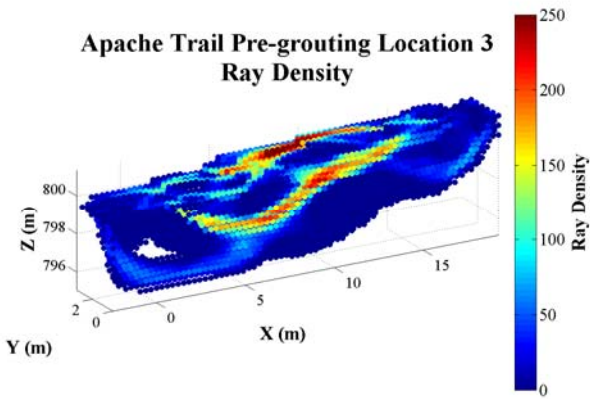
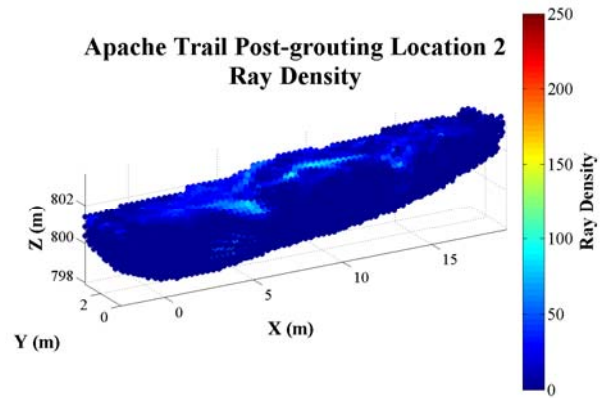
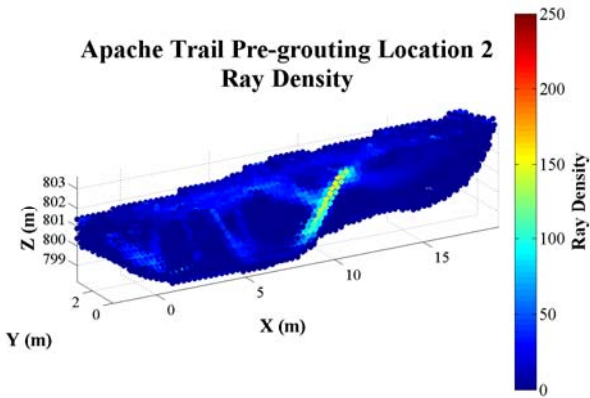
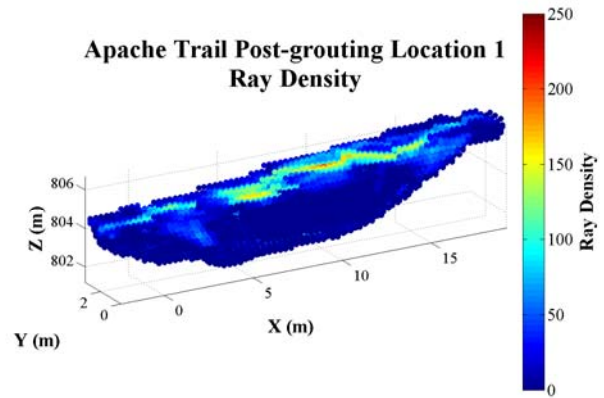
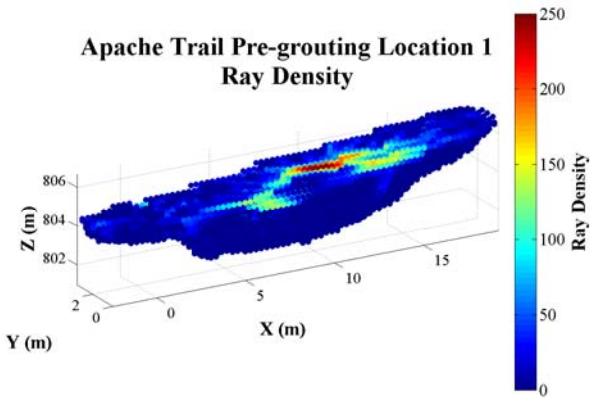


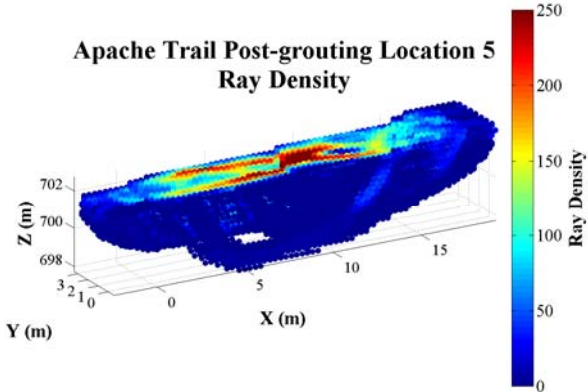
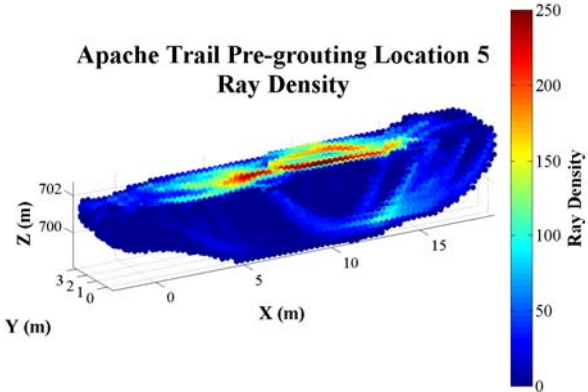
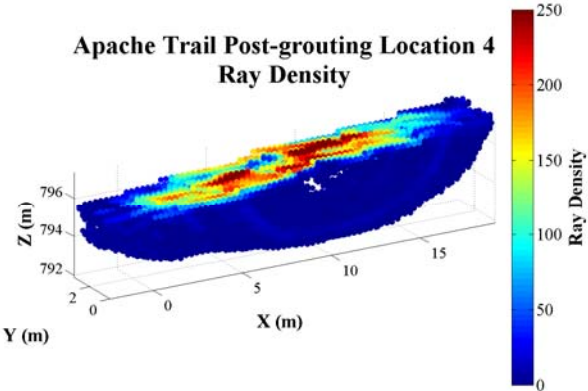
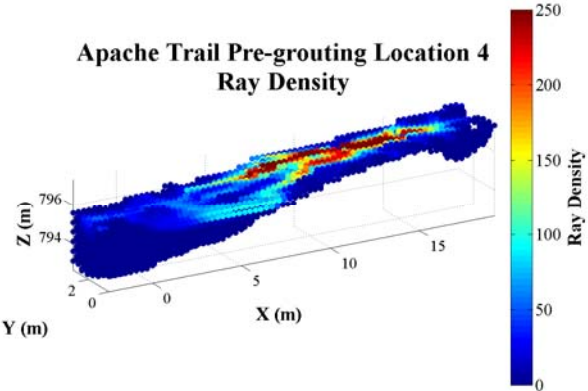


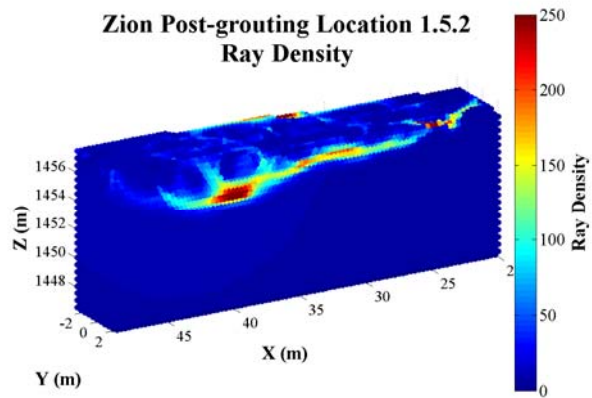
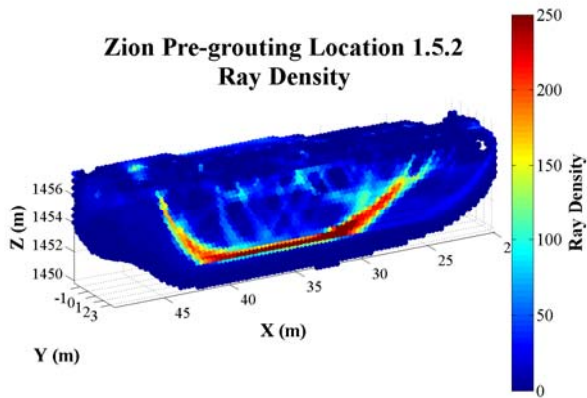
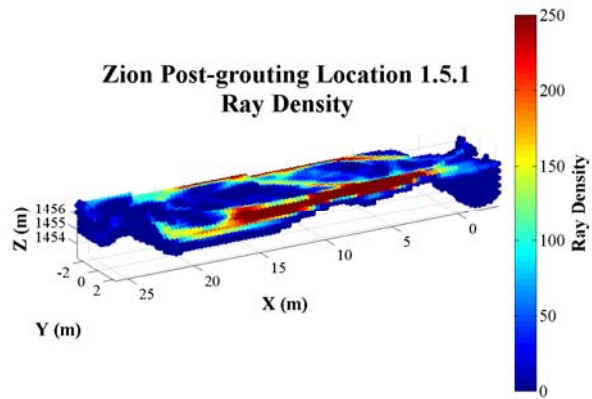
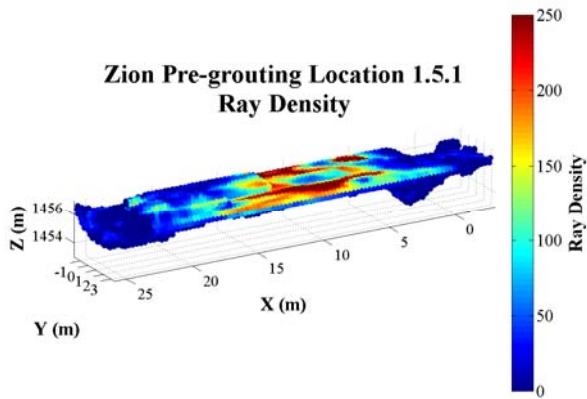
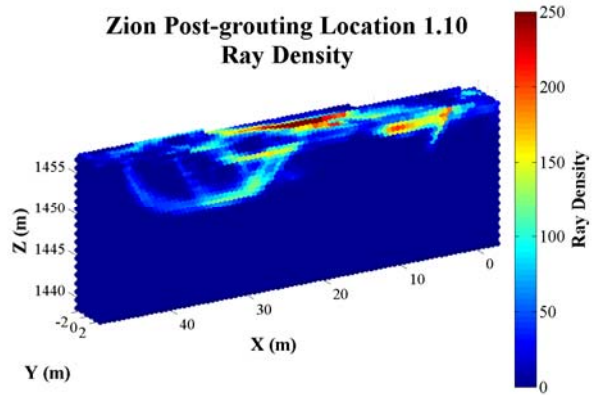
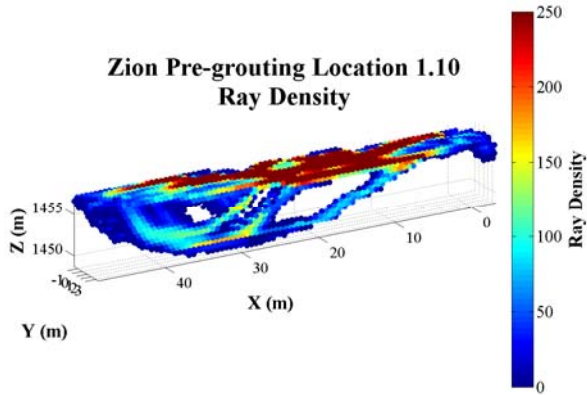


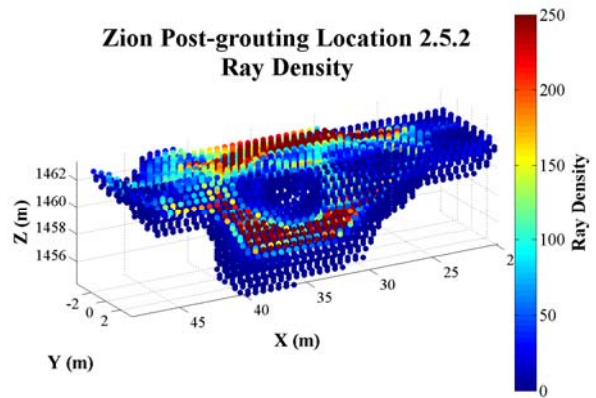
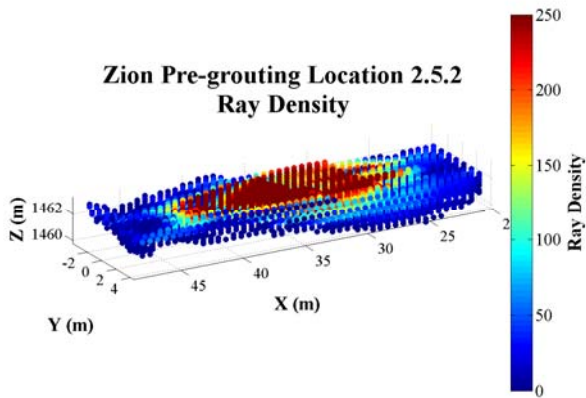
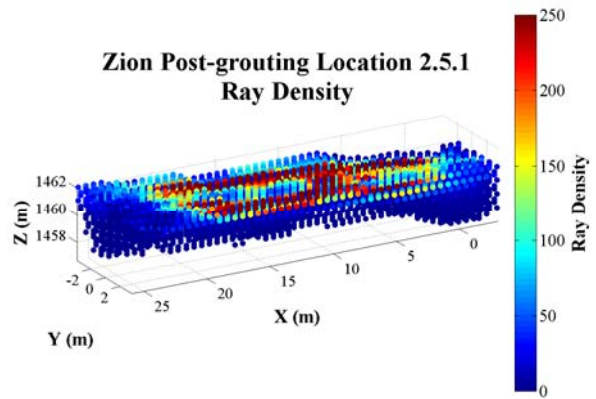
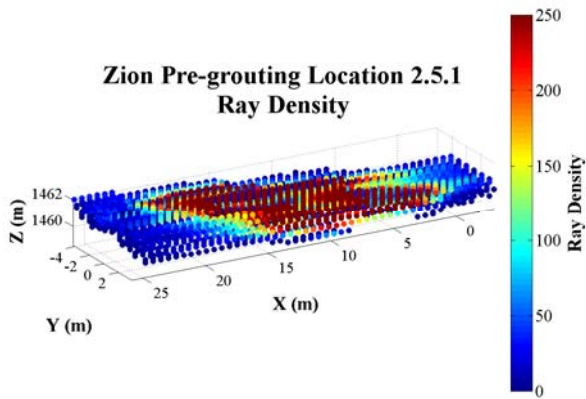
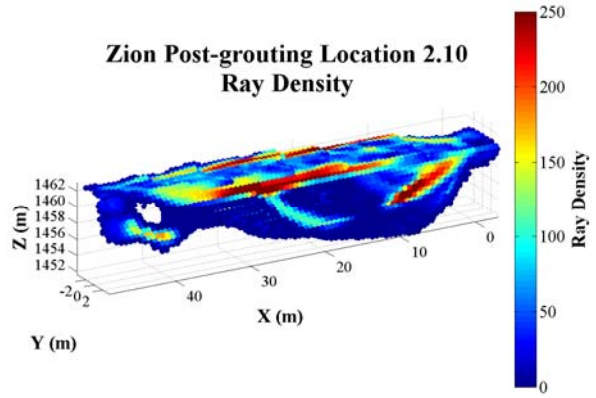
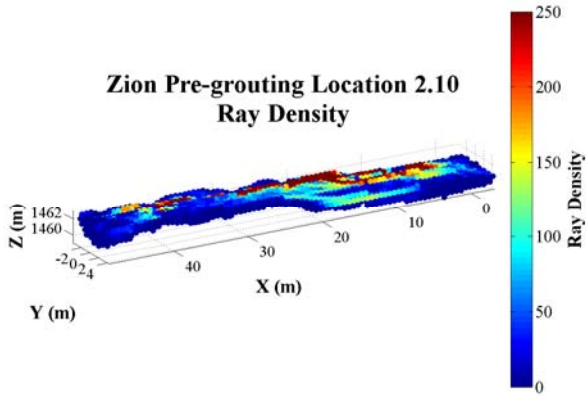


APPENDIX E – RAY DENSITIES









(blank page)